Title

Topics in Quantum Gravity and Quantum Information

Author

Caginalp, Reginald

Publication Date

2024

Peer reviewed|Thesis/dissertation

Topics in Quantum Gravity and Quantum Information

by

Reginald Caginalp

A dissertation submitted in partial satisfaction of the

requirements for the degree of

Doctor of Philosophy

in

Physics

in the

Graduate Division

of the

University of California, Berkeley

Committee in charge:

Professor Yasunori Nomura, Chair
Professor Raphael Bousso
Professor Richard Borcherds

Spring 2024

Topics in Quantum Gravity and Quantum Information

Abstract

Topics in Quantum Gravity and Quantum Information

by

Reginald Caginalp

Doctor of Philosophy in Physics

University of California, Berkeley

Professor Yasunori Nomura, Chair

This dissertation explores numerous applications of concepts from quantum information theory to quantum gravity, the AdS/CFT correspondence, as well as holographic dualities more generally. A recurring theme will be the notion that geometric quantities in the bulk are dual to information-theoretic quantities in the boundary.

The Ryu-Takayanagi formula and related results tell us that entanglement entropies in the CFT are given in terms of the areas of minimal surface in the bulk. This geometric formula for entanglement entropy imposes inequalities on the entanglement entropies of various CFT regions for static spacetimes, known as the holographic entropy cone. We will numerically investigate the validity of the five-region inequalities for a specific dynamical spacetime, a collapsing black hole spacetime. We find that, for all cases considered, all of the inequalities are satisfied when the null energy condition is satisfied in the bulk, while all of the inequalities are violated if the null energy condition is not satisfied in the bulk. This provides some evidence for the validity of the five-region inequalities in general settings in AdS/CFT with a dynamical bulk. We then discuss the complexity-action and complexity-volume conjectures in the setting of holographic Friedmann–Robertson–Walker universes, which are more realistic cosmological models than AdS space. These conjectures pass some non-trivial consistency checks in these settings. Following this, operator complexity is studied numerically for one- and two-qubit systems using Nielsen complexity geometry. Even though these are relatively simple systems, some interesting similarities are found with the behavior of complexity for more interesting, larger systems. Finally, we explore the use of sandwiched Renyi relative entropy in holography, and in finite-dimensional models of quantum error correction.

Contents

List of Figures

Acknowledgments

First and foremost, I would like to express my sincere appreciation to my dissertation advisor, Yasunori Nomura. I am deeply grateful for his outstanding dedication to my scientific development. I feel extremely fortunate that I was able to come to Berkeley and complete my PhD under his supervision.

I would also like to thank Raphael Bousso and Richard Borcherds for serving on my dissertation committee, as well as Heather Gray for being a part of my qualifying exam committee.

I am grateful to the other students, postdocs, and faculty in the BCTP, including Ning Bao, Ven Chandrasekaran, Newton Cheng, Ben Concepcion, Hugo Marrochio, Masamichi Miyaji, Chi Murdia, Geoff Penington, Pratik Rath, Kyle Ritchie, Tom Rudelius, Arvin Shahbazi-Moghaddam, Vincent Su, Misha Usatyuk, and Liz Wildenhain, for their support and for many useful discussions. I thank Matt Headrick for the guidance and suggestions he provided to me in numerous conversations and correspondences.

Finally, I thank my family for all of their love and support throughout my life. I am indebted to them for all of their constant support, guidance, and encouragement.

Chapter 1

Introduction

1.1 Quantum Gravity, Black Holes, and Holographic Duality

Two of the cornerstones of modern physics, quantum mechanics and general relativity, have revolutionized humanity's understanding of the natural world. In certain settings, they depart radically from classical physics, and many of their most consequential predictions have been experimentally and observationally verified to a striking level of accuracy.

However, quantum mechanics and general relativity appear to be incompatible if one tries to combine them in the most naive way. Applying the usual methods of quantum field theory to the metric tensor of general relativity results in a non-renormalizable theory. This suggests that the theory of quantum gravity may require a significant departure from classical general relativity in how we conceive of space and time. Although classical general relativity is expected to break down at around the Planck scale (around 10^{19} GeV, many orders of magnitude above the energy scales achieved in any current or near-term particle accelerators), there are many tantalizing hints of the nature of quantum gravity within general relativity and quantum field theory.

An important example of this was the discovery that using classical general relativity and quantum field theory on a curved background, black holes seem to obey a set of thermodynamic laws [13]. In this formalism, a black hole has an entropy associated with it, known as the Bekenstein-Hawking entropy [15], proportional to the area A of its event horizon,

$$S_{BH} = \frac{A}{4G_N},$$

where G_N is Newton's gravitational constant, and we are working in units where $\hbar = k_B = c = 1$. This is striking for several reasons. Firstly, in statistical mechanics, entropy is the logarithm of the number of microstates of a given system. However, in classical general relativity, a black hole is completely described by its mass, charge, and angular momentum. This seems to imply that in the full quantum theory of gravity, black holes should have

microstates, with associated entropy $\frac{A}{4G_N}$. In addition, the Bekenstein-Hawking formula seems to suggest that the entropy of a black hole scales with its event horizon *area*, rather than with its *volume*, as in most classical systems. This result has led to conjectures on bounds on the entropy of a matter configuration in a given spacetime region [14, 17, 16]. A couple of decades after the discovery of the Bekenstein-Hawking bound, the holographic principle was proposed by 't Hooft and Susskind, which states that a theory of quantum gravity of a given volume should be encoded on the boundary of that volume [90, 1].

Furthermore, Hawking discovered, by analyzing quantum fields on a classical curved spacetime, that black holes radiate at a small but nonzero temperature [53, 54]. This is in sharp contradiction to the expectations from classical general relativity, which predicts that nothing can escape from inside a black hole. The discovery that black holes radiate also implies that they gradually lose mass and will eventually evaporate, leaving only thermal radiation behind. However, this is in tension with the expectation that the laws of physics should conserve information. To see this, consider a star which collapses to form a black hole. The black hole will eventually evaporate, leaving only the thermal radiation. The initial star contains information about its constituent particles, their locations, velocities, and so on. After the star has collapsed into a black hole and then evaporated, the resulting cloud of radiation, according to Hawking's calculation, will be described only by a small number of parameters. Therefore, there is an apparent loss of a large amount of information. This peculiarity is known as the black hole information paradox. A significant amount of research over the last several decades has been dedicated to trying to resolve this paradox. In the last few years, there has been substantial progress towards solving this problem in favor of information conservation, and in showing in detail what happens to the information [82, 7, 81, 6].

Another important series of developments in the search for a theory of quantum gravity has been the research on string theory, which posits that the fundamental particles of nature are strings rather than particles. The vibrational modes of the string are quantum fields, one of which is the gravitational field. In this way, string theory provides an ultraviolet-complete theory of quantum gravity. This line of research has led to many important and beautiful developments in theoretical physics and in pure mathematics. One particularly pivotal advance was the discovery of the AdS/CFT correspondence by Maldacena in 1997 [71, 49, 96]. The AdS/CFT correspondence posits that any theory of quantum gravity in $(d+1)$-dimensional asymptotically Anti-de Sitter (AdS) space (known as the "bulk" theory) is equivalent to a conformal field theory (CFT) in d dimensions (known as the "boundary"). The work of Maldacena therefore used string theory to provide a concrete realization of the holographic principle. This remarkable equivalence of a theory with gravity to one without gravity has been very useful in improving our understanding of quantum gravity, since quantum field theory is relatively well understood. In addition, these holographic dualities have been useful in studying strongly-coupled quantum field theories, which have had numerous applications to other areas of theoretical physics, such as condensed matter physics and nuclear physics.

AdS space is a homogeneous and isotropic solution to the vacuum Einstein equations

of general relativity with a negative cosmological constant, $\Lambda < 0$. However, cosmological observations indicate that our Universe is not AdS, and in fact indicate that the cosmological constant is positive. Therefore, it would be of interest to try to develop holographic descriptions of gravity for more realistic Friedmann-Robertson-Walker (FRW) universes. In AdS/CFT, the holographic principle is realized by proposing that the bulk theory is encoded on the conformal boundary of AdS space. It is therefore natural to investigate the surfaces that encode the holographic description of gravity in FRW spacetimes. Much work has been done in this direction in recent years [77, 78, 79, 86]. In particular, it has been proposed that holographic descriptions of gravity are encoded in the holographic screens. For a given spacetime, a holographic screen is a codimension-1 that is foliated by marginally trapped or marginally anti-trapped codimension-2 surfaces. These codimension-2 surfaces that foliate the holographic screen are known as leaves. These holographic screens satisfy several properties that are key features of the AdS/CFT correspondence. These results have been used to obtain information about the entanglement structure of the holographic duals of gravity theories in FRW spacetimes.

A major theme in research into the holographic dualities (as well as quantum field theory) over the last 15 years has been the use of quantum information theoretic quantities and methods to gain insight into holography and quantum gravity, and vice versa. This dissertation explores several uses of quantum information-theoretic concepts to better understand various holographic dualities.

1.2 Quantum Information, Entanglement, and Holographic Duality

A major advance in understanding the role that entanglement and quantum information play in the AdS/CFT correspondence was the discovery of the Ryu-Takayanagi (RT) formula [85]. Consider a CFT state ρ with a static semi-classical bulk dual, and suppose Σ is a Cauchy slice of the bulk at a moment of time-reflection symmetry, and suppose A is a boundary subregion. If we approximate the Hilbert space of the CFT as factorizable, that is,

$$\mathcal{H}_{CFT} = \mathcal{H}_A \otimes \mathcal{H}_{\bar{A}},$$

where $\bar{A}$ is the complement of A, then we can calculate the reduced density matrix on A by tracing out the complement of A, $\rho_A = \mathrm{Tr}_{\bar{A}}(\rho)$. The entanglement entropy, or von Neumann entropy, of the boundary subregion A can be calculated as usual

$$S(A) = -\mathrm{Tr}(\rho_A \log \rho_A).$$

The Ryu-Takayanagi formula then states that

$$S(A) = \frac{\min_m \mathrm{Area}[m]}{4G_N},$$

where G_N is Newton's gravitational constant, and m is a codimension-2 surface in the bulk that shares its boundary with A (so that $\partial m = \partial A$), and is homologous to A (i.e., there exists a subset χ of the bulk such that $\partial\chi = m \cup A$). There exist several important generalizations to the Ryu-Takayanagi formula. For example, the Hubeny-Rangamani-Takayanagi formula [60] (which is equivalent to the maximin construction of Wall [94]) is the covariant generalization of the RT formula. In addition, perturbative corrections in G_N have been discussed in the literature [45]. It was recently proposed that the subregions of leaves that foliate holographic screens in FRW spacetimes obey an RT-like formula. This passes several basic consistency checks expected of an entanglement entropy, including strong sub-additivity [79, 86].

These formulae are remarkable for a number of reasons. First of all, that entanglement in the boundary theory is equivalent to areas in the bulk gravitational theory–entanglement is geometrized in the dual gravitational description. Computing entanglement entropies for quantum field theories is, in general, very difficult. For CFT states with semi-classical bulk duals, the RT formula (and its generalizations) allows us to compute entanglement entropies by calculating areas of minimal surfaces, which are in general much easier to compute. In addition, these formulas allow us to obtain a deeper understanding of the entanglement structures of CFT states with semi-classical bulk duals. The RT formula and its generalizations also play a prominent role in the connection between the AdS/CFT correspondence and quantum error correction [5, 40, 51, 50].

This geometric entanglement entropy formula also allows for an elegant proof of strong sub-additivity [58, 57, 94], which is an inequality that is true for an arbitrary quantum system [69, 68]. That is, for any three spatial CFT sub-regions A, B, C, the following inequality is obeyed

$$S(ABC) + S(B) \leq S(AB) + S(BC),$$

where, e.g., $S(ABC)$ denotes the entanglement entropy of $A \cup B \cup C$. In the same way, it has also been shown that for a holographic CFT state, monogamy of mutual entanglement is also obeyed [55, 57]. That is, again for three spatial CFT sub-regions A, B, C, we have

$$I(A : B) + I(A : C) \leq I(A : BC),$$

where I denotes the mutual information between two regions. The mutual information between two regions A and B is defined as

$$I(A : B) = S(A) + S(B) - S(AB).$$

Monogamy of mutual entanglement is not obeyed by all quantum systems, so this provides some insight into the special entanglement structure of holographic CFT states. More generally, for n CFT spatial sub-regions obeying the RT formula, one can derive the general set of inequalities obeyed by CFT states with holographic duals. This set of constraints is known as the holographic entropy cone, and was derived by Ref. [12] for static spacetimes.

Another fascinating idea involving the interplay between quantum information concepts in the boundary and geometric quantities in the bulk is the role that complexity may play

in holography. To understand the motivation for this proposal, consider an AdS black hole. This is dual to the CFT in a thermal state. Consider a maximal volume slice anchored at boundary time t. Classically, this volume grows forever, proportionally to t, and the AdS/CFT correspondence implies that there must be some boundary quantity (that is dual to this volume) that must grow linearly with time. The entanglement entropy saturates after a relatively small amount of time [52], so this led to the proposal that the computational complexity of the CFT state may be proportional to the maximal-slice volume in the bulk. This is known as the complexity-volume proposal [89]. The computational complexity of a quantum state $|\psi\rangle$ is the minimum number of "simple" gates (i.e., gates acting on a very small number of degrees of freedom) it takes to build up $|\psi\rangle$ from a simple, unentangled reference state. In a system with N degrees of freedom, the complexity of a state usually grows linearly with time until t is of order e^N, at which point it saturates, up until it experiences Poincare recurrences at very late times [91]. This conjecture also passes a number of other consistency checks [91]. Therefore, the complexity is a good candidate for the CFT dual of a maximal-volume slice in the bulk. This proposal was followed by the complexity-action proposal [25, 26], which posits that the complexity of a CFT state is proportional to the action of a certain subset of the bulk, called the Wheeler-deWitt patch, rather than a bulk volume.

This dissertation explores aspects of the interplay between quantum information, quantum field theory, as well as holographic dualities and quantum gravity.

Chapter 2 explores the validity of the five-region holographic entropy cone inequalities in dynamical spacetimes by considering a specific example of a dynamical spacetime, an AdS_3-Vaidya spacetime (i.e., a collapsing shell of matter that forms a black hole). We study this by numerically solving the geodesic equation in the bulk. We find that, for all cases considered, all of the five-region inequalities are satisfied when the null energy condition is satisfied in the dynamical bulk spacetime, and that all of the inequalities can be violated when the dynamical bulk spacetime does not satisfy the null energy condition. These results provide evidence that the five region inequalities of the holographic entropy cone are valid in dynamical spacetimes. This chapter is based on Ref. [28].

Chapter 3 applies the holographic complexity conjectures to the context of holographic descriptions of gravity in FRW spacetimes. We first discuss the complexity-action conjecture applied to a flat FRW universe with one component. In this case, the complexity grows proportionally to t^2, regardless of the value of w, the ratio of the pressure to the energy density. We then discuss the holographic complexity for a flat FRW universe sourced by a single scalar field that is undergoing a transition. The calculations show that the complexity decreases when the entanglement entropy decreases. In addition, we show that the magnitudes of the fractional decreases are significantly larger for the computational complexity than for the corresponding decreases in entanglement entropy. This is to be expected from basic physical considerations, since entanglement is computationally expensive. We find in this setting that the gravitational action has many complexity-like properties, while the total action is negative, and thus is an ill-defined dual to the complexity of the boundary theory. This is in contrast to the complexity-action conjecture in the context of AdS/CFT. Finally,

we discuss the implications of the complexity-volume conjecture, and find that the results are similar to those of the complexity-action conjecture. This chapter is based on Ref. [27].

Chapter 4 numerically analyzes the complexity of unitary time-evolution and precursor operators using Nielsen complexity geometry for one- and two-qubit systems. We find that the complexity of one- and two-qubit unitary time-evolution operators initially increase linearly with time. The complexities of the precursor operators display switchback-effect-like growth if we choose the cost factors so that the complexity geometry has negative curvature. This chapter is based on Ref. [30].

Chapter 5 discusses the role of sandwiched Renyi relative entropy in AdS/CFT. In particular, we discuss this quantity in the context of finite-dimensional models of holographic quantum error correction. In the setting of operator algebra error correction, we consider a natural generalization of sandwiched Renyi relative entropy for finite-dimensional von Neumann algebras. We then prove that the equality of bulk and boundary sandwiched Renyi relative entropy is equivalent to algebraic encoding of bulk and boundary states, the RT formula, the equality of bulk and boundary relative entropy, and subregion duality. This discussion adds one more item to the equivalence of the last four items, which was first established as a theorem in this setting by Ref. [51]. Following this, we explore the sandwiched Renyi relative entropy defined using modular operators. It is discussed how this is the definition naturally suited to finite-dimensional models of holographic error correction. Lastly, in order to gain insight into corrections to the equality of bulk and boundary sandwiched Renyi relative entropy, we discuss some numerical calculations of sandwiched Renyi relative entropy for a simple random tensor network model of holography. This chapter is based on Ref. [29].

Chapter 2

The Holographic Entropy Cone in AdS-Vaidya Spacetimes

2.1 Introduction

Recent work has unveiled deep connections between gravity and entanglement. The AdS/CFT correspondence [71, 49, 96] states that any theory of quantum gravity in $(d+1)$-dimensional anti-de Sitter space (AdS_{d+1}) is equivalent to a conformal field theory (CFT) in d dimensions. The Ryu-Takayanagi (RT) [85] formula and its covariant generalization, the Hubeny-Rangamani-Takayanagi (HRT) formula [60], posit that the entanglement entropies of holographic CFTs are given in terms of minimal or extremal areas. These have been derived from the basic AdS/CFT dictionary [67, 41]. In general, entanglement entropies of quantum field theories are difficult to compute. It is of great interest to try to determine which types of states are dual to semi-classical AdS bulks. The fact that holographic entanglement entropies are given by minimal areas should therefore enable us to constrain the entanglement structure of holographic states.

It is simple to show that if we have three spatial CFT regions, A, B, C, then the RT formula implies strong subadditivity [58, 57]:

$$S(ABC) + S(B) \leq S(AB) + S(BC).$$

The above inequality is, of course, true for all quantum states [69, 68], though the general proof is technically complicated. In addition, holographic entropies obeying the RT formula obey the constraint of monogamy of mutual information [55, 57]:

$$I(A : BC) \geq I(A : B) + I(A : C).$$

Unlike strong subadditivity, this constraint is not obeyed by all quantum systems. In addition, recent work [12] has shown that holographic entanglement entropies for n regions obey a set of inequalities known as the *holographic entropy cone*, assuming the RT formula holds. Recently, the exact holographic entropy cone for five regions has been obtained [59].

However, it is not known in general if these inequalities are valid for the covariant HRT formula.

Using the maximin formalism of Wall [94], it is possible to show that (assuming the null-energy condition holds in the bulk), strong subadditivity and monogamy of mutual information hold for the HRT formula. However, the validity of the inequalities for the entropy cone for the HRT formula for five or more regions remains unknown. Indeed, [84] showed that the set of five-region inequalities provable with the maximin formalism is less strong than the entropy cone inequalities.

Understanding the validity of the entropy cone inequalities in the dynamical, HRT case is thus an important step towards understanding the structure of holographic states. In this chapter, we will numerically calculate the entanglement entropies for an AdS_3-Vaidya spacetime, and examine the validity of the five-region entropy cone inequalities, using the HRT formula. This is a very simple setting to test these inequalities, since the HRT surfaces will be geodesics (not higher-dimensional surfaces), and the AdS_3-Vaidya solution is a very simple dynamical spacetime.

We find that the inequalities are all valid, in the cases we examined, as long as the bulk obeys the null energy condition. If the bulk violates the null energy condition, then all the inequalities are violated. This is analogous to the situation for strong subadditivity, which requires the NEC to hold in the bulk. We believe that this provides strong evidence for the validity of the five-region inequalities when the bulk is dynamical. Moreover, the shape of the curves resemble those of the strong subadditivity curves. This may hint that there is a reformulation of the HRT prescription for which both strong subadditivity and the five-region inequalities are valid. Indeed, this has already been done in certain limits for the positive-energy spacetime we considered here [10].

Understanding the validity of these inequalities in general, as well as further study of the entanglement of holographic states, will be very important in furthering our understanding of quantum gravity.

Our results build on previous work on the validity of the five-region inequalities for dynamical bulks. [47, 46] numerically verified the inequalities for a holographic model of two 1+1 dimensional heat baths joined at $t = 0$. It has also been shown that they are valid for large, late-time CFT regions in collapsing black hole spacetimes [10]. Shortly after the posting of the paper [28] (upon which this chapter is based), a related paper [37] appeared, with very interesting results. They showed that the five-region inequalities are valid for the HRT formula in the context of AdS_3/CFT_2. Our work provides strong evidence for the validity of the conclusions of [37] by providing explicit numerical calculations. We also provide a detailed analysis of HRT surfaces in AdS_3-Vaidya spacetimes that should be useful in other contexts. The results presented here are closely analogous to [31, 4, 83], which numerically studied the validity of strong subadditivity and monogamy of mutual information for AdS_3-Vaidya spacetimes. Similar computations have been done in the context of the quantum null energy condition [44].

2.2 Setup

Consider a holographic CFT with a Cauchy slice Σ of a static bulk, at a moment of time reflection symmetry. Let A be a boundary subregion. The Ryu-Takayanagi formula posits that

$$S(A) = \frac{\min_m \text{Area}}{4G_N},$$

where m is a codimension-2 surface in the bulk (with $\partial m = \partial A$) homologous to A. That is, there is a bulk region χ such that $\partial\chi = A \cup m$. The Hubeny-Rangamani-Takayanagi formula is the covariant generalization of this equation. If A is some spacelike CFT subregion, then the HRT formula says that

$$S(A) = \frac{\min_{\text{extremal } m} \text{Area}}{4G_N},$$

where extremal m means that m is a co-dimension 2 spacelike surface that extremizes the area and has $\partial m = \partial A$ and is homologous to A.

We will consider the planar AdS_3-Vaidya spacetime, with metric

$$ds^2 = -(r^2 - m(v))dv^2 + 2drdv + r^2dx^2.$$

The null-energy condition (i.e., $T_{\mu\nu}k^\mu k^\nu \geq 0$ for all lightlike k) is satisfied if and only if dm/dv is positive.

We can re-write this metric in more standard coordinates, t and r, with

$$v = t + g(r), g'(r) = \frac{1}{f}$$

$$\implies dv = dt + g'(r)dr = dt + \frac{dr}{f},$$

which means

$$\begin{aligned} ds^2 &= -f(dt^2 + \frac{dr^2}{f^2} + 2\frac{dtdr}{f}) + 2drdt + 2\frac{dr^2}{f} + r^2dx^2 \\ &= -fdt^2 + \frac{dr^2}{f} + r^2dx^2. \end{aligned} \tag{2.1}$$

We will consider a thin-shell limit,

$$m(v) = \pm m\Theta(v),$$

which represents a shell of infalling null matter. The plus sign satisfies the null energy condition and corresponds to positive energy matter–inside the shell, the metric is pure AdS_3, outside the shell, the metric corresponds to a black hole, i.e., the BTZ metric. The minus sign violates the null energy condition; this choice represents a shell of negative-energy

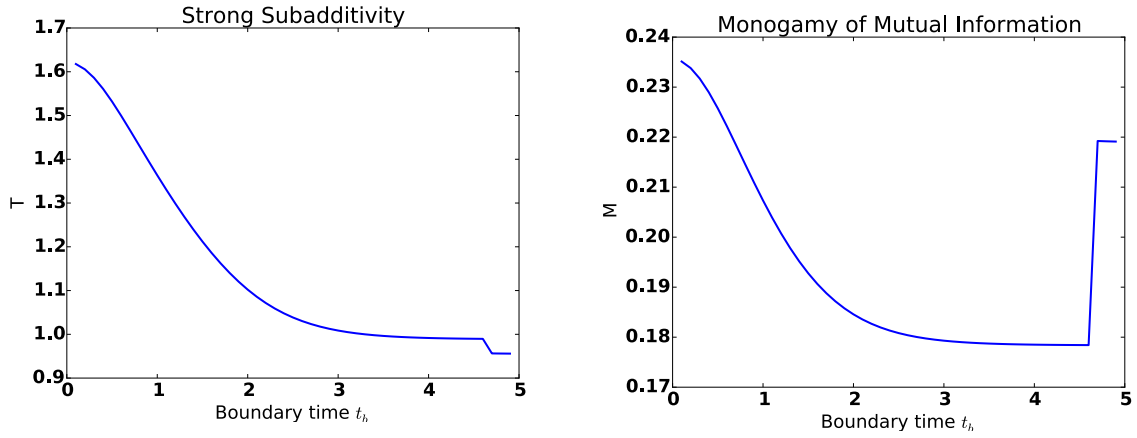

Figure 2.1: The quantities T (left) and M (right) plotted vs t_b. We see that $T > 0$ and $M > 0$ so strong subadditivity and monogamy of mutual information are always satisfied. The jumps at late times are due to numerical errors.

null matter so that outside the matter, the metric is pure AdS, while inside it is BTZ. We will consider both cases, starting with the positive-energy metric. For simplicity, we will set $m = 1$.

For AdS, we have $f = r^2$ so that

$$g' = -\frac{1}{r} \implies v = t - \frac{1}{r}.$$

Meanwhile for BTZ, we have $g = r^2 - 1$, which gives

$$g' = -\frac{1}{r^2 - 1} \implies g = -\tanh^{-1}\frac{1}{r} \implies v = t - \tanh^{-1}\frac{1}{r}.$$

Our discussion of geodesic kinematics largely follows that of [31].

2.3 Positive Energy Vaidya Metric

We wish to obtain enanglement entropies in the CFT dual to the Vaidya metric. The HRT prescription tells us that we need to calculate the areas of the extremal codimension 2 surfaces that are anchored at the boundary of the CFT subregion. In our case, this corresponds to spacelike geodesics. We discuss the geodesic kinematics in the Appendix A.1.

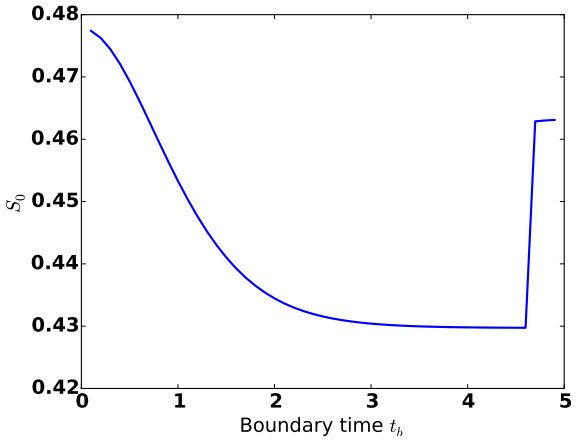

Figure 2.2: The quantity S_0 plotted vs t_b. We see that $S_0 > 0$ so the corresponding inequality is always satisfied. The jump at late times is due to numerical errors.

Constant-Time Intervals

We begin by testing strong subadditivity. We consider adjacent three regions A, B, C, all at constant time t_b. We choose $\ell_A = 2, \ell_B = 4, \ell_C = 2$. We then consider the quantity

$$T(A, B, C) \equiv 4G_N[S(AB) + S(BC) - S(ABC) - S(B)]$$

as a function of the boundary time t_b. Strong subadditivity will be satisfied if and only if $T \geq 0$. $S(AB)$ is given by the length of a geodesic with $\ell_x = 6$ over $4G_N$. $S(BC)$ is identical. ABC is an interval of length 8, while B is an interval of length 4. Using this information, we can plot T as a function of t_b. This is done in Figure 2.1. We see that $T > 0$, so strong subadditivity is always satisfied.

We do the same calculation for monogamy of mutual information. Define

$$\begin{aligned} M &\equiv 4G_N[I(A:BC) - I(A:B) - I(A:C)] \\ &= 4G_N[S(A) + S(BC) - S(ABC) - S(A) - S(B) \\ &+ S(AB) - S(A) - S(C) + S(AC)] \\ &= 4G_N[-S(A) + S(BC) - S(ABC) - S(B) \\ &+ S(AB) - S(C) + S(AC)]. \end{aligned} \tag{2.2}$$

We plot this quantity as a function of t_b in Figure 2.1. Again, since $M > 0$, we see that monogamy of mutual information is always satisfied.

Next, we consider five regions. There are several inequalities that are valid for the RT formula for five regions. These bound the holographic entropy cone. For example, we have that

$$\begin{aligned} &S(A|BC) + S(B|CD) + S(C|DE) + S(D|EA) + S(E|AB) \\ &\geq S(ABCDE) \end{aligned} \tag{2.3}$$

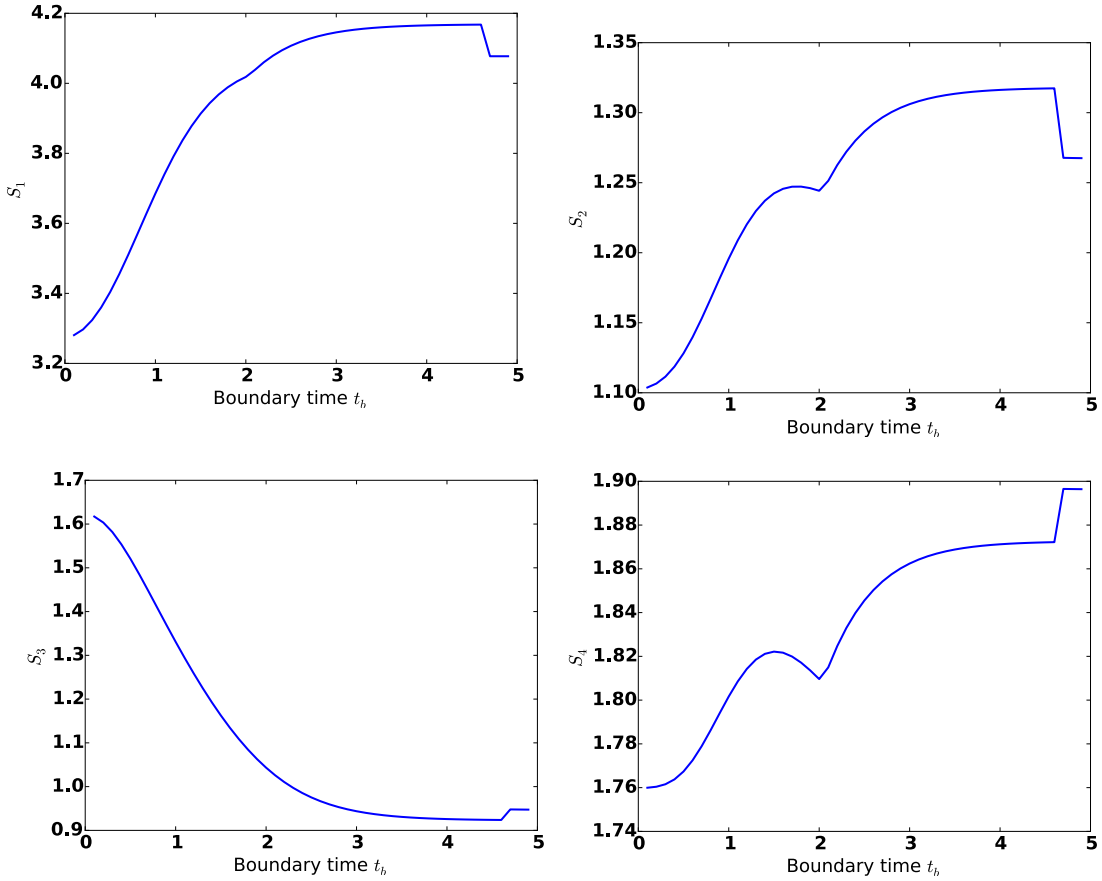

Figure 2.3: The quantities S_i $(i = 1, 2, 3, 4)$ plotted vs t_b. We see that $S_i > 0$ for all i so the corresponding inequalities given in the main text are always satisfied. The jumps at late times are due to numerical errors.

(see [12]). Here $S(X|Y) \equiv S(XY) - S(Y)$ is the conditional entropy. To test this in the non-static case, consider 5 regions A, B, C, D, E, all of which are constant time intervals on the boundary. Take $\ell_A = \ell_C = \ell_E = 2$, $\ell_B = \ell_D = 4$. Then define the quantity

$$\begin{aligned} S_0 \equiv 4G_N[&S(A|BC) + S(B|CD) + S(C|DE) + S(D|EA) \\ &+ S(E|AB) - S(ABCDE)]. \end{aligned} \tag{2.4}$$

We plot this as a function of t_b. See Figure 2.2. We see that $S_0 > 0$ so this inequality is always satisfied in this non-static case.

There are several more inequalities for the holographic five-region case [12]. For example,

$$\begin{aligned} &2S(ABC) + S(ABD) + S(ABE) + \\ &S(ACD) + S(ADE) + S(BCE) + S(BDE) \geq \\ &S(AB) + S(ABCD) + S(ABCE) + S(ABDE) + \\ &S(AC) + S(AD) + S(BC) + S(BE) + S(DE), \end{aligned} \tag{2.5}$$

$$\begin{aligned} &S(ABE) + S(ABC) + S(ABD) + S(ACD) + S(ACE) + \\ &S(ADE) + S(BCE) + S(BDE) + S(CDE) \geq \\ &S(AB) + S(ABCE) + S(ABDE) + S(AC) + \\ &S(ACDE) + S(AD) + S(BCD) + S(BE) + S(CE) + S(DE), \end{aligned} \tag{2.6}$$

$$\begin{aligned} &S(ABC) + S(ABD) + S(ABE) + S(ACD) + S(ACE) + S(BC) + S(DE) \geq \\ &S(AB) + S(ABCD) + S(ABCE) + S(AC) + S(ADE) + S(B) + S(C) + S(D) + S(E), \end{aligned} \tag{2.7}$$

$$\begin{aligned} &3S(ABC) + 3S(ABD) + 3S(ACE) + S(ABE) + S(ACD) \\ &+ S(ADE) + S(BCD) + S(BCE) \\ &+ S(BDE) + S(CDE) \geq 2S(AB) + 2S(ABCD) + 2S(ABCE) \\ &+ 2S(AC) + 2S(BD) + 2S(CE) \\ &+ S(ABDE) + S(ACDE) + S(AD) + S(AE) + S(BC) + S(DE). \end{aligned} \tag{2.8}$$

For each of these inequalities, we define the quantities S_i to be $4G_N$ times the left-hand side minus $4G_N$ times the right-hand side for $i = 1, 2, 3, 4$. Inequality i will be satisfied if and only if S_i is positive. We plot each of these quantities as functions of t_b. See Figure 2.3. We see that for each i, S_i is positive so that the five-region inequalities are all satisfied in this case, even though the spacetime is not static.

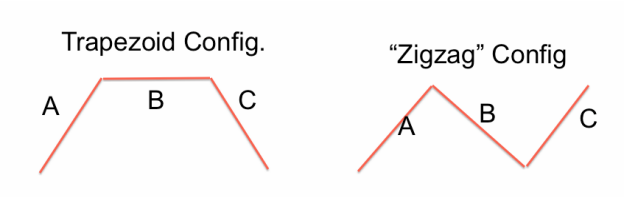

Figure 2.4: The covariant "trapezoid" and "zigzag" configurations. In both cases, each of the components (A, B, and C) have $\Delta x = 1$.

Spacelike Intervals with Nonzero Δt

We now consider the case where the interval is not constant-time. Again, the details of the kinematics are discussed in Appendix A.1.

To find the geodesic length for a given set of parameters, we proceed as follows. If $t_b < 0$, we solve for the AdS geodesic. We then calculate $v(\tau) = t(\tau) - \frac{1}{r(\tau)}$. If v never crosses 0, the geodesic is entirely in the AdS bulk. If it crosses 0, then the geodesic has a portion in the BTZ spacetime. We then numerically find the values of r_c, p_x, E_A that correspond to the given values of $\Delta x, \Delta t, t_b$. We then substitute these results back into our formula for geodesic length. Similarly, if $t_b \geq 0$, we calculate the pure BTZ solution, and see if $v(\tau) = t(\tau) - \tanh^{-1}(\frac{1}{r(\tau)})$ is ever negative, there is a component in the AdS bulk. We numerically find the values of r_1, E_A, p_x that correspond to the values of $\Delta x, \Delta t, t_b$ and use these to find the geodesic length.

Finally, we are ready to test the entropy inequalities for regions that are not purely spacelike. We begin by testing strong sub-additivity. We test two cases, the "trapezoidal" case, and the "zigzag" case; both of these are shown in Figure 2.4. We plot the quantity

$$S(AB) + S(BC) - S(B) - S(ABC)$$

(times $4G_N$) for these regions as a function of the boundary start time of the region A, for a variety of values of $\Delta t/\Delta x$, fixing $\Delta x = 1$. We show the results in Figures 2.5. These curves show that strong sub-additivity is obeyed for these regions.

We now test the five-region inequalities. We use the same labeling scheme for the inequalities as used above, in the constant-time case. We consider the three configurations shown in Figure 2.6. We consider a variety of values of $\Delta t/\Delta x$, again fixing the value of Δx for each component to be 1. We plot these curves as functions of the boundary start time t_b. We do this for the zigzag configuration in Figure 2.7, the configuration with 2 flat components in Figure 2.8, and the configuration with 1 flat component in Figure 2.9 We see that the inequalities are all satisfied, and that the shapes of the curves strongly resemble those of the strong subadditivity.

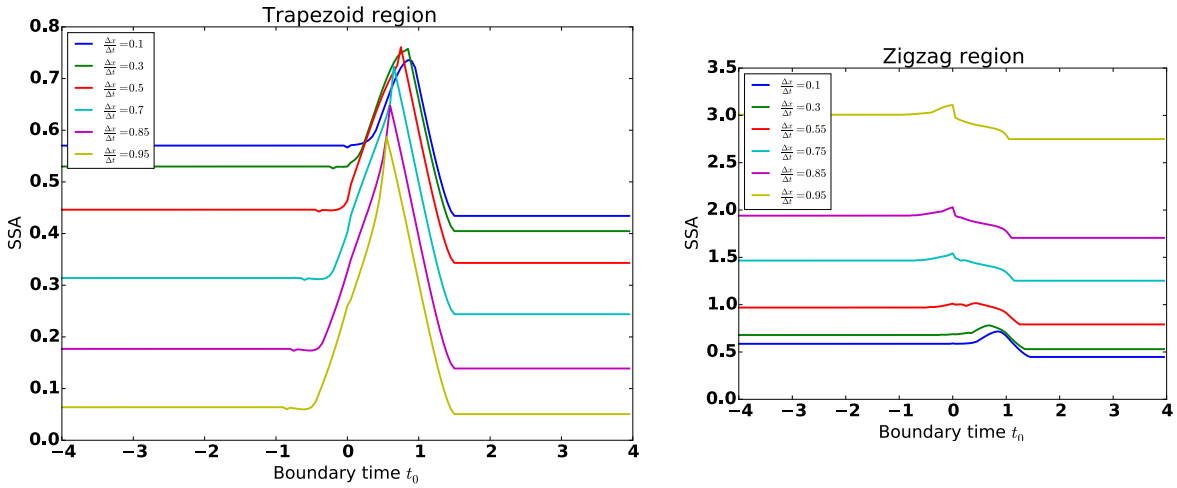

Figure 2.5: Strong subadditivity is verified for the trapezoid and zigzag configurations.

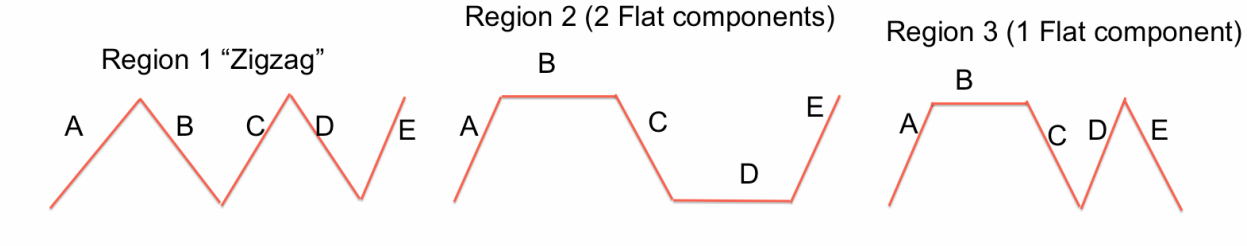

Figure 2.6: The three configurations we consider. Each of the components has its Δx fixed to be 1.

2.4 Negative Energy Vaidya Metric

We now consider the negative-energy Vaidya metric. As discussed above, this violates the null energy condition. We will see that strong subadditivity is violated, as well as the five-body inequalities. The geodesic kinematics are discussed in A.1.

We consider five adjacent constant-time intervals, A, B, C, D, E. A, C, and E have width 2, while B and D have width 4. To start with, we plot strong subadditivity for a couple collections of regions in Figure 2.10. We see that strong subadditivity is violated, which is expected since our metric violates the null energy condition.

Next, we check the five-region inequalities. We use the same numbering scheme as before (with labels 0 through 4), and we plot $4G_N$ times the left hand side minus $4G_N$ times the right hand side of each of the inequalities. We show the results in Figure 2.11. We see that all of the inequalities are violated for this spacetime, roughly in the places where strong

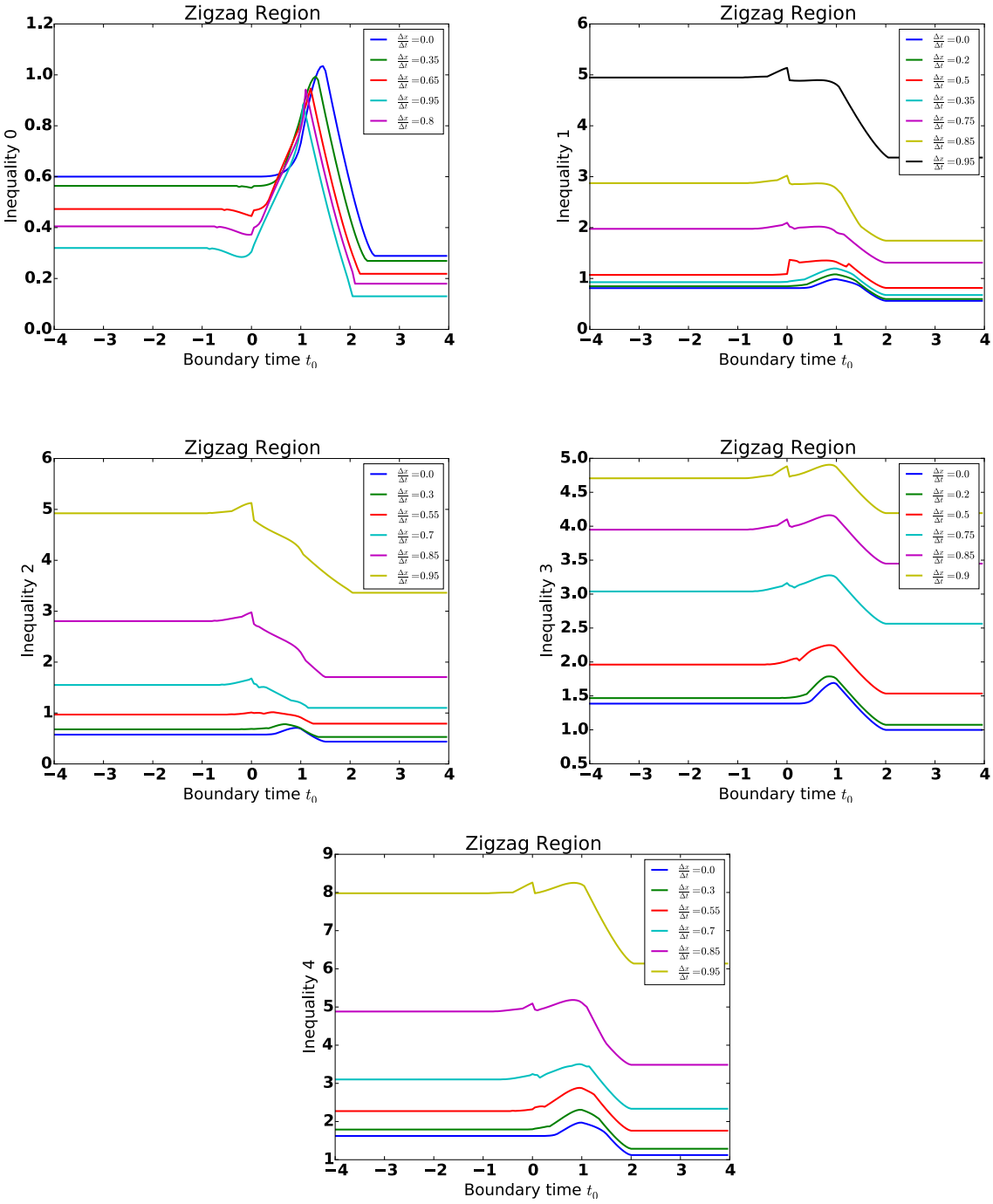

Figure 2.7: The inequalities plotted vs t_b for the zigzag region for a variety of values of $\Delta t/\Delta x$. We see that the inequalities are all satisfied.

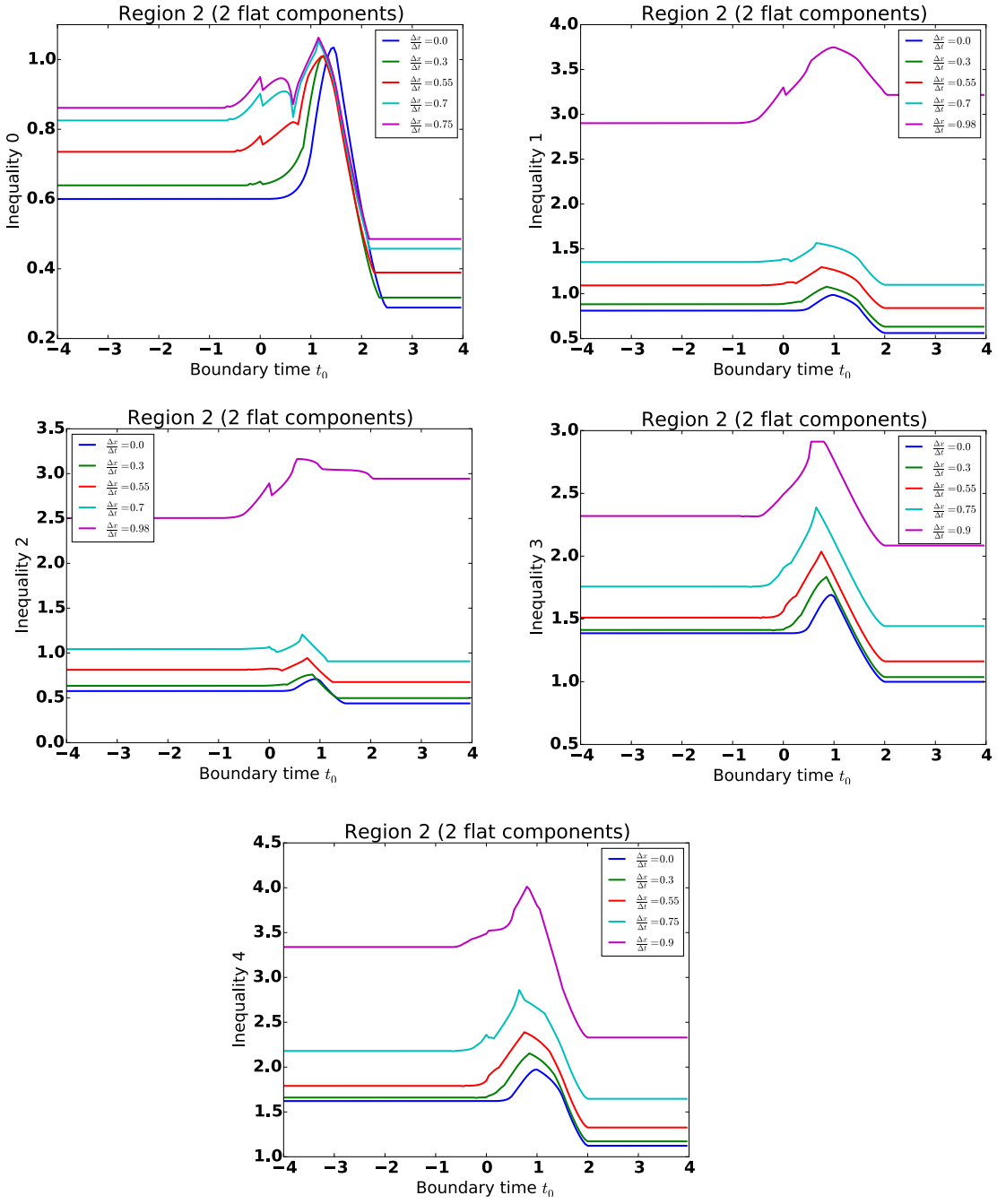

Figure 2.8: The inequalities plotted vs t_b for the Region 2 (with 2 flat components) for a variety of values of $\Delta t/\Delta x$. We see that the inequalities are all satisfied.

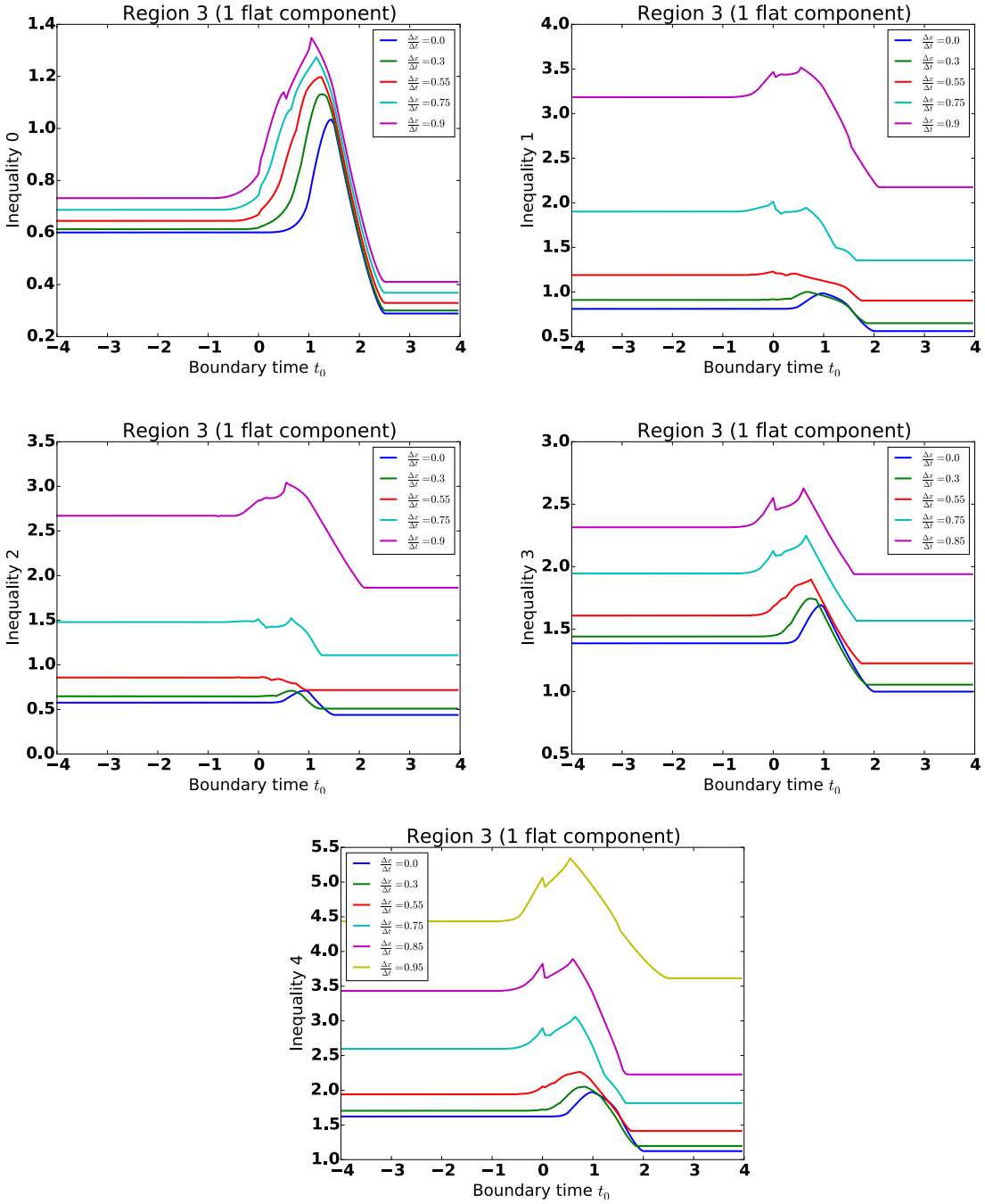

Figure 2.9: The inequalities plotted vs t_b for the Region 3 (with 1 flat component) for a variety of values of $\Delta t/\Delta x$. We see that the inequalities are all satisfied.

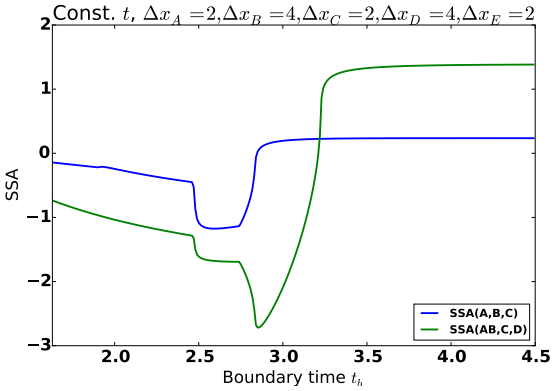

Figure 2.10: Strong subadditivity versus boundary time t_b for the negative-energy Vaidya spacetime. We see that strong subadditivity is violated. Here, we consider strong subadditivity for regions A, B, and C, as well as for AB, C, and D.

subadditivity is violated. Furthermore, we once again see that the curves for the five-region inequalities resemble the strong subadditivity curves.

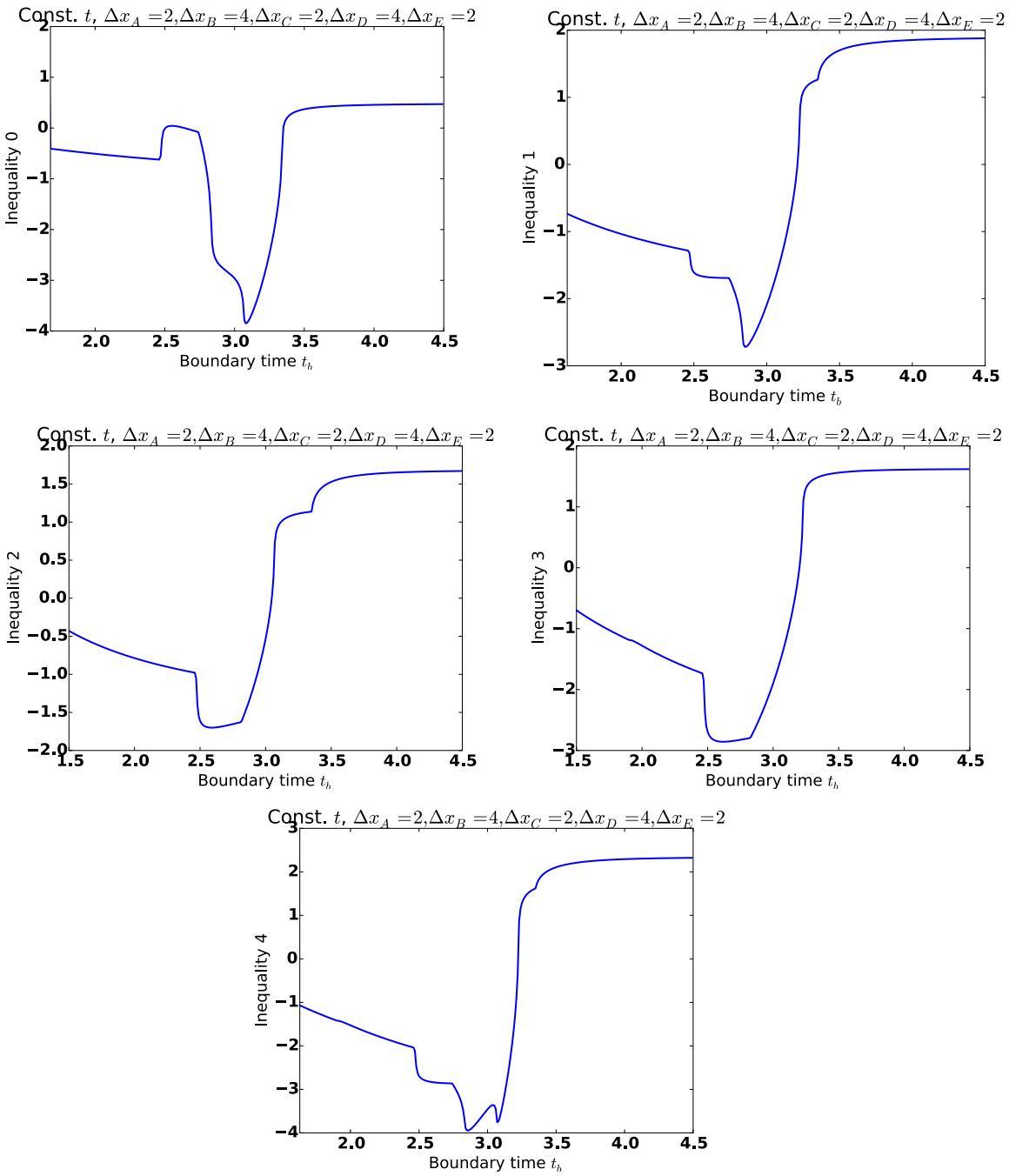

Figure 2.11: The inequalities plotted vs t_b. We see that the inequalities are all violated for this spacetime that violates the null energy condition.

Chapter 3

Holographic Complexity in FRW Spacetimes

3.1 Introduction

Recent work has revealed deep connections between between gravity, spacetime, and information. The AdS/CFT correspondence posits that any theory of quantum gravity in $d+1$-dimensional anti-de Sitter space (AdS) is equivalent to a conformal field theory (CFT) in d dimensions [71, 49, 96]. This correspondence is a concrete realization of the holographic principle, which conjectures that the degrees of freedom in a theory of quantum gravity are encoded in one fewer dimension.

The celebrated Ryu-Takayanagi formula [85] (and its covariant generalization, the Hubeny-Rangamani-Takayanagi formula [60]) of the AdS/CFT correspondence posits an equivalence between entanglement entropy in a holographic CFT and minimal surfaces in the bulk. This has led to an improved understanding of the rich interplay between the spacetime in the bulk theory, and information in the boundary theory.

There has been much recent speculation about the possible role of complexity in the AdS/CFT correspondence. This arises from the following consideration. If we consider the maximum volume slice anchored at boundary time t, of an AdS black hole, the volume will grow linearly with t. Moreover, it will (classically) grow forever. However, the entanglement entropy saturates after a relatively short time. Thus, there must be some CFT quantity that encodes this growth. Even after the saturation of the entanglement entropy, the quantum state continues to evolve subtly in time, and the entanglement entropy is too crude of a measure to detect these changes. A promising candidate for the CFT dual of the volume growth is the *complexity*. Consider some state $|\psi\rangle$ in a Hilbert space $\mathcal{H}$, and some "simple" reference state $|\psi_0\rangle \in \mathcal{H}$. For example, in a system of n qubits, the state $|\psi_0\rangle$ could be the unentangled state $|00\cdots0\rangle$. Then the complexity $\mathcal{C}(|\psi\rangle)$ is defined as the minimum number of simple gates (meaning they act on some $O(1)$ number of degrees of freedom) needed to take $|\psi_0\rangle$ to $|\psi\rangle$. The exact value of the complexity is, of course, dependent on details such as

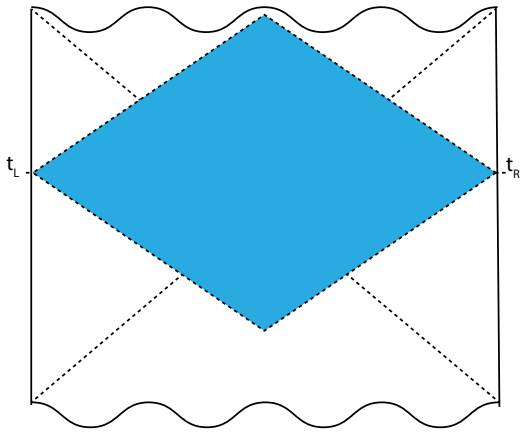

Figure 3.1: The Wheeler-de Witt patch of a two-sided AdS black hole. It is defined as the bulk domain of dependence for a slice between t_L and t_R, shaded in light blue

what gates are allowed, what the tolerance is, and so on. However, the qualitative behavior does not depend on these details: the complexity, in general, grows linearly with time for a large amount of time after the entanglement entropy saturates.

This line of reasoning led to the complexity-volume conjecture, which says that the CFT quantity dual to the maximum-volume slice is the complexity of the CFT state. Issues related to various ad-hoc factors in the complexity-volume conjecture led to the complexity action conjecture. Consider a AdS two-sided black hole. Then the complexity-action conjecture posits that the complexity of the state CFT state $|\psi(t_L, t_R)\rangle$ is given by [25]

$$\mathcal{C} = \frac{\mathcal{I}_{WdW}}{\pi\hbar},$$

where $\mathcal{I}_{WdW}$ is the action on the Wheeler-de Witt patch, which is defined as the bulk domain of dependence of any spacelike surface between t_L on the left boundary and t_R on the right boundary. See Figure 3.1. The authors of [25] argued that is natural for the complexity to be normalized so that the constant of proportionality is $\frac{1}{\pi\hbar}$. In this way, when one fixes the normalization for one particular black hole, it is such that all other black holes saturate the upper limit on the rate of computation.

However, cosmological observations indicate that our Universe is not AdS (which requires $\Lambda < 0$), but in fact has $\Lambda > 0$. However, it is believed that holography holds in more general spacetimes than AdS space [17, 16]. A considerable amount of recent work has been done in trying to understand the structure of holography in general spacetimes. It

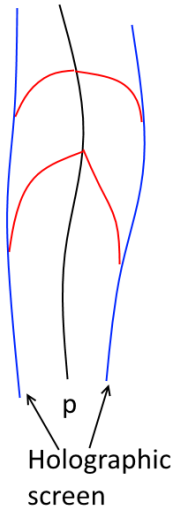

Figure 3.2: The construction of a holographic screen. At a point τ on the line $p(\tau)$, we follow the past null geodesics until they have zero expansion. Continuing in this way for the entire curve p, we have a codimension-1 surface that is foliated by leaves $\sigma(t)$.

is believed that the details of the holographic theory are encoded on a *holographic screen*, which is a codimension-1 surface foliated by marginally trapped (or marginally anti-trapped) codimension-2 surfaces known as *leaves*. (Recall that a codimension-2 surface will have two orthogonal null congruences, labelled by k and ℓ. The surface is called *marginal* if one of the expansions, say θ_k, vanishes. It is called *marginally trapped* if $\theta_\ell < 0$, and *marginally anti-trapped* if $\theta_\ell > 0$.) Recently, it was shown that holographic screens obey an area law [18, 19, 20].

The proposal of [86, 79] is that, in general spacetimes, the holographic description of this gravity theory in the bulk lives on this holographic screen. In particular, [86] propose an analogy with the Ryu-Takayanagi formula for gravity in AdS spacetime. Specifically, if $\sigma(t)$ is a leaf of the holographic screen and $\Gamma \subset \sigma(t)$ is a subset of the leaf, then the entanglement entropy of the Γ is given by

$$S(\Gamma) = \frac{\text{Area}(E_\Gamma)}{4G_N},$$

where E_Γ is the extremal-area codimension-2 surface that is anchored on Γ: $\partial E_\Gamma = \partial\Gamma$.

It is shown in [86] that entropies in the putative holographic dual theory to an FRW spacetime obey the basic consistency checks that would expected. In particular, they satisfy a maximin-like formulation, and therefore obey strong subadditivity. Given these successes in lifting the holographic entanglement entropy conjectures to non-AdS spaces, it is natural to investigate the consequences of the holographic complexity conjectures in non-AdS spacetimes.

The purpose of this chapter is to examine the holographic complexity conjectures to

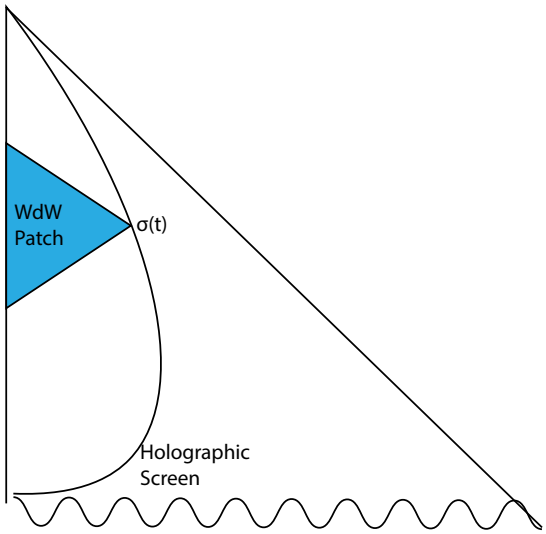

Figure 3.3: The Wheeler-de Witt patch for a general spacetime. It is the domain of dependence of a slice that is interior to a leaf $\sigma(t)$ of the holographic screen, shaded in light blue.

more general spacetimes, in the same spirit as the hologaphic entropy conjecture for the holographic screens. Specifically, we study the same quantity (the action of the Wheeler-de Witt patch over $\pi\hbar$), but modify the WdW patch so that it is the domain of dependence of the interior of the leaf $\sigma(t)$. See Figure 3.3. We also examine the behavior of maximal-volume slices. We begin by reviewing the construction of the holographic screens.

3.2 Holographic Screens

We recall the construction of holographic screens. First, we pick some timelike path $p(\tau)$ through the spacetime. At each τ, we fire a congruence of null geodesics in the past direction from $p(\tau)$. When the expansion parameter θ on this congruence reaches 0, at some point in the past, this will be the location of the leaf of the holographic screen. By doing this for all values of τ, we construct a codimension-one surface that is foliated by "leaves" that have one expansion parameter vanishing. See Figure 3.2. In the case of AdS space, as we show below, this reduces to the conformal boundary.

AdS Space

First, we analyze AdS spacetimes. Consider, for example, AdS_3 in global coordinates, with the AdS scale set to 1. The metric is given by

$$ds^2 = -(1+r^2)dt^2 + \frac{dr^2}{1+r^2} + r^2 d\phi^2.$$

In these coordinates, r ranges from 0 to ∞, with the conformal boundary located at $r = \infty$. We choose our timelike path to simply be the line $r = 0$. We now consider radial geodesics fired into the past from $r = 0$. Because ∂_t is a Killing vector, the quantity

$$E = g_{tt}k^t = -(1+r^2)(k^t)$$

is conserved, and $E > 0$ since the geodesics are past-directed. (We have defined $k^\alpha \equiv \frac{dx^\alpha}{d\lambda}$.) Because the geodesic is null, we must have that

$$-(1+r^2)(k^t)^2 + \frac{(k^r)^2}{1+r^2} = 0$$

so that

$$k^t = \frac{E}{1+r^2},\ k^r = E.$$

One can readily verify that $k^\alpha \nabla_\alpha k_\beta = 0$ so this does indeed satisfy the geodesic equations. We compute the expansion parameter to find

$$\theta = g^{\alpha\beta}\nabla_\alpha k_\beta = \frac{E}{r}.$$

Therefore, we see that the expansion θ of this null congruence goes to 0 only at the boundary, $r \to \infty$. The holographic screen for AdS spacetime is the conformal boundary. Moreover, it is clear that the holographic screen for AdS will always be the conformal boundary, regardless of our choice for our timelike path $p(\tau)$ through the spacetime.

FRW Cosmologies

Next, we examine FRW cosmologies. The metric for this is given by

$$ds^2 = -dt^2 + a^2(t)\left(\frac{dr^2}{1-kr^2} + r^2 d\Omega_2\right),$$

where $a(t)$ is the scale factor. $k = 0$ for a flat Universe, $+1$ for a closed Universe, and -1 for an open Universe. The equations governing the evolution of a are the Friedmann equations

$$\frac{\dot{a}^2}{a^2} + \frac{k}{a^2} = \frac{8\pi\rho}{3},$$

$$\dot{\rho} = -3\frac{\dot{a}}{a}(\rho + P).$$

We now find the holographic screen for the FRW metric. Again, we pick our path $p(\tau)$ through the spacetime to be the line $r = 0$. We now study past directed null geodesics. The geodesic equation

$$\frac{dk^t}{d\lambda} + \Gamma^{\alpha}_{\beta\gamma} k^{\beta} k^{\gamma} = 0,$$

(where λ is an affine parameter) gives

$$\frac{dk^t}{d\lambda} + \frac{a\dot{a}}{1 - kr^2}(k^r)^2 = 0.$$

Meanwhile, the geodesic is null so that $k^{\alpha} k_{\alpha} = 0$ or

$$(k^r)^2 = \frac{1 - kr^2}{a^2}(k^t)^2$$

so that

$$\frac{dk^t}{d\lambda} + \frac{\dot{a}}{a}(k^t)^2 = 0.$$

This equation is solved by $k^t = -\frac{\text{const}}{a}$. We calculate the expansion of this congruence of null geodesics. The result is

$$\theta = g^{\alpha\beta} \nabla_{\alpha} k_{\beta} = \frac{2\text{const}(\sqrt{1 - kr^2} - r\dot{a})}{ra^2}.$$

The holographic screen will be at time t and at the radius when $\theta = 0$, which is given by

$$r = \frac{1}{\sqrt{\dot{a}(t)^2 + k}}.$$

3.3 Complexity-Action Conjecture in FRW Spacetimes

We begin by computing the complexity given by the complexity-action conjecture [25]. The contributions wil be the bulk Einstein-Hilbert term, a GHY term for spacelike boundaries, which we consider first. In section 3.3 below, we consider the null boundary terms and the corner terms.

We will consider a flat ($k = 0$) Universe with one component that has the equation of state

$$P = w\rho.$$

Then the scale factor behaves as (from the Friedmann equations)

$$a(t) = ct^{\frac{2}{3(1+w)}}.$$

The r-coordinate of the holographic screen, at time t_b is given by

$$r = \frac{3(1+w)}{2} \frac{1}{ct_b^{\frac{-1-3w}{3(1+w)}}}.$$

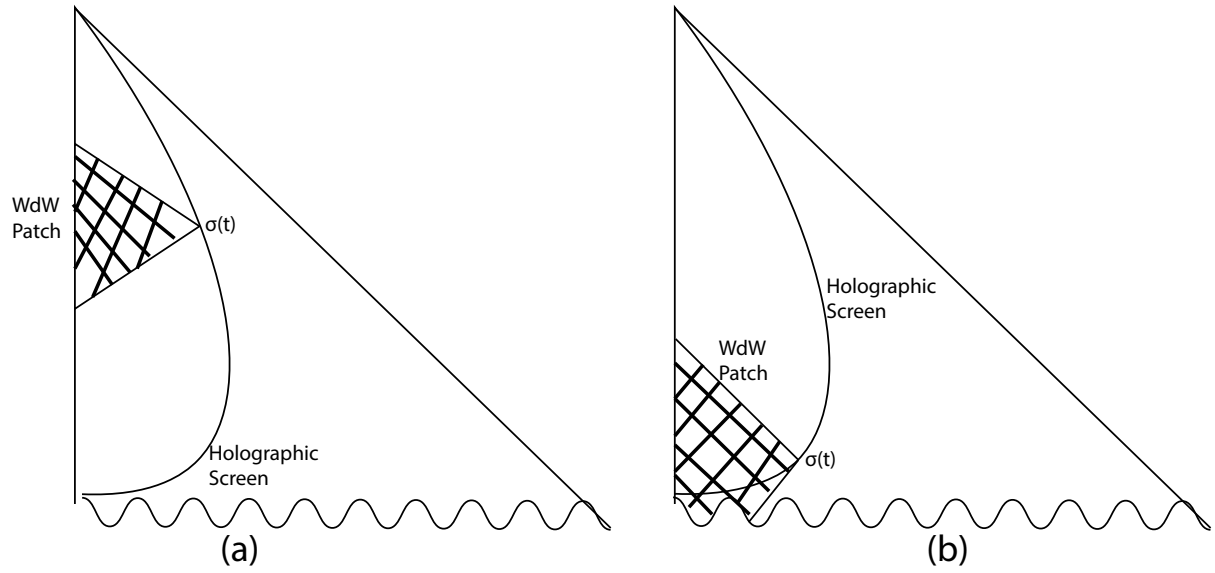

Figure 3.4: The Wheeler-de Witt patch for a FRW spacetimes. In some cases, (a) the WdW patch does not touch the Big Bang singularity. In others, (b), it touches the singularity and there will be a GHY boundary term associated to this boundary of the WdW patch in the singularity.

We define the scaled coordinates

$$\rho = \frac{2}{3(1+w)} c t_b^{\frac{-1-3w}{3(1+w)}} r,$$

$$\eta = \frac{2}{3(1+w)} \left(\left(\frac{t}{t_b} \right)^{\frac{1+3w}{3(1+w)}} - 1 \right).$$

The metric then becomes

$$\begin{aligned} ds^2 = & \frac{9(1+w)^2 t_b^2}{4} \left(\frac{1+3w}{2} \eta + 1 \right)^{\frac{4}{1+3w}} \\ & \cdot [-d\eta^2 + d\rho^2 + \rho^2 d\Omega_2^2]. \end{aligned} \tag{3.1}$$

The leaf of the holographic screen is at $\eta = 0$, $\rho = 1$. We first consider the upper half of the WdW patch, the part with $\eta \geq 0$.

Inward, future-directed geodesics from the leaf satisfy $\rho = 1 - \eta$. The inward, past-directed geodesics from the leaf have $\rho = 1 + \eta$. Under certain conditions, these geodesics will intersect the big bang singularity, $t = 0$. We do this by linearly extrapolating back to

find the value of ρ at $t = 0$. If $\rho > 0$ at this point, it will intersect the singularity. If $\rho < 0$, the WdW patch terminates at some strictly positive value of t. See Figure 3.4. When $t = 0$,

$$\eta = -\frac{2}{3(1+w)}$$

so that

$$\rho = 1 + \eta = 1 - \frac{2}{3(1+w)} = \frac{1+3w}{3(1+w)}.$$

Thus, if $w < -1/3$, the WdW patch does not intersect the singularity, while if $w > -1/3$ it does.

We first consider the upper half of the WdW patch, the part with $\eta \geq 0$. The bulk contribution to the gravitational action from this region is given by

$$\mathcal{I}_{up} = \frac{1}{16\pi G_N} \int_0^1 d\eta \int_0^{1-\eta} d\rho \sqrt{-g} R \int d\Omega_2,$$

where R is the Ricci scalar. Using Mathematica, we find that

$$\begin{aligned} &R = \\ &9(\rho^2 t^2 (w+1)^2)^{-1} 2^{\frac{8}{3w+1}-1} (\eta + 3\eta w + 2)^{-\frac{8}{3w+1}} \\ &\cdot \left(1 - 16^{\frac{1}{-3w-1}} (\eta + 3\eta w + 2)^{\frac{4}{3w+1}-2} \left((\eta + 3\eta w + 2)^2 + 4\rho^2(6w-5)\right)\right). \end{aligned} \tag{3.2}$$

We then perform the integration to obtain

$$\begin{aligned} \mathcal{I}_{up} = \frac{t^2}{4G_N} 2^{-\frac{6}{3w+1}-2} 3^{\frac{2}{3w+1}-1} (w+1)^{\frac{2}{3w+1}} [(3w-5)(3w+2)(3w+4)(3w+7)]^{-1} \\ \cdot (2^{\frac{6}{3w+1}+3} \left(-162w^4 - 675w^3 - 531w^2 + 513w + 515\right) (3w+3)^{\frac{6w}{3w+1}} + \\ 81(w+1)^3 \left(5(w+1)(3w-1)(3w+2)(3w+3)^{\frac{4}{3w+1}} + 16^{\frac{1}{3w+1}} (3w-5)(3w+4)(3w+7)\right)). \end{aligned} \tag{3.3}$$

We now consider the lower half of the WdW patch. We begin by considering the case where it does not intersect the Big Bang singularity. We fire past-directed light rays from the leaf, which satisfy $\rho = 1 + \eta$, so they will hit $\rho = 0$ when $\eta = -1$. The bulk contribution to the gravitational action for the lower WdW patch is then given by

$$\mathcal{I}_{low} = \frac{1}{16\pi G_N} \int_{-1}^0 d\eta \int_0^{1+\eta} d\rho \sqrt{-g} R \int d\Omega_2.$$

We perform this integral to obtain

$$\mathcal{I}_{low} = \frac{t_b^2}{4G_N}[(3w-5)(3w-1)(3w+2)(3w+4)(3w+7)]^{-1}3\cdot 2^{-\frac{6}{3w+1}-2}(w+1)(8^{\frac{2}{3w+1}+1}(3w-1)$$
$$\cdot\left(3w\left(36w^3+84w^2+w-86\right)-85\right)-16^{\frac{1}{3w+1}}(3w-5)(3w+4)(3w+7)(1-3w)^{\frac{2}{3w+1}+3}+$$
$$5(w+1)(3w+2)(1-3w)^{\frac{6}{3w+1}+4}). \quad (3.4)$$

The total bulk gravity action for the WdW patch is, then, (for $w < -1/3$):

$$\mathcal{I}^{WdW}_{bulk,gravity} = \mathcal{I}_{low} + \mathcal{I}_{up} =$$
$$\frac{t_b^2}{4G_N}[2^{-\frac{6}{3w+1}-2}(\frac{1}{3w+1}(9(8^{\frac{2}{3w+1}+1}(3w-1)\left(3w\left(36w^3+84w^2+w-86\right)-85\right)$$
$$-16^{\frac{1}{3w+1}}(3w-5)(3w+4)(3w+7)(1-3w)^{\frac{2}{3w+1}+3}$$
$$+5(w+1)(3w+2)(1-3w)^{\frac{6}{3w+1}+4})(w+1))$$
$$+9^{\frac{1}{3w+1}}(2^{\frac{6}{3w+1}+3}\left(-162w^4-675w^3-531w^2+513w+515\right)(3w+3)^{\frac{6w}{3w+1}}+$$
$$81(w+1)^3\left(5(w+1)(3w-1)(3w+2)(3w+3)^{\frac{4}{3w+1}}+16^{\frac{1}{3w+1}}(3w-5)(3w+4)(3w+7)\right))$$
$$\cdot(w+1)^{\frac{2}{3w+1}})]$$
$$\cdot[3(3w-5)(3w+2)(3w+4)(3w+7)]^{-1}. \quad (3.5)$$

Next, we consider the case where the WdW patch does intersect the Big Bang singularity, which is the case when $w > -1/3$. As can be seen from Figure 3.4, there will be a Gibbons-Hawking-York boundary term associated to the boundary, where the WdW patch intersects the singularity. The upper bulk WdW patch remains unchanged, while the action associated to the lower WdW patch has to be modified – we need to integrate η from its value at the initial singularity (when $t = 0$) to 0. Thus, we have

$$\mathcal{I}_{low} = \frac{1}{16\pi G_N}\int_{-\frac{2}{3(1+w)}}^{0} d\eta \int_0^{1+\eta} d\rho\sqrt{-g}R\int d\Omega_2.$$

We preform this integral on Mathematica to obtain the total bulk gravity action

$$\mathcal{I}^{WdW}_{bulk,gravity} = \mathcal{I}_{low} + \mathcal{I}_{up} = \frac{t_b^2}{4G_N}\frac{3}{2}\{(\frac{4(w+1)\left(3w\left(36w^3+84w^2+w-86\right)-85\right)}{(3w-5)(3w+2)(3w+4)(3w+7)} - \frac{4^{\frac{1}{3w+1}+1}9^{\frac{1}{-3w-1}}w\left(\frac{1}{w+1}\right)^{\frac{2}{3w+1}}}{3w+2} - \frac{9^{-\frac{3}{3w+1}-1}64^{\frac{1}{3w+1}}(3w-1)(3w(3w(3w(9w(2w+7)+37)-101)-179)-100)\left(\frac{1}{w+1}\right)^{\frac{6}{3w+1}}}{(3w-5)(3w+4)(3w+7)})+ [2^{-\frac{6}{3w+1}-2}3^{\frac{2}{3w+1}-1}(2^{\frac{6}{3w+1}+3}\left(-162w^4-675w^3-531w^2+513w+515\right)(3w+3)^{\frac{6w}{3w+1}}+ 81(w+1)^3 \cdot\left(5(w+1)(3w-1)(3w+2)(3w+3)^{\frac{4}{3w+1}}+16^{\frac{1}{3w+1}}(3w-5)(3w+4)(3w+7)\right))(w+1)^{\frac{2}{3w+1}}] [(3w-5)(3w+2)(3w+4)(3w+7)]^{-1}\}. \tag{3.6}$$

Now, the boundary term is given by

$$\mathcal{I}_{GHY} = \frac{1}{8\pi G_N}\int d^3x\sqrt{h}K,$$

where h is the induced metric on the boundary, while K is the trace of its extrinsic curvature. We consider a $\eta =$ const slice. The normal vector is given by $n_\eta = \sqrt{g_{\eta\eta}}$, all other components 0. We can compute $K_{\mu\nu} = \nabla_\mu n_\nu$ and then take the trace $K = K^\mu_{\ \mu}$. The ρ integral ranges from 0 to $1+\eta$. Evaluating the geometric quantities on Mathematica, we obtain

$$\begin{aligned}\mathcal{I}_{GHY} &= \frac{1}{2G_N}\int_0^{1+\eta} d\rho\rho^2\left[-9t_b^2(w+1)^2(\eta\frac{1+3w}{2}+1)^{\frac{4}{3w+1}-1}\right] \\ &= \frac{-9t_b^2}{2G_N}(w+1)^2(\eta\frac{1+3w}{2}+1)^{\frac{4}{3w+1}-1}\int_0^{1+\eta} d\rho\rho^2 \\ &= \frac{-3t_b^2}{2G_N}(w+1)^2(\eta\frac{1+3w}{2}+1)^{\frac{4}{3w+1}-1}(1+\eta)^3. \end{aligned}\tag{3.7}$$

This is for a surface at η – the term of interest is obtained as we go to the big bang, i.e., by taking the limit $\eta \to \eta_{\text{Big Bang}} = -\frac{2}{3(1+w)}$. Taking this limit, we obtain

$$\mathcal{I}_{GHY} = \frac{-3t_b^2}{2G_N}(w+1)^2(\frac{2-3w}{3+3w})^{\frac{4}{3w+1}-1}(\frac{1+3w}{3+3w})^3.$$

Notice how both the GHY term and the bulk terms are both proportional to t_b^2. This is in contrast to the case of black holes in AdS, where generically, the WdW action is linear

in t. A possible (very schematic) explanation for this is follows. Roughly speaking, in any system we expect that the rate of change of the complexity to be proportional to its entropy [91]:

$$\frac{d\mathcal{C}}{dt} \sim S.$$

In the case of AdS/CFT, the entropy is a constant – as we evolve forward in time in the boundary Hilbert space, we are in a constant time-slice of the CFT. The entropy is roughly the area of a time slice of the boundary (by the holographic principle), and this is of course unchanging. Therefore, we would expect that

$$\mathcal{C}_{AdS} \propto t.$$

However, in the case of FRW spacetimes, as we evolve forward in time, the Hilbert space changes. The dimension of the Hilbert space is roughly given by the area of the leaf. Hence, the complexity at boundary time t should grow as

$$\frac{d\mathcal{C}}{dt} \sim S \sim \frac{\text{Area}[\sigma(t)]}{G_N},$$

where as usual $\sigma(t)$ is a leaf of the holographic screen at time t. Now, one also has

$$\text{Area}[\sigma(t)] \sim \left(\frac{a(t)}{\dot{a}(t)}\right)^2 \sim t^2.$$

Thus, we would expect

$$\frac{d\mathcal{C}}{dt} \sim t^{O(1)},$$

which is what we found from the bulk computation. The relationship between the Hilbert spaces of each of the leaves and gravity theory is not yet established. It is possible that these effects will yield an $O(1)$ exponent for $d\mathcal{C}/dt$.

Null Boundary and Corner Terms

In addition to the bulk Einstein-Hilbert term, and the spacelike boundary GHY term, we also must consider null boundary terms and corner terms. This was first worked out in [66], and we follow their procedure, which we summarize in Appendix A.2.

For a given spacetime region W with a null component N of the boundary ∂W, its boundary and corner terms are given by

$$\mathcal{I}_N = \frac{sgn(N)}{8\pi G_N}\int_N d\lambda d\theta \sqrt{\gamma}\kappa + \frac{sgn(N)}{8\pi G_N}\int_N d\lambda d\theta \sqrt{\gamma}\Theta \log(l_c|\Theta|) + \frac{1}{8\pi G_N}\int_{B_1} d\theta\sqrt{\gamma}a_1 + \frac{1}{8\pi G_N}\int_{B_2} d\theta\sqrt{\gamma}a_2. \quad (3.8)$$

In the above equation, $sgn(N)$ is $+1$ if N is to the future of W, and -1 if it is to the past of W. Also, λ represents a parameterization of the null generators, and the coordinates θ label the different null generators of N. Meanwhile, B_1 and B_2 are the endpoints of the component N. The null geodesics will satisfy the equation

$$k^\mu \nabla_\mu k^\nu = \kappa k^\nu.$$

If λ is an affine parameterization, then κ is of course 0. Θ is the expansion of N, while γ is the transverse metric. Finally, l_c is an undetermined parameter in the counterterm. As we summarize in Appendix A.2, this is independent of the parameterization of the null geodesics.

For our case, we first consider the geodesics to have an affine parameterization, which eliminates the first term. Specifically, we choose our geodesics to be parameterized such that the tangent vectors are

$$k = \left(\frac{1}{a}, -\frac{1}{a^2}, 0, 0\right)$$

for the upper sheet and

$$m = \left(\frac{1}{a}, \frac{1}{a^2}, 0, 0\right)$$

for the lower sheet.

For the second term, we first consider the upper part of the boundary. For an FRW universe with equation of state $P = w\rho$, the scale factor evolves as

$$a = t^b, \ b \equiv \frac{2}{3(1+w)}.$$

The holographic screen is at location t_b, $r = \frac{1}{bt^{b-1}}$. The geodesic that composes the upper portion of the boundary will satisfy

$$r(t) = \frac{1}{bt_b^{b-1}} + \frac{-t^{1-b} + t_b^{1-b}}{1-b}.$$

Meanwhile, the expansion is

$$\Theta = \frac{-2bt^{-b-1}}{r},$$

while the transverse metric is

$$\sqrt{\gamma} = r^2 a(t)^2 d\Omega_2.$$

We can rewrite the integral over λ as an integral over t, integrating from t_b to the point when $r = 0$ along the null geodesic. This occurs when

$$t = t_{max} = \left(t_b^{1-b} + \frac{1-b}{bt_b^{b-1}}\right)^{\frac{1}{1-b}}.$$

The integral gives

$$\mathcal{I}^{up}_{surf} = \frac{1}{8\pi G_N (b-1) b^2} * \\ [2t_b^{-b}(b\left(t_b t^b - b^2 t t_b^b\right)\log\left(\frac{2(b-1)b^2 l_c t_b^b}{t\left(t_b t^b - b t t_b^b\right)}\right) - b^2\left(b^2+1\right) t t_b^b \\ + (b-1)^2 b^2 t t_b^b \, {}_2F_1\left(1, \frac{1}{b-1}; \frac{b}{b-1}; \frac{t_b^{1-b} t^{b-1}}{b}\right) \\ + (b+1) t_b t^b)]_{t=t_b}^{t=t_{max}}. \quad (3.9)$$

We now calculate the surface counterterm for the lower part of the boundary. In this case, the null geodesic is described by

$$r(t) = \frac{1}{b t_b^{b-1}} + \frac{t^{1-b} - t_b^{1-b}}{1-b}.$$

The t integral runs from t_{min}, the value of t when the expression above for $r(t)$ reaches 0, to t_b. We have that

$$t_{min} = \left(t_b^{1-b} - \frac{1-b}{b t_b^{b-1}}\right)^{\frac{1}{1-b}}.$$

$$\mathcal{I}^{low}_{surf} = \frac{-1}{8\pi G_N} \frac{1}{(b-1)b^2} 2t_b^{-b}[b^4 t t_b^b + b\left(b^2 t t_b^b - 2b t_b t^b + t_b t^b\right)\log\left(\frac{2(b-1)b^2 l_c t_b^b}{t\left(b t t_b^b - 2b t_b t^b + t_b t^b\right)}\right) + \\ b^2 t t_b^b - (b-1)^2 b^2 t t_b^b \, {}_2F_1\left(1, \frac{1}{b-1}; \frac{b}{b-1}; \frac{(2b-1) t_b^{1-b} t^{b-1}}{b}\right) - 2b^2 t_b t^b - b t_b t^b + t_b t^b]_{t=t_{min}}^{t=t_b}. \quad (3.10)$$

Meanwhile, we consider the corner terms. They are given by

$$\mathcal{I}_{corner} = \frac{1}{8\pi G_N} \int a dS,$$

where

$$a = \pm \log\left|\frac{k \cdot m}{2}\right|,$$

with k and m being the two normal vectors to the null sheets that join at the corner. The sign is determined is follows. If $W \subset J^+(N)$, and the corner is at the past end of N, or if $W \subset J^-(N)$, and the corner is at the future end of N, then the sign is positive. In all other cases, it is negative. In our case, the sign is negative. We know that

$$k = \left(\frac{1}{a}, -\frac{1}{a^2}, 0, 0\right)$$

for the upper sheet and

$$m = \left(\frac{1}{a}, \frac{1}{a^2}, 0, 0\right)$$

for the lower sheet. Thus, the corner term for the joint between the null sheet fired in towards the future, and the null sheet fired inwards towards the past is:

$$\begin{aligned} \mathcal{I}_{corner} &= -\frac{1}{8\pi G_N} \frac{t_b^{2b}}{b^2 t_b^{2b-2}} \log\left[\frac{1}{2}\left|-\frac{1}{a^2} - \frac{1}{a^2}\right|\right] 4\pi \\ &= -\frac{1}{2G_N}\frac{t_b^2}{b^2}\log\left[\frac{1}{t_b^{2b}}\right] = \frac{1}{G_N}\frac{t_b^2}{b}\log(t_b). \end{aligned} \tag{3.11}$$

Role of the Constant l_c in the Counterterm

We comment briefly on the role of the arbitrary parameter l_c in the counterterm discussed above. It was observed [33] that the CA proposal tells us that the complexity of an AdS_{d+1}-Vaidya geometry has a term

$$\mathcal{C} = \frac{L^{d-1}}{4\pi^2 G_N}\frac{V(\Sigma)}{\delta^{d-1}}\log\left(\frac{(d-1)l_c}{L}\right) + \cdots,$$

where L is the AdS scale, δ is the bulk UV cutoff, and $V(\Sigma)$ is the volume of a boundary Cauchy slice Σ.

Recent work [34, 62] has also investigated the complexity of Gaussian states in free field theories. While these are *a priori* very different from the kinds of field theories expected to have holographic duals (large-N, strongly-coupled field theories), there are some interesting similarities between the complexities of these two systems.

Consider a free scalar field ϕ with its conjugate momentum π. A Gaussian state $|S\rangle$ is one that is annihilated by a certain operator:

$$\left(\sqrt{\frac{\alpha_k}{2}}\phi(k) + i\frac{1}{\sqrt{2\alpha_k}}\pi(k)\right)|S\rangle = 0.$$

The usual ground state corresponds to a Gaussian state with $\alpha_k = \omega_k$ for all k. The reference state, $|R(M)\rangle$, is taken to be a Gaussian state with $\alpha_k = M$ for all k, where M is some fixed scale. The target state is taken to be an approximate ground state, $\left|m^\Lambda\right\rangle$, with $\alpha_k = \omega_k$ if $k < \Lambda$ and $\alpha_k = M$ if $k > \Lambda$, so that Λ serves as a UV cutoff. The complexity in going from the reference state $|R(M)\rangle$ to the target state $\left|m^\Lambda\right\rangle$ is given by

$$\mathcal{C} \sim \mathrm{Vol}\cdot\Lambda^d\left|\log\left(\frac{M}{\Lambda}\right)\right|,$$

where Vol represents the volume of the time-slice of the spacetime where our quantum field theory lives.

Comparing these two results, it seems plausible that the ambiguity in the gravitational action (parameterized by l_c) is related to the ambiguity in choosing the reference state in the quantum field theory calculation (which in this case is parameterized by M). Much less is known about the holographic duals of FRW spacetimes (compared with the AdS case), however, in the dual description of FRW gravitational theories, presumably there exist ambiguities in defining the complexity. It seems reasonable that these ambiguities will again be the analog of the ambiguity parameterized by the parameter l_c in the counterterm of the gravitational action.

3.4 Holographic Screen Complexity in an FRW Spacetime undergoing a Transition

We wish to calculate the holographic screen complexity for a flat FRW Universe undergoing a transition from a state of matter with one equation of state to another. For concreteness, we consider a Universe where the matter is a scalar field ϕ, following section 3.2 of [79]. We consider a scalar field with potential

$$V(\phi) = 1 - e^{-k(\phi-\phi_0)^2} + s(\phi-\phi_0)\tanh(p(\phi-\phi_0)).$$

We consider two values of the parameters: a “steep" potential, with values

$$k = 5000, s = 0.01, p = 20, \phi_0 = 0.045,$$

and a “broad" potential, with values

$$k = 25, s = 0.01, p = 2, \phi_0 = 0.5,$$

as in [79]. The energy density of the scalar field is given by

$$\rho = \frac{1}{2}\dot{\phi}^2 + V(\phi),$$

so that the Friedmann equation is

$$\frac{1}{a}\frac{da}{dt} = \sqrt{\frac{8\pi}{3}}\sqrt{\frac{1}{2}\dot{\phi}^2 + V(\phi)},$$

where an overdot denotes a derivative with respect to t. The equation of motion for ϕ, meanwhile, is

$$\frac{d^2\phi}{dt^2} + 3\frac{\dot{a}}{a}\frac{d\phi}{dt} + V'(\phi) = 0,$$

where a prime denotes a derivative with respect to the scalar field ϕ. Therefore, we have

$$\frac{d^2\phi}{dt^2} + 3\sqrt{\frac{8\pi}{3}}\sqrt{\frac{1}{2}\dot{\phi}^2 + V(\phi)}\frac{d\phi}{dt} + V'(\phi) = 0.$$

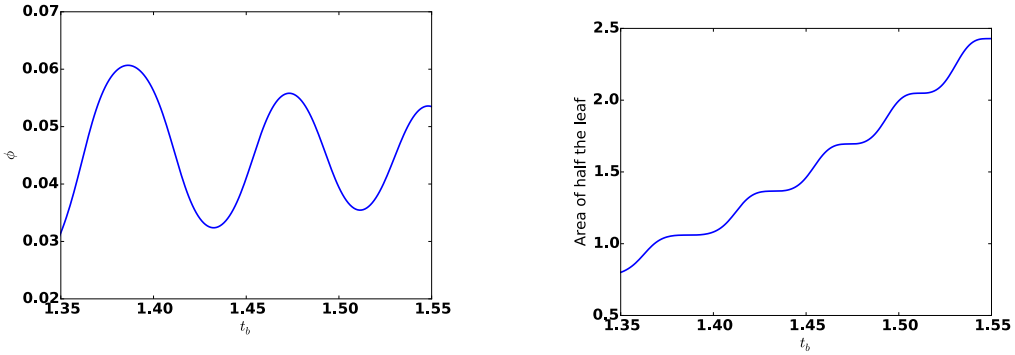

Figure 3.5: Numerical solution of ϕ (left), as well as the area of the half leaf (right), for the steep potential.

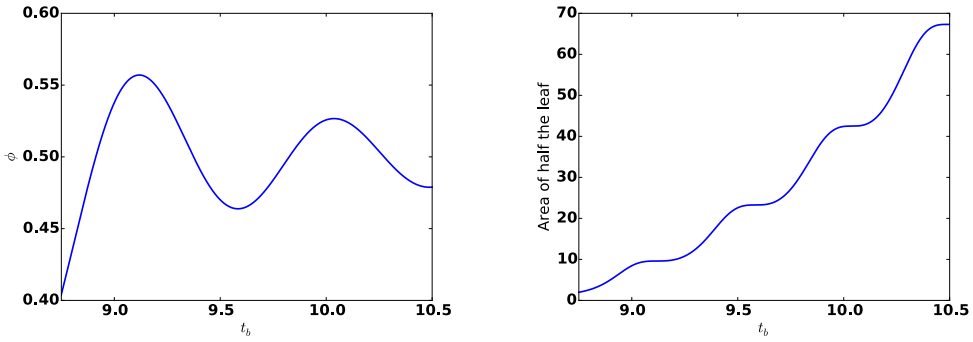

Figure 3.6: Numerical solution of ϕ (left), as well as the area of the half leaf (right), for the broad potential.

We integrate this numerically, together with the Friedmann equation. We plot ϕ as a function of t, as well as the area of half the holographic leaf, in Figure 3.5 for the steep potential and 3.6 for the broad potential. In addition, we also plot the proper area of the leaf of holographic $\sigma(t)$.

The Wheeler-de Witt patch associated to $\sigma(t_b)$ is given by

$$0 \leq r \leq \tilde{r}(t), t_{low} \leq 0 \leq t_{up},$$

where $\tilde{r}(t)$ is given by

$$r_{AH}(t) - \int_{t_b}^{t} \frac{dt'}{a(t')}$$

if $t < t_b$, and

$$r_{AH}(t) + \int_{t_b}^{t} \frac{dt'}{a(t')}$$

if $t > t_b$. t_{low} and t_{up} are, of course, the points where $\tilde{r}(t) = 0$. The Ricci scalar of the flat FRW metric

$$ds^2 = -dt^2 + a^2(t)(dr^2 + r^2 d\Omega_2^2)$$

is given by

$$R = 6\left[\frac{\ddot{a}}{a} + \left(\frac{\dot{a}}{a}\right)^2\right].$$

The gravity action of the WdW patch is given by

$$\begin{aligned}\mathcal{I}_{grav} &= \frac{1}{16\pi}\int_{WdW} d^4x\sqrt{-g}R \\ &= \frac{3}{8\pi}\int d\Omega_2 \int_{t_{low}}^{t_{up}} dt \int_0^{\tilde{r}(t)} drr^2(\ddot{a}a^2 + \dot{a}^2 a) \\ &= \frac{1}{2}\int_{t_{low}}^{t_{up}} dt\tilde{r}(t)^3(\ddot{a}a^2 + \dot{a}^2 a). \end{aligned} \quad (3.12)$$

Meanwhile, the action of the scalar field is given by

$$\begin{aligned}\mathcal{I}_{sc} &= \int_{WdW} d^4x\sqrt{-g}\left(\frac{1}{2}\dot{\phi}^2 - V(\phi)\right) \\ &= \frac{1}{3}\int d\Omega_2 \int_{t_{low}}^{t_{up}} dt\tilde{r}(t)^3\left(\frac{1}{2}\dot{\phi}^2 - V(\phi)\right)\end{aligned} \quad (3.13)$$

so that the total action on the WdW patch is given by

$$\mathcal{I}_{WdW} = \mathcal{I}_{grav} + \mathcal{I}_{sc}.$$

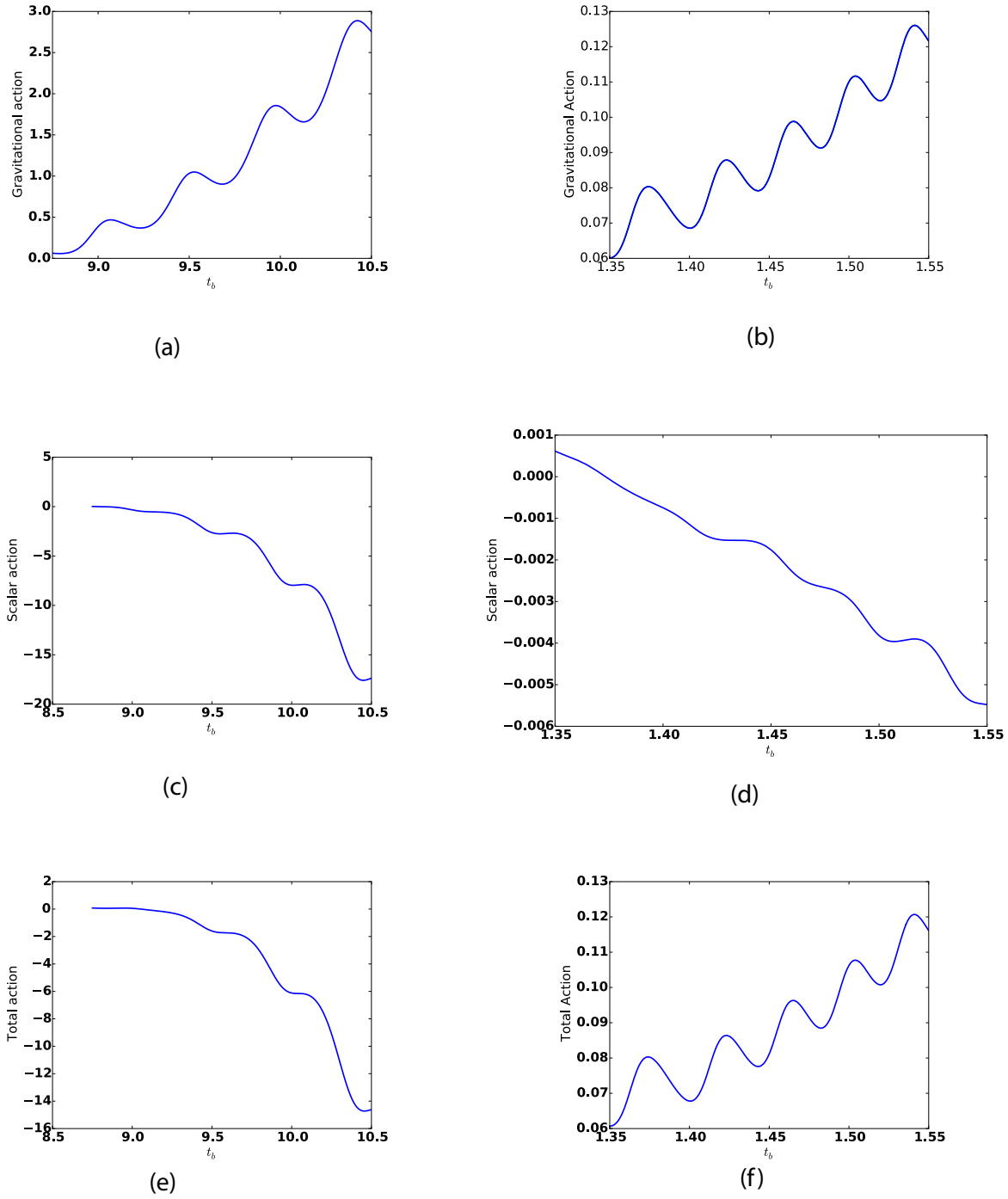

Figure 3.7: WdW actions for the steep and broad potentials. (a) Gravitational WdW action for the steep potential. (b) Gravitational WdW action for the broad potential. (c) Scalar WdW action for the steep potential. (d) Scalar WdW action for the broad potential. (e) Total WdW action for the steep potential. (f) Total WdW action for the broad potential

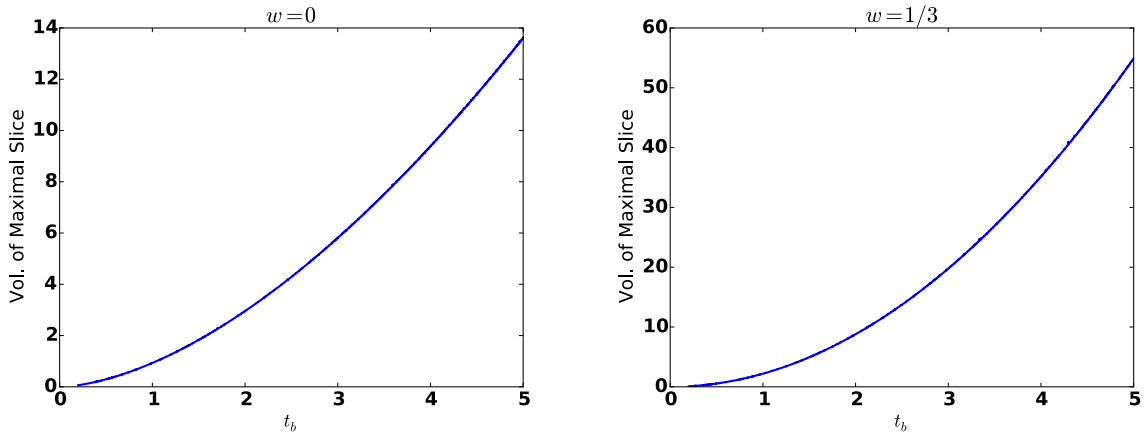

Figure 3.8: Maximal volume vs boundary time for a single-component flat FRW Universe. The a $w = 0$ (matter) universe is on the left, while the $w = 1/3$ (matter) universe is on the right.

We calculate numerically these actions, and plot the results in Figure 3.7. In Figure 10 of [79], the authors find that, when the area of the leaf is flat as a function of t_b, the entanglement entropy decreases very slightly. We see in Figure 3.7 that the gravitational WdW action decreases during exactly these periods of t_b–the complexity decreases when the entanglement entropy decreases. Moreover, the authors of [79] found that the entanglement entropy decreased only very slightly. The decreases in the WdW gravitational action are bigger–they are some $O(1)$ fraction of the increases.

For the “steep" potential, the scalar action is much less than the gravitational action. However, for the broad potential this is not the case. Indeed, the scalar action is negative so that the total action is negative. Hence, the total action in this case appears to be unsuitable as a measure of circuit complexity. Therefore, in this case, the gravitational action (as opposed to the total action) behaves more like a complexity. Furthermore, we shall see below that the gravitational action qualitatively agrees with the expectations from the complexity-volume conjecture. This is in contrast to other settings, such as charged black holes in AdS, which require their total actions (gravitational plus Maxwell) to have similar behavior as complexity. Of course, there are many ways to define complexity in putative holographic duals to gravitational theories (depending on tolerance, gate set, etc.), so perhaps the different actions in the gravity theory correspond to different measures of complexity. Moreover, it is conceivable that the appropriate way to measure complexity in a holographic CFT is very different from the appropriate way to measure it in the holographic dual to FRW gravitational theories. This may explain why two different quantities behave like complexity in the two different settings.

3.5 Complexity-Volume Conjecture for FRW Spacetimes

We wish to analyze the complexity-volume conjecture. In the AdS/CFT context, this states that if a CFT state $|\psi\rangle$ at time t is dual to some bulk geometry, then the complexity of $|\psi\rangle$ is given by the volume of the maximum-volume slice that is anchored at boundary time t [89]:

$$\mathcal{C}(|\psi\rangle) \sim \max V.$$

We examine the generalization of this conjecture to the FRW context by calculating the maximum volume slice inside of the holographic screen. We do this for an FRW universe dominated by one component, as well as one undergoing a transition.

Flat One-Component Universe

In this case, we have one dominant matter component with equation of state

$$P = w\rho.$$

The Friedmann equation gives

$$a \propto t^{\frac{2}{3(1+w)}}.$$

The holographic screen, at time t will be located at

$$r = \frac{1}{\dot{a}(t)}.$$

We need to find the maximum-volume slice inside of (t, r). This will be spherically-symmetric, and will have coordinates $r(\lambda), t(\lambda)$. The volume will be given by

$$\text{Volume} = \int d\Omega_2 \int d\lambda r^2 \sqrt{-a(t)^2 \left(\frac{dt}{d\lambda}\right)^2 + \left(\frac{dr}{d\lambda}\right)^2}.$$

Therefore, we need to extremize the functional

$$I[t(\lambda), r(\lambda)] = \int d\lambda \sqrt{-r^4 a(t)^2 \left(\frac{dt}{d\lambda}\right)^2 + a(t)^2 \left(\frac{dr}{d\lambda}\right)^2},$$

subject to the initial conditions $r(0) = r$, $t(0) = t$. This is done by solving the equations

$$\frac{dr^2}{d\lambda^2} + \frac{2}{r}\left(\frac{dr}{d\lambda}\right)^2 + \frac{2}{ra(t)^2}\left(\frac{dt}{d\lambda}\right)^2 + 2\frac{\dot{a}(t)}{a(t)}\frac{dr}{d\lambda}\frac{dt}{d\lambda} = 0,$$

$$\frac{dt^2}{d\lambda^2} + a(t)\dot{a}(t)\left(\frac{dr}{d\lambda}\right)^2 + \frac{4}{r}\frac{dr}{d\lambda}\frac{dt}{d\lambda} = 0.$$

We solve these equations numerically, and calculate the volumes of maximal slices for points on the holographic screen. We do this for matter (with $w = 0$) and for radiation ($w = 1/3$). The results are shown in Figure 3.8.

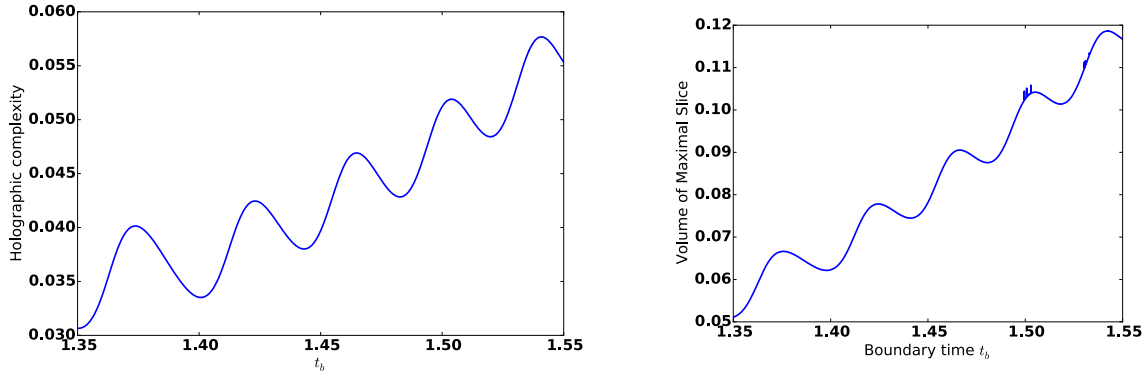

Figure 3.9: Holographic complexity for the steep potentials. The action for the WdW patch for the steep potential is on the left, while the maximum volume slice is shown on the right.

FRW Universe Undergoing a Transition

We now consider the flat FRW universe that undergoes a transition, sourced by a scalar field. We previously saw that the bulk gravitational action of the WdW patch increases when the entanglement entropy increases, and decreases when the entanglement entropy decreases. We numerically solve for the scale factor for the previously-considered "steep" potential, and then solve for the maximal slices. We show the results for the CV conjecture (as well as the results for the CA conjecture for comparison) in Figure 3.9. We see that the behavior is qualitatively very similar. The maximal volume increases and decreases essentially in the same time periods that the action of the WdW patch increases and decreases.

3.6 The de Sitter Limit

In this section, we analyze the de Sitter limit, which corresponds to $w \to -1$. de Sitter space has natural thermodynamic variables associated to it, so it is interesting to see how this limit behaves with respect to those variables.

We have that the bulk WdW action is (for $w < -1/3$):

$$\mathcal{I}^{WdW}_{bulk,gravity} = \frac{t_b^2}{4G_N}[2^{-\frac{6}{3w+1}-2}(\frac{1}{3w+1}(9(8^{\frac{2}{3w+1}+1}(3w-1)\left(3w\left(36w^3+84w^2+w-86\right)-85\right)$$
$$-16^{\frac{1}{3w+1}}(3w-5)(3w+4)(3w+7)(1-3w)^{\frac{2}{3w+1}+3}$$
$$+5(w+1)(3w+2)(1-3w)^{\frac{6}{3w+1}+4})(w+1))$$
$$+9^{\frac{1}{3w+1}}(2^{\frac{6}{3w+1}+3}\left(-162w^4-675w^3-531w^2+513w+515\right)(3w+3)^{\frac{6w}{3w+1}}+$$
$$81(w+1)^3$$
$$\cdot\left(5(w+1)(3w-1)(3w+2)(3w+3)^{\frac{4}{3w+1}}+16^{\frac{1}{3w+1}}(3w-5)(3w+4)(3w+7)\right))$$
$$\cdot(w+1)^{\frac{2}{3w+1}})][3(3w-5)(3w+2)(3w+4)(3w+7)]^{-1}. \tag{3.14}$$

We take the de Sitter limit $w \to -1$ to find that

$$\lim_{w\to -1}\mathcal{I}^{WdW}_{bulk,gravity} = \frac{t_b^2}{4G_N}\frac{87}{1024}.$$

For a dS universe, we would perhaps expect that

$$\frac{d\mathcal{C}}{dt} = TS,$$

where T and S are the standard thermodynamic values for the dS patch,

$$T = \frac{H}{2\pi},\ S = \frac{\pi}{H^2},$$

where H is the Hubble constant. Clearly, this does not agree with the limit $w \to -1$ of the FRW result; not even the scaling with t matches. It is possible that this disagreement is to be expected, since the causal structure of the spacetime changes discontinuously at $w = -1$. This question merits further study.

3.7 Relations to Lloyd's Bound

In the original complexity-action paper [25], it was noted that the normalization of the complexity

$$\mathcal{C} = \frac{\mathcal{I}_{WdW}}{\pi\hbar},$$

lead to black holes saturating Lloyd's bound [70] on the rate of computation. That is, when one calculates the complexity using the complexity-action proposal, a black hole of mass M satisfies

$$\frac{d\mathcal{C}}{dt} = \frac{2M}{\pi}.$$

In the FRW cases discussed in this chapter, the complexity grows faster than linearly (for example, in the case of a Universe with a single component, it grows as t^2). Hence, it seems that the rate of complexity growth can be arbitrarily high, violating Lloyd's bound.

However, it was later shown that (in the AdS black hole geometries) $\frac{d\mathcal{C}}{dt}$ approaches this bound from above [32]. Additionally, it was later found that there are cases where Lloyd's bound is violated even in the late-time limit [36, 93]. Therefore, even in AdS cases, the above normalization of complexity leads to values that do not always obey Lloyd's bound.

3.8 Conclusions and Open Questions

In this chapter, we have examined the possible role of complexity in holographic theories of FRW spacetimes. We generalized the complexity-action and complexity-volume dualities from AdS to several FRW spacetimes. Specifically, for a flat FRW Universe with one component, we found that the WdW action grows as t^2, regardless of the matter content. This is to be contrasted with the behavior of the the WdW action for a black hole in AdS, where the complexity grows linearly with time. In the AdS case, the holographic theory is encoded in a set of degrees of freedom that remain fixed with time. However, in the FRW case, the holographic theory is encoded on the leaf $\sigma(t)$ which is growing in time, so one would expect the complexity to grow faster for the holographic dual to FRW spacetimes. For a FRW Universe sourced by a scalar field, undergoing a transition, the gravitational WdW action decreases during the time intervals when the entanglement entropy decreases. The fractional decreases in the gravitational action are much larger than the corresponding decreases in the entanglement entropy. This is consistent with the intuition that entanglement is computationally expensive. We then examined the complexity-volume conjecture, where we find similar qualitative behavior with the complexity-action results. While our work is speculative, we believe that the apparent consistency of the results are noteworthy. We close with some possible avenues of further study.

First, it is interesting that, in the FRW cases, the quantity that behaves most like a complexity is the *gravitational*, rather than the *total* action. In other settings, for example, charged AdS black holes, it is the total (gravity plus Maxwell) action that seems to be dual to complexity [25]. In the FRW setting, the total action is negative, which is of course not a sensible result for complexity. Complexity in the putative holographic theory is, of course, only defined up to choices in parameters like the tolerance, gate set, etc. It is conceivable that the different WdW actions correspond to different definitions of complexity. Furthermore, since a holographic CFT and the holographic dual to the FRW universe are very different theories (see, for example, [77]), it is plausible that they require different measures of complexity. The precise holographic dictionary between actions and volumes and complexities clearly merit further research. Our results provide more explicit tests of holographic complexity conjectures, which may lead to clarification on this dictionary.

It is also noteworthy that in the case of an FRW universe with one component, the scaling of the complexity with time is t^2, independent of the value of w. This is reminiscent of the

butterfly velocities in holographic theories of FRW spacetimes [78]. It would be interesting to explore the relationship between butterfly velocities and complexity, and to see if there is some common explanation for the w-independence of the scaling of these two quantities.

It would also be interesting to try to better understand the de Sitter (i.e., $w \to -1$) limit. In particular, the holographic screen degenerates to the past/future infinity of dS space. It is possible that a better understanding of the FRW Universe and its $w \to -1$ limit will lead to an improved understanding of quantum gravity in dS.

Our analysis in this chapter has largely focused on flat FRW spacetimes. We comment briefly on the non-flat case here. Previously analysis has considered the entanglement entropy per degree of freedom (for a region Γ of holographic screen σ), which is

$$Q(\Gamma) = \frac{S_\Gamma}{(V_\Gamma)/4},$$

where S_Γ is the entanglement entropy of Γ and V_Γ is the volume of the the subregion Γ of the holographic screen. Specifically, for a curvature-dominate open universe, it was found that this quantity was lower than for the flat spacetimes [79]. As we have discussed, entanglement is computationally expensive, presumably this also means that there is less complexity per degree of freedom. Moreover, it is likely that (as in some of the cases studied above) there is a much bigger gap for the complexities of the curvature-dominated universe versus the flat ones than for their respective entanglement entropies. More detailed investigation of this question clearly merits future work.

Finally, it is has been argued that the holographic theory of FRW spacetimes fall into one of two structures, which have been termed the “Russian nesting doll" structure, and the “spacetime equals entanglement" structure [79]. It would be interesting to see if the results obtained in this chapter could be useful in obtaining a better understanding of the way the bulk FRW spacetimes are encoded in their boundary theories, and the structure of their Hilbert spaces.

Chapter 4

Complexity of One- and Two-Qubit Systems

4.1 Introduction

Recent work has shown that information plays a fundamental role in gravity, holography and the structure of spacetime. The crucial role of information is often most easily studied in the context of the Anti-de Sitter (AdS)/Conformal Field Theory (CFT) correspondence, which posits an equivalence between quantum gravity in $(d+1)-$dimensional AdS space and a CFT in d dimensions [71, 49, 96]. An explicit example is the Ryu-Takayanagi (RT) formula [85, 60], which states that the entanglement entropy of a CFT subregion is equivalent to the area of a minimal surface in AdS anchored on the entangling surface of the CFT subregion. This information-theoretic entry in the AdS/CFT 'dictionary' has led to many important results in understanding holographic duality including, for example, entanglement wedge reconstruction [5, 40]. Such advances have motivated a push to understand how other information-theoretic probes are realized in a theory of quantum gravity.

A recent proposal along these lines regards the role that quantum complexity may play in holographic duality [89, 25, 26]. Given a state $|\Psi\rangle$ in a Hilbert space $\mathcal{H}$, the complexity $\mathcal{C}(|\Psi\rangle)$ is the minimum number of "simple" gates that one must act on a "simple" reference state $|\Psi_0\rangle \in \mathcal{H}$ to obtain $|\Psi\rangle$. For example, in a system of qubits, "simple" gates might be chosen to be those that act on a small number of qubits, and a reference state might by the untangled state $|000\cdots0\rangle$. A closely-related concept is the complexity of a unitary operator, which is the minimum number of "simple" gates we need to compose to obtain the desired unitary operator. We discuss the approach to operator complexity taken in this chapter, Nielsen complexity geometry, in more detail in Section 4.2.

Although the precise values of complexity depend on details such as the tolerance, the precise set of "simple" gates chosen, and so on, complexities obey some simple qualitative features. For example, a system of a large number of qubits with a generic Hamiltonian H has time-evolution unitary $U(t) = \exp(-iHt)$. In this scenario, one expects that the

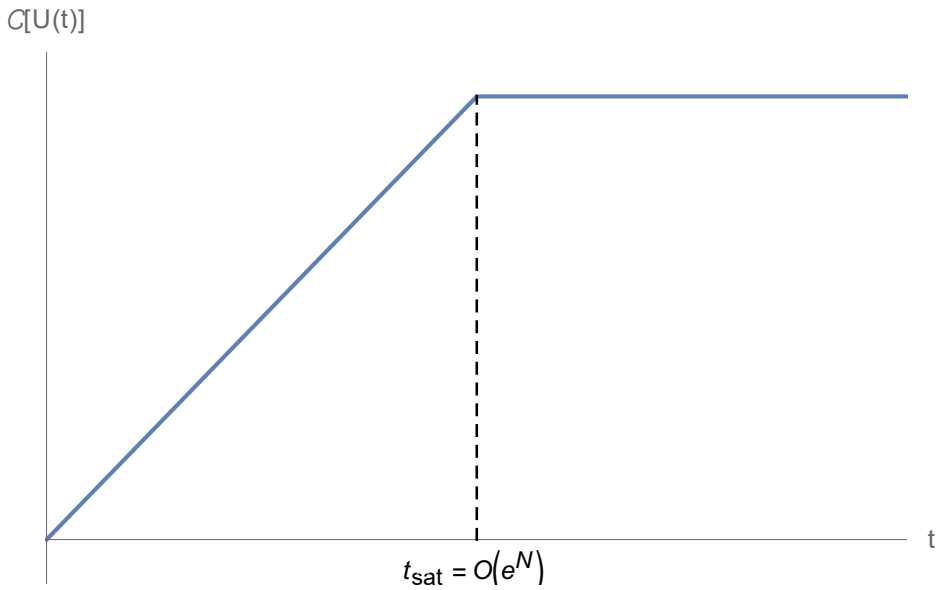

Figure 4.1: Schematic of complexity of a unitary time-evolution operator versus time. Initially, the complexity grows linearly with time, before saturating at some time that is exponential in the number of degrees of freedom N. At very late times, there will be Poincare recurrences (not shown here).

complexity of $U(t)$ will grow linearly with time, at least initially. However, at a certain point, the complexity will saturate and be approximately constant thereafter [91]. This was shown explicitly by [9]. See Figure 4.1. Previous work by Brown and Susskind argued for a thermodynamics of complexity [23]. In particular, they argued that the complexity of a quantum system with N qubits is related to an entropy of a classical system with 2^N degrees of freedom. They argue for a "second law of complexity," which says that any system with non-maximal complexity will be overwhelmingly likely to increase its complexity. Moreover, they argue that a system that does not have maximal complexity can use this as a resource (which the authors of [23] dub "uncomplexity") for quantum computation.

Another interesting feature of complexity of these systems is the so-called switchback effect [92, 24]. This involves precursor operators, which are the time-evolved "simple" operators. As an example, for a simple 'initial' operator W_0 (on a qubit system W_0 could be $X \otimes I \otimes \cdots \otimes I$), the precursor operator $W(t)$ is

$$W(t) = e^{-iHt} W_0 e^{iHt}.$$

Initially, the operator $W(t)$ is not very complex, since it still is mostly along the "simple" direction, W_0. However, after a time of order a scrambling time, the complexity begins to grow linearly [92, 24]. This delay in complexity growth on the order of a scrambling time is the switchback-effect. It can be intuitively understood as the delay for $W(t)$ to be begin to

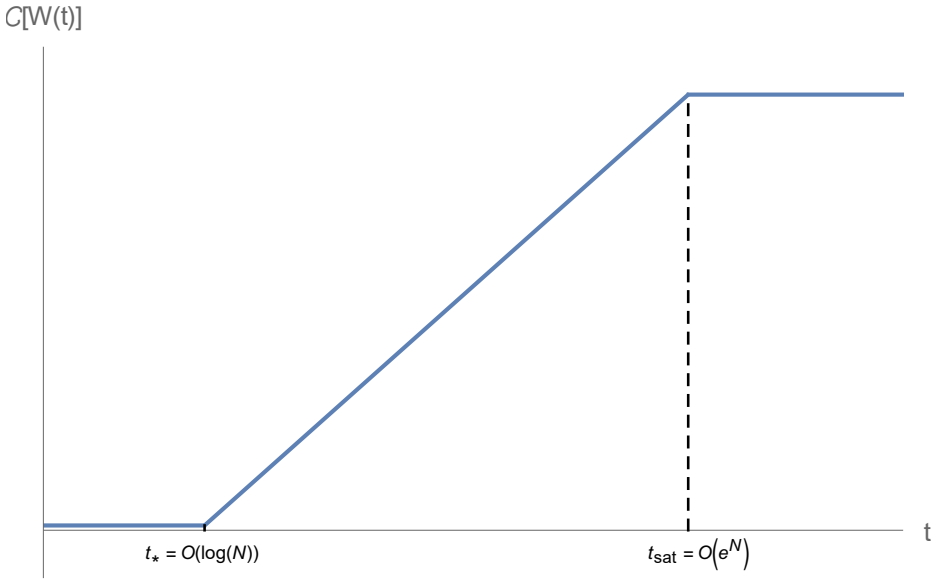

Figure 4.2: Schematic of complexity of a precursor operator versus time. Initially, the complexity is very small, up until the scrambling time t_*, at which point it begins to grow linearly with time, before saturating at some time that is exponential in the number of degrees of freedom N. At very late times, there will be Poincare recurrences (not shown here).

be supported on "complicated" operators since at small times $W(t)$ will consist primarily of "simple" gates which do not contribute to its complexity. In particular, consider the small-t expansion of the above precursor. By the Baker-Campbell-Hausdorff formula, there will be nested commutators of W_0 and H. H is a sum of terms that act on a small number of qubits. As t increases, the terms with larger numbers of nested commutators increase. These terms with a higher number of nested operators will generate terms with support on a larger number of qubits, and will thus have high complexity. As these high-complexity terms are multiplied by higher powers of t, it takes a larger amount of time for them to become significant. Once $W(t)$ has support on a large number of degrees of freedom, its complexity will of course be large. See Figure 4.2. A key element of the switchback effect in large N systems is the negative curvature of complexity geometry [92, 24], which we explain in greater detail in later sections.

There has been much recent work exploring the role complexity may play in holographic systems. In a two-sided AdS black hole, it was observed that the entanglement entropy of one side quickly saturates [52]. However, the volume of the maximum slice of the black hole keeps growing forever, at least classically. The AdS/CFT duality then asserts that this volume should be dual to some CFT quantity. The essence of the holographic complexity proposals [89, 25, 26] is that the dual of this quantity in the CFT side is the computational

complexity.

The two main proposals are the complexity-volume (CV) proposal [89] and the complexity-action (CA) proposal [25, 26]. Consider a state $|\Psi\rangle$ in a holographic CFT with a semi-classical dual. The complexity-volume proposal says that the complexity of the state $|\Psi\rangle$ is equal to the volume of the maximal volume slice (i.e., co-dimension 1 surface) through the bulk. The complexity-action proposal says that the complexity of $|\Psi\rangle$ is the action of the Wheeler-de Witt patch, which is defined as the domain of dependence of the maximum volume slice.

Although these proposals are somewhat speculative, they pass some non-trivial checks. For example, some recent work has investigated complexity in simple quantum field theories such as the free scalar field [34, 62]. These are quite different from the types of strongly-coupled, large-N field theories that are expected to have semi-classical holographic duals, but there are some intriguing similarities between these. In particular, in the analysis of the states in free quantum field theories, there are ambiguities in the reference state. It is tempting to identify these with the ambiguities in the bulk gravitational action [66]. Moreover, there is a logarithmic divergence in the UV cutoff in the field theory calculation, which is similar to the logarithmic divergence in the near-boundary cutoff in the complexity-action bulk calculation.

Importantly, these holographic complexity proposals also reproduce the switchback effect [92, 24], with the standard scrambling time for black holes, $t_* = \frac{\beta}{2\pi} \log N^2$, where β is the inverse temperature of the black hole, and N is the rank of the gauge group on the CFT side of the duality [87, 88]. Namely, the complexity of a precursor is low up until the scrambling time t_*, at which point it begins to grow linearly.

The purpose of this chapter is to help bridge the gap between these qualitative expectations of the CV and CA proposals, and notions of complexity in the boundary theory of holographic systems. Specifically, we will calculate the complexity of various operators in one- and two-qubit systems, using the framework of Nielsen complexity geometry, and analyze their behavior in time. This will allow us to quantitatively calculate complexity and compare with the qualitative intuition above. In this approach, we assign a metric to the space of unitaries, making some directions have a much larger cost than others. In a large-N system, we may assign gates that act on more than two degrees of freedom have a very large cost. The complexity of a given unitary U is then given by the length of the minimal-length path (i.e., geodesic) between the identity operator I and the target unitary U. See Figure 4.3

For the operators we consider in this chapter, we will find the following features: the complexity of unitary time evolution operators grows linearly with time, at least initially, as expected. For choices of complexity geometry that are negatively curved, the precursors show the qualitative behavior described above. The initial rate of growth is slow and then it begins quicken, entering a regime of linear growth of complexity in time; however, the distinction between the two regimes is not as pronounced as it is in the large-N case.

Our calculations provide support for the aforementioned conjectures in a concrete setting with explicit computations. In particular, we provide a first numerical study of precursor complexity in small systems. Previous work analyzed the geodesics in complexity space using the Euler-Arnold formalism [8, 9]. The paper [8] analyzed the "binding complexity" of various qubit states that are analogous to multi-boundary wormholes in AdS/CFT. These

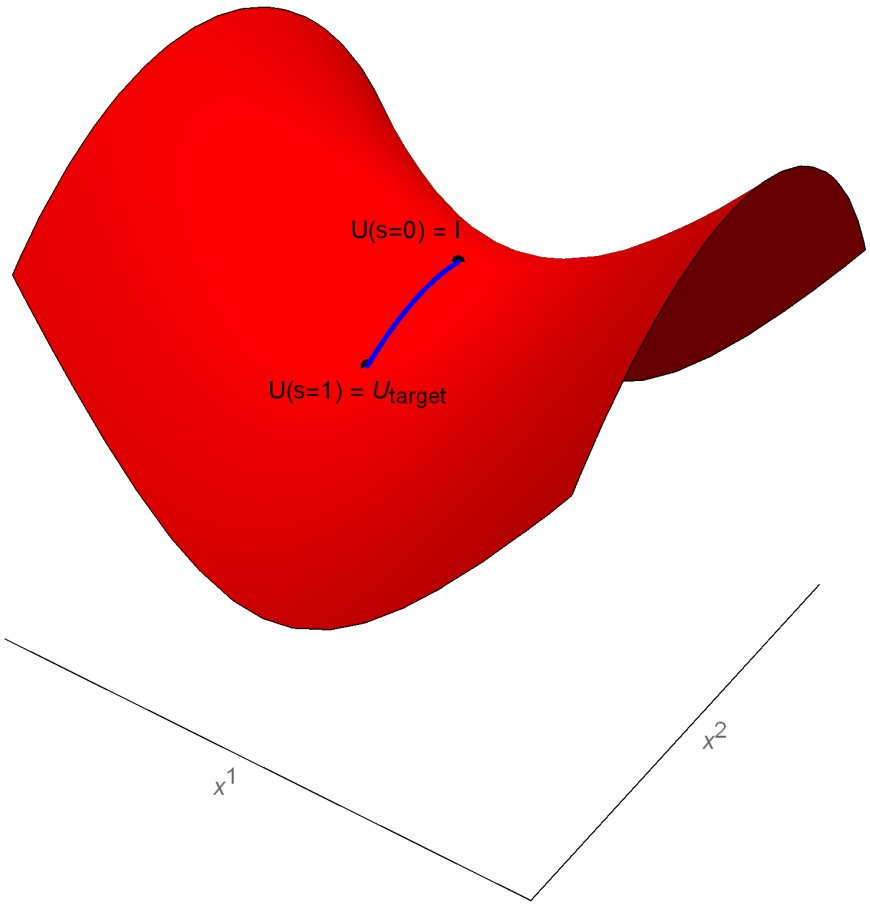

Figure 4.3: Schematic of complexity geometry. The intrinsic curvature, described by the complexity metric, of the unitary manifold (red surface) covered by coordinate patch (x^1, x^2) is visualized as extrinsic curvature in an embedding space. The blue line is the minimum-length path between the identity operator I and the target unitary, U_{target}.

calculations showed that the binding complexities behave similarly to the expectations from the holographic complexity proposals. The work in [9] considered the complexity of unitary time-evolution operators for one-qubit systems, as well as an analysis of the SYK model.

We begin with a brief review of Nielsen complexity geometry. We then investigate complexity in one-qubit geometries, considering a geometry where the Z-direction is much harder than the X and Y-directions. We find that the complexity of the unitary time-evolution operator grows linearly with time for early times. The complexity of precursors initially grows slowly, before then growing linearly, mimicking the behavior of large-N systems discussed above. We discuss how precursors are sensitive to the degree of the anisotropy in unitary space, while the time-evolution operators are not. We then consider two-qubit systems. As expected, at early times, complexity of the time-evolution unitary grows linearly with time. If we choose one-qubit gates to be easier and a Hamiltonian consisting of single qubit terms, then the complexity of a precursor is constant with time. However, if we take the two-qubit gates to be easier and a Hamiltonian consisting of two-qubit terms, we find that the complexity of precursors grows slowly at first, and then begins to grow linearly. Although this latter choice is unusual from a laboratory perspective, it gives a better model of the switchback effect. We use units where $\hbar = 1$ throughout.

4.2 Nielsen Complexity Geometry

We briefly review Nielsen complexity geometry which we will be using throughout [74, 76, 75, 43, 48]. Suppose that we have a system of N qubits, and a general unitary U in the group of unitaries that act on the N qubits, $SU(2^N)$. Any such unitary, U, can be parameterized by 4^N-1 parameters $x_1, x_2, \ldots, x_{4^N-1}$ indicating the extent of that unitary along each generator of $SU(2^N)$. A general metric on this space of unitaries is given by

$$ds^2 = \mathrm{Tr}(idUU^\dagger T_I)\mathcal{I}_{IJ}\mathrm{Tr}(idUU^\dagger T_J), \tag{4.1}$$

where T_I is a generator of $SU(2^N)$ (which later we will take to be a tensor product of Pauli matrices), and $\mathcal{I}_{IJ}$ is the cost factor. We will take $\mathcal{I}_{IJ}$ to be diagonal; hence, $\mathcal{I}_{IJ}$ characterizes the 'hardness' of applying the generator T_I. With the parametrization by coordinates, x^I, the corresponding group element $U \in SU(2^N)$ is given by

$$U(x^I) = \exp\bigl(ix^I T_I\bigr).$$

To find the complexity of a unitary, U_{target}, we first need to solve the geodesic equation

$$\frac{d^2x^I}{ds^2} = -\Gamma^I_{JK}\frac{dx^J}{ds}\frac{dx^K}{ds}$$

subject to the boundary conditions

$$U(x^I(s=0)) = I,\ U(x^I(s=1)) = U_{target},$$

where the Γ^I_{JK} are the usual Christoffel symbols for the Nielsen complexity metric 4.1. The complexity of our target unitary will then by given by the length of the minimal geodesic,

$$\mathcal{C}[U_{target}] = \int_0^1 \sqrt{g_{IJ}\frac{dx^I}{ds}\frac{dx^J}{ds}}ds,$$

where g_{IJ} is the Nielsen complexity metric.

In the later sections, we generate random Hamiltonians satisfying certain conditions, and then compute the complexity of the time-evolution unitary and of precursors with Nielsen metric such that "easy" gates have a lower cost factor than "hard" gates. We will always take the Hamiltonian to be a sum of "easy" terms.

In our subsequent discussions, we will often have a target unitary and need to calculate its coordinates. Orthogonality of the $SU(2^N)$ generators:

$$\mathrm{Tr}(T_I T_J) = 2^N \delta_{IJ},$$

allows us to compute the coordinates of a unitary U_{target} via

$$ix^I = 2^{-N}\mathrm{Tr}(\log(U_{target})T_I). \tag{4.2}$$

We can then numerically solve the geodesic equation, subject to the boundary conditions that the geodesic starts at the identity ($x^I = 0$) and ends at the coordinates of the target unitary. We numerically calculate the values of the metric and Christoffel symbols. We use the Matlab function `bvp4c` to solve the boundary value problem given by the system of ODE's resulting from the geodesic equation. The boundary conditions are $x^I(s = 0) = 0$, corresponding to the identity, and $x^I(s = 1)$ being the coordinates of target unitary, given by 4.2. The function `bvp4c` uses a collocation method to solve the system of ODE's with boundary conditions. The function subdivides the interval [0,1] into subintervals, and discretizing the system of ODE's and boundary conditions, which turns it into an algebraic system of equations for values of the solution at the mesh points. It then numerically solves these algebraic systems.

4.3 One Qubit System

In this section, we consider complexity in a one-qubit system. Specifically, we consider the setup explored in [22], where the X- and Y-directions are considered "easy" and the Z-direction is considered "hard". The Z-direction is taken to be 10 times harder than the X- and Y-directions.

First, we take our Hamiltonian to be a sum of the easy terms, explicitly,

$$H = J_1 X + J_2 Y,$$

and consider the unitary time-evolution operator $U(t) = e^{-iHt}$. We numerically solve the geodesic equations as described above for a sample Hamiltonian, and plot the complexity

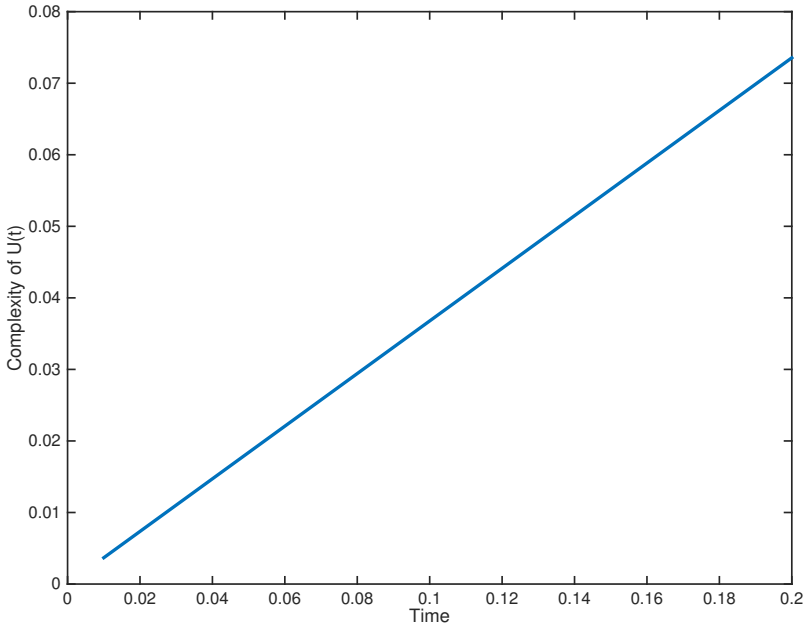

Figure 4.4: Complexity of a unitary time-evolution operator versus time for a one qubit system described in the main text. The complexity of this operator grows linearly with time, at least initially. The time axis is in units of seconds.

$\mathcal{C}[U(t)]$ as a function of time in Figure 4.4. We use the values $J_1 = 0.4387s^{-1}$, $J_2 = 0.3816s^{-1}$, and $\mathcal{I}_{XX} = \mathcal{I}_{YY} = 0.1$, $\mathcal{I}_{ZZ} = 1$. However, our answers for complexity will be equivalent for various classes of J_i. For the time-evolution operator, $U(t)$, for a fixed time t, the geodesic will lie in the isotropic subspace spanned by the X and Y directions. Hence, if we apply a rotation to J_1, J_2, the complexity will not change–the only thing that changes the complexity is an overall rescaling of J_i, which can absorbed into a rescaling of time t. A similar story applies for precursors, in that the complexity will be equivalent for various classes of choices of J_i and W_0. See Appendix A.3 for more details.

Initially, before any recurrence time, we see the complexity of $U(t)$ grows linearly with time, exactly as expected. However, as t increases, there are topological obstructions or 'conjugate points' and the length of the shortest path from I to $U(t)$ stops increasing. To illustrate this point with a concrete example, we plot the complexity of $U(t)$ for a larger range of time in Figure 4.5. The complexity initially grows linearly with time, until it reaches a maximum value, at time $t = \pi/\sqrt{J_1^2 + J_2^2}$. For our Hamiltonian, this occurs at $t = 5.4031s$. We discuss this in more detail in Appendix A.3. It then starts to decrease linearly to zero, at which point it begins to increase linearly again. This process repeats itself indefinitely. This agrees with the qualitative behavior of the complexity of a one-qubit unitary obtained

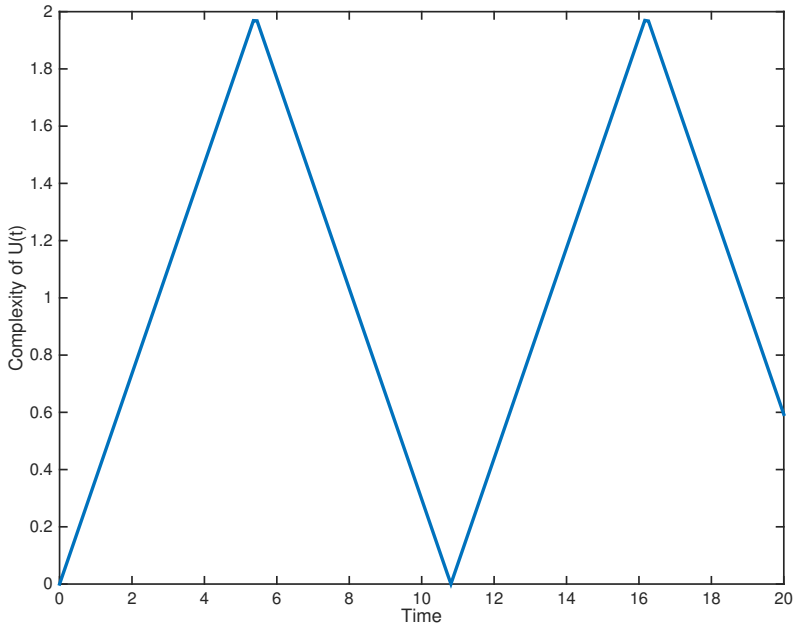

Figure 4.5: Complexity of a unitary time-evolution operator versus time for the one qubit system described in the main text. The complexity of this operator grows linearly with time, then linearly decreases to zero, at the Poincaré recurrence time. This process repeats itself indefinitely. The time axis is in units of seconds.

in [9]. These dips in the complexity are the one-qubit versions of Poincaré recurrences. As discussed in the introduction, in a system with N degrees of freedom, we expect that the complexity will grow linearly up until a time that is $O(\exp(N))$. In our numerical work, we will only be concerned with regimes well before the appearance of topological obstructions or conjugate points.

Now we consider a precursor, $W(t)$, which will be a time-evolved "easy" operator. In our one-qubit case, we will consider the operators

$$W(t) = e^{-iHt} i X e^{iHt}$$

and

$$W(t) = e^{-iHt} i Y e^{iHt},$$

where we have chosen the normalization so that $\det W(t) = 1$ and $W(t) \in \mathrm{SU}(2)$. We numerically solve the geodesic equations, and plot the complexity $\mathcal{C}[W(t)]$ as a function of time in Figure 4.6, using the same parameters as Figure 4.4.

When $t = 0$, $W(t) = W_0$ is entirely along an easy direction. However, for nonzero t, we will of course have terms proportional to the commutator $[W_0, J_1 X + J_2 Y] \supset Z$,

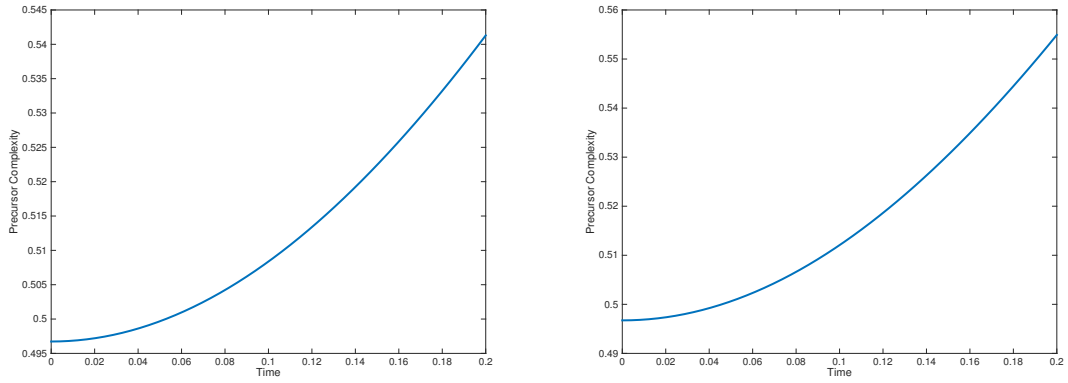

(a) $W_0 = iX$. (b) $W_0 = iY$.

Figure 4.6: Complexity of a precursor operator versus time, for the one-qubit system described in the main text, for different choices of the operator W_0. The time axis is in units of seconds.

which is a hard direction. In this case, the hardness of Z generates negative curvature in the complexity geometry and is somewhat reminiscent of the switchback effect for large-N systems, as discussed above. That is, the precursor will be a sum of nested operators which are initially suppressed for small times, but become more important for large times. The nested commutators for the large-N case generate terms that are very complex. Hence, the complexity is initially suppressed, and then begins to grow. Indeed, we see that the rate of growth of $\mathcal{C}[W(t)]$ is somewhat suppressed for some time, and then it begins to grow linearly, though of course the difference between the two regimes is less stark than we expect in the large-N case. Therefore, it appears that this negative-curvature model of one-qubit complexity is a very simple toy model of information scrambling.

To see the connection between negatively-curved geometry and the structure of the commutators more concretely, consider the following argument of Brown and Susskind [22]. Say that we have two "easy" directions, $\mathcal{O}_1$ and $\mathcal{O}_2$. Then the Baker-Campbell-Hausdorff formula tells us the following:

$$e^{i\mathcal{O}_1 t} e^{i\mathcal{O}_2 t} = \exp\left[i(\mathcal{O}_1 + \mathcal{O}_2)t - \frac{1}{2}[\mathcal{O}_1, \mathcal{O}_2]t^2 + \cdots \right].$$

We can think of the LHS as starting from the identity matrix I, and then traveling a distance t in the $\mathcal{O}_1$ direction to a point P, and then a distance t along the $\mathcal{O}_2$ to a point Q. The RHS is taking a path from the identity directly to the point Q. If the commutator $[\mathcal{O}_1, \mathcal{O}_2]$ is hard, then the length of the "hypotenuse" (the direct path from the identity matrix to the point Q) will be longer than what it would be in flat space. This is a generic property of negatively-curved geometries. On the other hand, if the commutator $[\mathcal{O}_1, \mathcal{O}_2]$ is easy, then the length of the "hypotenuse" will be shorter than what it would be in flat space. This is a

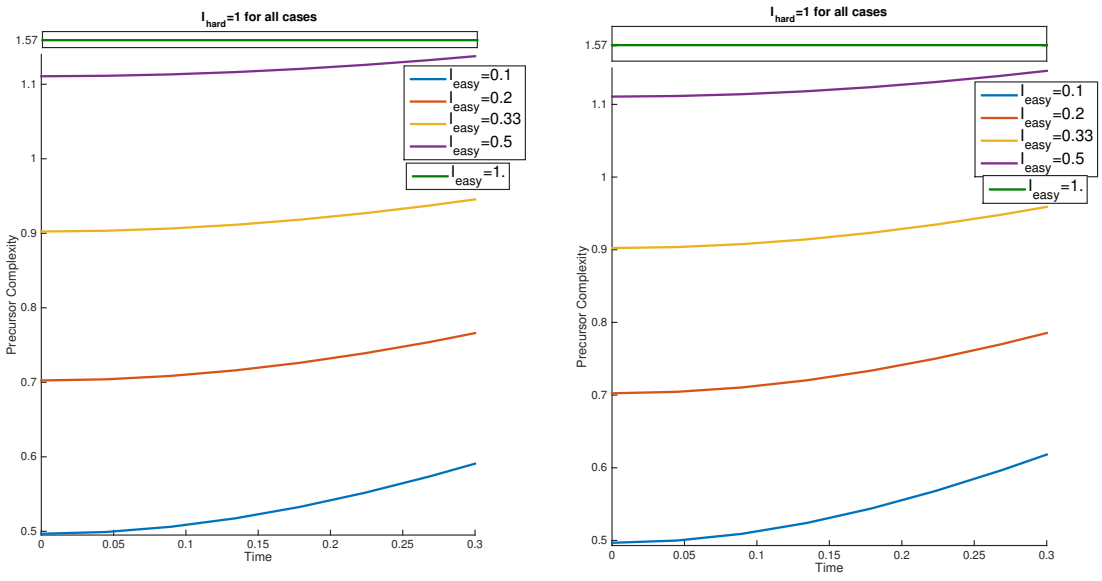

(a) $W_0 = iX$.

(b) $W_0 = iY$.

Figure 4.7: Complexity of a precursor operator versus time, for the one-qubit system described in the main text, for different choices of the operator W_0 for various penalty factors. The very lowest curves in each panel correspond to the plots shown in Figure 4.6. The time axis is in units of seconds. Note that there is a jump in the vertical axis.

property of positively curved spaces. Indeed, in the present setup, with $\mathcal{I}_{XX} = \mathcal{I}_{YY} = 0.1$, we can calculate, for example, the scalar curvature at the origin (the identity matrix), which is given by $\mathcal{R} = 10(8 - 20\mathcal{I}_{ZZ})$ [22]. Hence, the (curvature of the) complexity geometry will be negative when the Z gate is much harder than the other directions and positive when the Z gate is easier.

Finally, we plot the complexity of the same precursors considered above (with the same Hamiltonian) with various penalty factors, in Figure 4.7. We can see that as we decrease the "easy" penalty factor relative to the hard one, the switchback effect becomes more pronounced, as expected. Indeed, for the case where both penalty factors are 1 (i.e., the metric is isotropic), the complexity is a constant as a function of time. We explain this last case in detail analytically in the next section. Therefore, we see explicitly that this anisotropy in complexity space that generates the negative curvature is essential to the switchback-like-behavior in precursor operators.

Hence, we see that precursors are a more sensitive probe of the complexity geometry, and in particular, the anisotropy, since their qualitative behavior is affected by the introduction of certain types of anisotropies, as we have shown. Indeed, the unitary time-evolution operator

will be entirely in the easy subspace, and so will not be affected by this type of anisotropy. [1]

4.4 Hard Two-Qubit Gates, Easy One-Qubit Gates

Generally, when one introduces measures of complexity, gates that act on a small numbers of qubits are considered "easy," while those that act on larger numbers of qubits are considered "hard." Thus, when considering a model of circuit complexity for two-qubit systems, one expects that the natural choice is to assign gates that act non-trivially on both qubits a higher penalty factor than those that act on only one qubit. However, we will see in this section that this is not suitable as a model for the switchback effect. In fact, the reverse (i.e., assigning one-qubit gates a much larger penalty factor than their two-qubit counterparts) seems to be a geometry that much better illustrates the switchback effect. This latter model is discussed in the next section.

Consider a precursor operator in this model with a large cost factor for the two-qubit gates. In this case, our "local" Hamiltonian is one built out of easy, i.e., one-qubit operators. In general, it will take the form

$$H = \sum_i \left(J_{1i}\ \sigma_i \otimes I + J_{2i}\ I \otimes \sigma_i \right).$$

We numerically solve the geodesic equations to calculate the complexity of the unitary time evolution operator $U(t)$ corresponding to this type of Hamiltonian (using the geometry described previously). We plot the results in Figure 4.8. Explicitly, the cost factor will be taken to be 0.1 for one-qubit gates, and 1.0 for two-qubit gates. We use the following coefficients in the Hamiltonian:

$$J_{1X} = 0.9390, J_{1Y} = 0.8759, J_{1Z} = 0.5502, J_{2X} = 0.6225, J_{2Y} = 0.5870, J_{2Z} = 0.2077,$$

where each J_{ij} is given in units of s^{-1}. We see that it is linear in time for early times, as expected.

Recall that a precursor takes the form

$$W(t) = e^{-iHt} W_0 e^{iHt},$$

where W_0 is an "easy" operator, a one-qubit operator in this case. As the Hamiltonian is a sum of commuting single-body terms we can clearly see that $W(t)$ will also be a single-body operator as the evolution does not generate any operators on the second qubit. Say for concreteness that $W_0 = iX \otimes I$ (the overall factor is chosen so that $W(t)$ has determinant

[1] An explicit discussion of the different features of the Nielsen metric probed by precursor and time-evolution unitary complexity is given in appendix A.3.

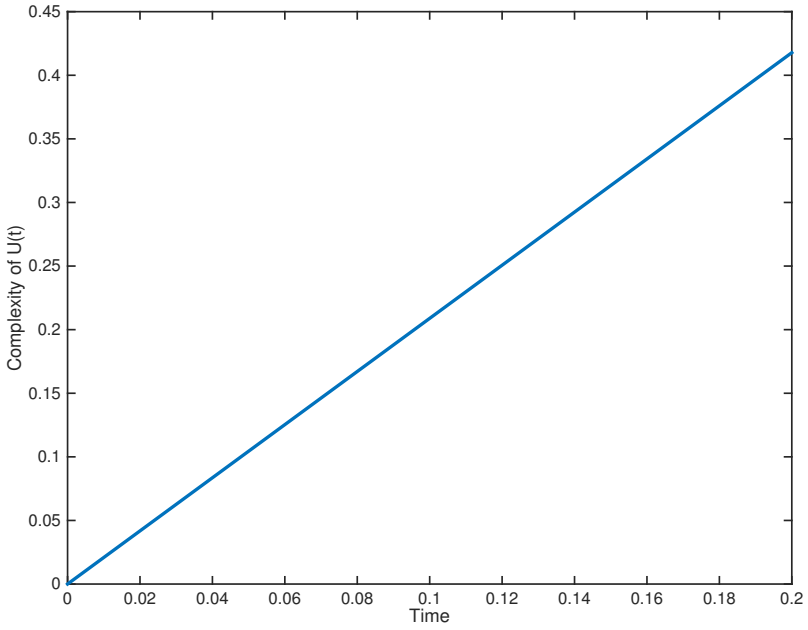

Figure 4.8: Complexity of a unitary time-evolution operator versus time with one-qubit gates being easier than two-qubit gates. The complexity of this operator grows linearly with time. The time axis is in units of seconds.

1). Then our precursor $W(t)$ becomes

$$\begin{aligned} W(t) &= \exp\left(-i\sum_i \left(J_{1i}\sigma_i \otimes I + J_{2i} I \otimes \sigma_i\right) t\right) iX \otimes I \exp\left(i\sum_i \left(J_{1i}\sigma_i \otimes I + J_{2i} I \otimes \sigma_i\right) t\right) \\ &= \exp\left(-i\sum_i \left(J_{1i}\sigma_i\right) t\right) iX \exp\left(i\sum_i \left(J_{1i}\sigma_i\right) t\right) \otimes I. \end{aligned} \tag{4.3}$$

As we are now only considering single-qubit operators, the matrix exponentials can be easily computed giving schematic form of (for example)

$$\begin{aligned} W(t) &= \exp\left(i\sum_i \alpha_i\sigma_i\right) iX \exp\left(-i\sum_i \alpha_i\sigma_i\right) \\ &= \left(\cos(\alpha)\, I + i\sum_i \hat{\alpha}_i\sigma_i \sin\alpha\right) iX \left(\cos(\alpha)\, I - i\sum_i \hat{\alpha}_i\sigma_i \sin\alpha\right), \end{aligned} \tag{4.4}$$

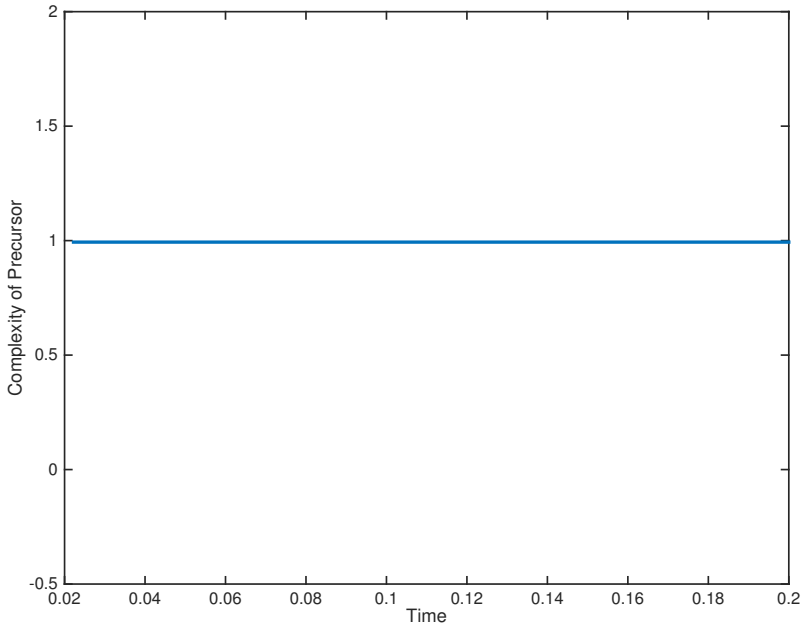

Figure 4.9: Complexity of a precursor operator versus time, with one-qubit gates being easier than two-qubit gates. In this case, $W_0 = iX \otimes I$. The complexity of the precursor is constant in time, as explained in the main text. The time axis is in units of seconds.

where $\alpha \equiv \sqrt{\alpha_1^2 + \alpha_2^2 + \alpha_3^2}$, and $\hat{\alpha}_i \equiv \alpha_i/\alpha$, are t-dependent parameters. Using the identity

$$\sigma_i \sigma_j = I\delta_{ij} + i\epsilon_{ijk}\sigma_k,$$

we can show that $W(t)$ has no term proportional to the identity, since, by cyclicity of trace, $\mathrm{Tr}W(t) = \mathrm{Tr}W(0) = 0$.

Therefore, for all time t, the precursor $W(t)$ will have no term proportional to the identity, since all the Pauli matrices are traceless. We can write $W(t)$ in the form

$$W(t) = \exp\left(i \sum_i \beta_i(t)\sigma_i\right).$$

We can expand this as

$$W(t) = \exp\left(i \sum_i \beta_i(t)\sigma_i\right) = \left(\cos\left(\beta(t)\right) I + i \sum_i \hat{\beta}_i(t)\sigma_i \sin\beta(t)\right),$$

where $\beta(t) \equiv \sqrt{\beta_1(t)^2 + \beta_2(t)^2 + \beta_3(t)^2}$, and $\hat{\beta}_i(t) \equiv \beta_i(t)/\beta(t)$.[2]

[2]See appendix A.3 for an explicit calculation of $\beta_i(t)$.

Because $W(t)$ has no term proportional to the identity, we must have $\cos\beta = 0$ so that $\beta = \frac{\pi}{2}$ for all time. In this geometry, all one-qubit directions have the same cost, so we would expect that the complexity of the precursor will be constant throughout time. Once again, we solve the geodesic equations, and plot the complexity of $W(t)$ versus time in Figure 4.9. We see that $\mathcal{C}[W(t)]$ is constant with respect to time. (Note that this is exactly the same reason why the complexity of a precursor was constant in time for the one-qubit case with an isotropic metric discussed at the end of the last section.) Although we chose $W_0 = iX \otimes I$ for concreteness, the complexity of $W(t)$ will be constant in time for any choice of one-qubit operator W_0 with $\det W_0 = 1$, using the exact same logic as above. However, different choices of W_0 will result in different values for the complexity. Hence, this geometry is poorly-suited to model the switchback effect. Indeed, as discussed above, since the commutator of two "easy" directions is "easy," the complexity geometry is not negatively-curved and we should not expect the precursor to display switchback-effect-like behavior.

We now turn to the other case (where the two-qubit gates have a lower cost factor than the one-qubit gates), which seems to be a better model of the switchback effect.

4.5 Easy Two-Qubit Gates, Hard One-Qubit Gates

In this section, we consider a geometry in which the two-qubit gates are "easy" while the one-qubit gates are "hard." While this may seem counter-intuitive from the perspective of large-N systems (where gates that act on a small number of qubits are easy), we shall see that the geometry that results from this choice seems to illustrate the switchback effect. In this case, the Hamiltonian will be a sum of "easy" terms,

$$H = \sum_{ij} J_{ij}\ \sigma_i \otimes \sigma_j.$$

The unitary time-evolution operator is then $U(t) = \exp(-iHt)$. We solve the geodesic equation numerically, and use this to calculate the complexity $\mathcal{C}[U(t)]$. We plot the results in Figure 4.10, for Hamiltonian 1 in Table 4.1. The Hamiltonians in this table were found by randomly generating the nine two-qubit operator coefficients. As expected, the complexity grows linearly in time.

Recall that a precursor in this geometry will have the form

$$W(t) = e^{-iHt} W_0 e^{iHt},$$

however now W_0, being "easy," will of course act non-trivially on both qubits. At $t = 0$, this operator will only have non-zero coordinates in an "easy" direction. However, as we increase t, we will have terms in $W(t)$ that result from the commutator of terms in the Hamiltonian and W_0. In general, these will lead to terms that act non-trivially on only one qubit. For example, if $W_0 = -X \otimes X$, $[W_0, X \otimes Y]$ will be proportional to $I \otimes Z$, which is a "hard" gate. Note that this is a somewhat similar mechanism to what happens

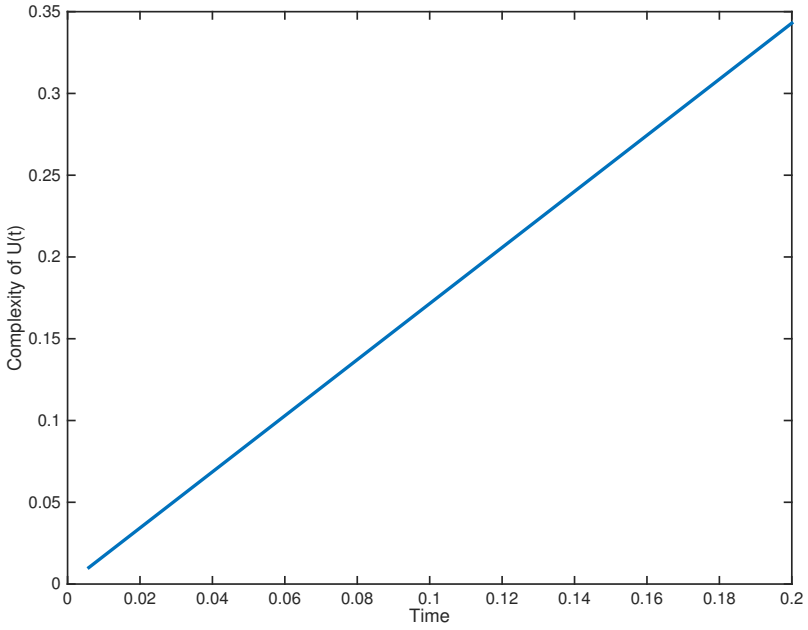

Figure 4.10: Complexity of a unitary time-evolution operator versus time with one-qubit gates being harder than two-qubit gates. The complexity of this operator grows linearly with time. The time axis is in units of seconds.

to the complexity of precursors in large-N systems. As discussed above, this structure of the commutator (specifically that the commutator of two "easy" operators yields a "hard" operator) is a reflection of the negative curvature of unitary space that is a key component of switchback-like time evolution of precursor complexity. This should be contrasted with the situation above, where the "easy" gates were taken to be the one-qubit operators. In this case, the commutator of two "easy" gates is another "easy" gate. Therefore, even though *physically* (in, for example, a laboratory setting) this setup (in which two-qubit gates are taken to be easier than one-qubit) gates is not a good model of complexity, it is a good mathematical toy model of the switchback effect. In particular, once again, we see that the negative curvature is necessary to generate switchback-like-behavior of precursor operator complexity.

When we calculate the complexity of $W(t)$ and plot the results as a function of time (see Figure 4.11), we see that for a brief initial period, the complexity grows slowly, and then it begins to grow much more rapidly, exactly as expected from the previous discussion. We do this calculation for the Hamiltonians given in Table 4.1. This behavior of complexity of precursors is very similar in form to the behavior of precursors in the usual systems with a much larger number of qubits [24, 92], suggesting that, qualitatively, the switchback effect

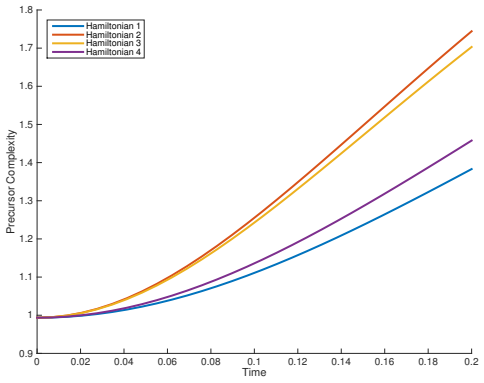

(a) $W_0 = -X \otimes X$

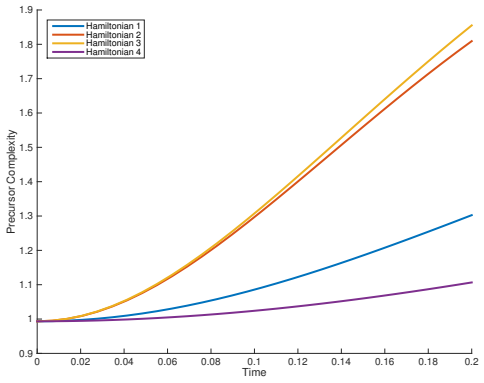

(b) $W_0 = -X \otimes Y$

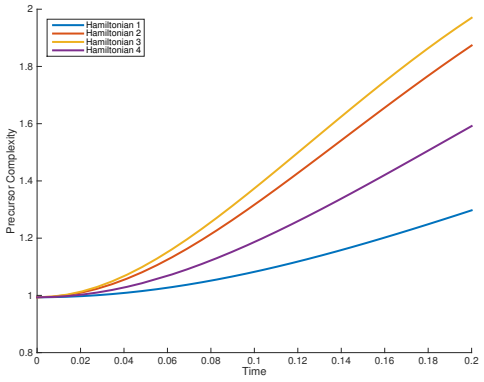

(c) $W_0 = -X \otimes Z$

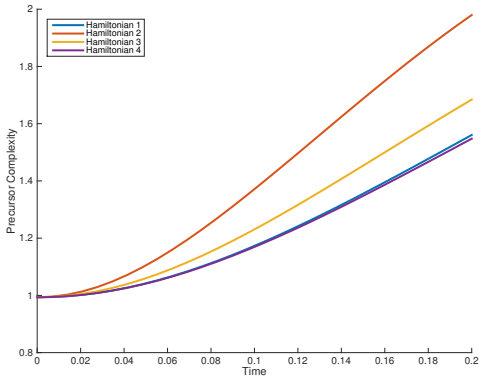

(d) $W_0 = -Y \otimes Z$

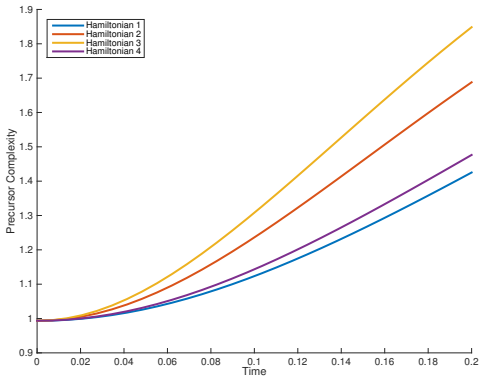

(e) $W_0 = -Y \otimes Y$

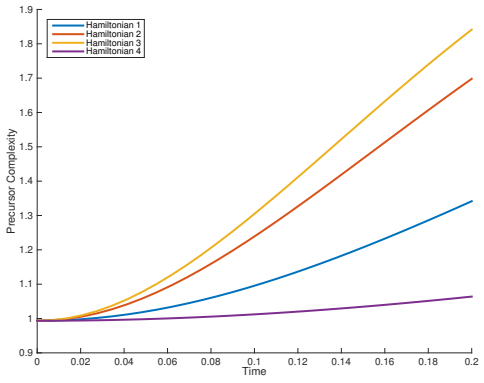

(f) $W_0 = -Z \otimes Z$

Figure 4.11: Complexity of a precursor operator versus time, with one-qubit gates being harder than two-qubit gates for various choices of the operator W_0, as well as for various choices of the Hamiltonian. The complexity of the precursor grows slowly at first, then begins to grow linearly. This is a result of a switchback effect similar to the one seen in systems with a large number of degrees of freedom. The time axis is in units of seconds. Note that the overall factor is chosen so that $\det W(t) = 1$.

	J_{11}	J_{12}	J_{13}	J_{21}	J_{22}	J_{23}	J_{31}	J_{32}	J_{33}
H_1	0.1888	0.0012	0.3164	0.6996	0.6253	0.5431	0.4390	0.2874	0.5017
H_2	0.9649	0.1576	0.9706	0.9572	0.4854	0.8003	0.1419	0.4218	0.9157
H_3	0.7922	0.9595	0.6557	0.0357	0.8491	0.9340	0.6787	0.7577	0.7431
H_4	0.3922	0.6555	0.1712	0.7060	0.0318	0.2769	0.0462	0.0971	0.8235

Table 4.1: Hamiltonians considered in the main text. Each row in the table corresponds to $H = \sum_{ij} J_{ij}\ \sigma_i \otimes \sigma_j$. Each J_{ij} is in units of s^{-1}.

is related to the generation of "hard" operators via commutators of "easy" operators and the role of large N is simply to increase the number of "hard" operators relative to "easy" operators, sharpening the effect.

4.6 Conclusions and Future Directions

In this chapter, we have analyzed complexity of operators in one- and two-qubit systems, using Nielsen complexity geometry. This approach allows us to give a precise definition of operator complexity, and largely confirm our qualitative intuition for how this should behave. We have found that the unitary time-evolution operators grow linearly with time, as expected. It was also found that precursor operators grow more slowly at first, at least when we chose our "hard" and "easy" gates such that the resulting complexity geometry was negatively curved. For one-qubit systems, this occurred when we considered one of the three Pauli operators to be "hard," and the other two to be "easy." For two-qubit systems, to obtain negative curvature, we chose two-qubit gates to be "easy," while considering their one-qubit counterparts to be "hard." While this is somewhat counter-intuitive from, e.g., a laboratory point of view, this choice was necessary to generate negative curvature that is required to model many of the features of computational complexity.

There are several interesting ways in which our analysis could be extended, which we leave to future work. First of all, it would be worthwhile to try to extend these types of computations to larger numbers of qubits. In particular, it would be nice to consider a system of N qubits, where the one- and two-qubit gates are much less difficult than gates acting on larger numbers of qubits, reflecting laboratory conditions. In this setting it is natural to consider two-qubit operators "easy" and commutators of "easy" operators will generate larger "hard" operators. As evidenced by our two-qubit calculations, the production of "hard" operators (one-qubit in that case) by commutators of "easy" operators seems to be an important ingredient needed to observe (qualitatively) the switchback effect. We therefore expect that the behavior of precursor complexity will look more and more like the behavior expected for the large-N limit–very small complexity until the scrambling time, and then linear growth.

Furthermore, it would be interesting to analyze specific qubit models, especially those

that are of interest from the gravity point of view, such as the SYK model. For, e.g., the SYK model, the scrambling time is expected to scale logarithmically with the number of degrees of freedom. Presumably, then, these calculations would show that the time at which linear growth starts also scales logarithmically with the number of degrees of freedom.

However, doing these calculations for a larger number of degrees of freedom means analyzing a much more complicated geometric space, the dimension of which scales exponentially in the number of qubits, which poses a considerable computational challenge.

We expect that future work analyzing these types of problems will continue to illuminate the connections between information, holography, gravity, and spacetime, and in particular illustrate how bulk data is encoded in information-theoretic quantities in its holographic boundary dual.

Chapter 5

Sandwiched Renyi Relative Entropy in AdS/CFT

Recent work has uncovered the importance of quantum information in understanding quantum gravity. The anti-de Sitter/conformal field theory (AdS/CFT) correspondence states that any theory of quantum gravity in $(d+1)$-dimensional anti-de Sitter space is equivalent to a conformal field theory in d dimensions [71, 49, 96]. The Ryu-Takayagi formula [85] and the Hubeney-Rangamani-Takayagi [60] formula show that entanglement entropies in the CFT are equal to areas of minimal or extremal surfaces in the bulk. These formulae can be derived directly from the basic AdS/CFT dictionary [67, 41]. The role of the Renyi entropy, a generalization of entanglement entropy, in AdS/CFT has also been studied [38].

An important aspect of this connection has been the role that quantum error correction plays in the encoding of the bulk in the boundary [51, 50, 5, 40, 80, 42, 39, 2, 61]. In particular, [51] established a theorem demonstrating the equivalence between (i) subregion duality, (ii) the equality of bulk and boundary relative entropy, (iii) algebraic encoding, and (iv) the RT formula.

The purpose of this chapter is to discuss the role of sandwiched relative Renyi entropy in holographic quantum error correction. The sandwiched Renyi entropy is a generalization of the relative entropy, which reduces to the usual relative entropy if we take the limit of the Renyi index to 1. In particular, we show that the the equivalence of bulk and boundary relative Renyi entropy is equivalent to the conditions stated above (subregion duality, algebraic encoding, the RT formula, and the equivalence between bulk and boundary relative entropy) in the context of operator algebra quantum error correction with complementary recovery. Along the way, we will define a sandwiched relative Renyi entropy in the context of finite-dimensional von Neumann algebras. We will then show that this definition follows from the definition of relative Renyi entropy on general von Neumann algebras, which is defined from modular operators. Finally, we will discuss results from numerical simulations on a simple holographic tensor model which illustrates the behavior of the sandwiched relative Renyi entropy near a phase transition. These numerical calculation are a model for approximate error correction, in contrast to the theorem we will discuss which concerns an equivalence

between exact equality of bulk and boundary sandwiched Renyi relative entropies.

The sandwiched relative Renyi entropy has previously been used to illuminate the connections between information, entanglement, gravity, and quantum field theory. For example, [11] discussed the bulk dual of the so-called refined relative Renyi entropy. The quantum null energy condition (QNEC) [21] can be expressed as a second shape deformation of the relative entropy of a given state and the vacuum. For free quantum field theories, it has been shown that this can be generalized to the sandwiched Renyi relative entropies [72] for certain values of the Renyi index. Our work in the present chapter is closely related to the recent article [63] on corrections to the equality of bulk and boundary relative entropy in AdS/CFT.

We begin this chapter with a discussion of the basic definitions and properties of sandwiched relative Renyi entropy as well as a brief review of the theory of holographic quantum error correction.

5.1 Sandwiched Renyi Relative Entropy

Given a Hilbert space $\mathcal{H}$ and two density operators ρ, σ on the Hilbert space, the sandwiched relative Renyi entropy [73, 95, 65] is defined as

$$S_n(\rho||\sigma) \equiv \frac{1}{n-1} \log \left[\mathrm{Tr} \left[\left(\sigma^{\frac{1-n}{2n}} \rho \sigma^{\frac{1-n}{2n}} \right)^n \right] \right].$$

This is also known in the literature as the sandwiched Renyi divergence (SRD).

Proposition 1. *The sandwiched relative Renyi entropy is invariant under unitary transformations. That is, given a unitary transformation U on the Hilbert space $\mathcal{H}$, we have*

$$S_n(U\rho U^\dagger||U\sigma U^\dagger) = S_n(\rho||\sigma)$$

for any density matrices ρ, σ on $\mathcal{H}$.

Proof. This follows from the definition:

$$\begin{aligned} S_n(U\rho U^\dagger||U\sigma U^\dagger) &= \frac{1}{n-1} \log \left[\mathrm{Tr} \left[\left((U\sigma U^\dagger)^{\frac{1-n}{2n}} U\rho U^\dagger (U\sigma U^\dagger)^{\frac{1-n}{2n}} \right)^n \right] \right] \\ &= \frac{1}{n-1} \log \left[\mathrm{Tr} \left[\left(U\sigma^{\frac{1-n}{2n}} U^\dagger U\rho U^\dagger U\sigma^{\frac{1-n}{2n}} U^\dagger \right)^n \right] \right] = \frac{1}{n-1} \log \left[\mathrm{Tr} \left[\left(U\sigma^{\frac{1-n}{2n}} \rho \sigma^{\frac{1-n}{2n}} U^\dagger \right)^n \right] \right] \\ &= \frac{1}{n-1} \log \left[\mathrm{Tr} \left[U \left(\sigma^{\frac{1-n}{2n}} \rho \sigma^{\frac{1-n}{2n}} \right)^n U^\dagger \right] \right] = \frac{1}{n-1} \log \left[\mathrm{Tr} \left[\left(\sigma^{\frac{1-n}{2n}} \rho \sigma^{\frac{1-n}{2n}} \right)^n \right] \right] = S_n(\rho||\sigma). \end{aligned} \tag{5.1}$$

□

In addition to being invariant under unitary transformations, the sandwiched relative Renyi entropy is always strictly positive, unless the two density matrices are the same, in which case it is zero [73, 95, 65].

Proposition 2. *Let $\mathcal{H}$ be a Hilbert space, and let ρ, σ be two density matrices on $\mathcal{H}$. Then $S_n(\rho||\sigma) \geq 0$, and $S_n(\rho||\sigma) = 0$ if and only if $\rho = \sigma$.*

Moreover, the limit as $n \to 1$ of the relative Renyi entropy is the usual relative entropy [73, 95, 65].

Proposition 3. *Let $\mathcal{H}$ be a Hilbert space, and let ρ, σ be two density matrices on $\mathcal{H}$. Then*

$$\lim_{n \to 1} S_n(\rho||\sigma) = S(\rho||\sigma),$$

where

$$S(\rho||\sigma) \equiv Tr(\rho \log \rho) - Tr(\rho \log \sigma)$$

is the relative entropy.

In addition, the sandwiched Renyi relative entropy is monotonic in the Renyi index n [65].

Proposition 4. *Let $\mathcal{H}$ be a Hilbert space, and let ρ, σ be two density matrices on $\mathcal{H}$, and suppose $n_1, n_2 \in (0, \infty) \backslash \{1\}$ with $n_1 \leq n_2$. Then*

$$S_{n_1}(\rho||\sigma) \leq S_{n_2}(\rho||\sigma).$$

The sandwiched relative Renyi entropy obeys the data-processing inequality for $n \geq 1/2$. That is, when we apply a quantum channel to the density matrices, the sandwiched relative Renyi entropy decreases or stays the same. See, for example, [65] and references therein for a discussion.

Proposition 5. *Let $\mathcal{H}$ be a Hilbert space, let ρ, σ be two density matrices on $\mathcal{H}$, let $n \geq 1/2$, and let Λ be a quantum channel. Then*

$$S_n(\rho||\sigma) \geq S_n(\Lambda[\rho]||\Lambda[\sigma]).$$

5.2 Holographic Quantum Error Correction

We briefly review some aspects of the connection between quantum error correction and holography [50, 51]. Consider a finite-dimensional Hilbert space $\mathcal{H}$ that factorizes as $\mathcal{H} = \mathcal{H}_A \otimes \mathcal{H}_{\bar{A}}$, and a subspace $\mathcal{H}_{code} \subseteq \mathcal{H}$, and a von Neumann algebra $\mathcal{M}$ acting on the code subspace $\mathcal{H}_{code}$.

Then there exists a decomposition of $\mathcal{H}_{code}$,

$$\mathcal{H}_{code} = \oplus_\alpha (\mathcal{H}_{a_\alpha} \otimes \mathcal{H}_{\bar{a}_\alpha})$$

such that $\mathcal{M}$ is the set of all operators of the form $\oplus_\alpha(\mathcal{O}_\alpha \otimes I_{\bar{a}_\alpha})$ where the $\mathcal{O}_\alpha$'s are operators on $\mathcal{H}_{a_\alpha}$. In the above setup, $\mathcal{H}$ is the analog of the full Hilbert space of the conformal field theory, while $\mathcal{H}_{code}$ corresponds to a code subspace, e.g., the set of states that are perturbatively close to some smooth classical bulk geometry. $\mathcal{H}_A$ corresponds to the Hilbert space of some spatial region A in the CFT, while $\mathcal{M}$ represents the set of operators with support in the entanglement wedge of A, $\mathcal{E}(A)$.

These error correcting codes work by encoding a state on $\mathcal{M}$ in the "physical" Hilbert space $\mathcal{H}$. In particular, there are states χ_α on $\mathcal{H}_{\bar{a}_\alpha}$ and a unitary transfomation U_A on $\mathcal{H}_A$ such that a state $\tilde{\rho}$ on $\mathcal{H}_{code}$ is mapped to a state with the following density matrix on $\mathcal{H}_A$:

$$\tilde{\rho}_A = U_A \left[\oplus_\alpha (p_\alpha \rho_{a_\alpha} \otimes \chi_\alpha)\right] U_A^\dagger.$$

Each of the ρ_{a_α}'s is defined so that

$$p_\alpha \rho_{a_\alpha} = \mathrm{Tr}_{\bar{a}_\alpha} \tilde{\rho}_{\alpha\alpha},$$

where $\tilde{\rho}_{\alpha\alpha}$ is the αth block of the density matrix of $\mathcal{H}_{code}$. Furthermore, each of the ρ_{a_α}'s is normalized so that $\mathrm{Tr}\rho_{a_\alpha} = 1$, and $\sum_\alpha p_\alpha = 1$.

The above encoding satisfies an equivalent of the Ryu-Takayanagi formula. In particular,

$$S(\tilde{\rho}_A) = \mathrm{Tr}(\tilde{\rho}_A \mathcal{L}_A) + S(\rho_a : \mathcal{M}),$$

where $\mathcal{L}_A = \oplus_\alpha S(\chi_\alpha)(I_{a_\alpha} \otimes I_{\bar{a}_\alpha})$ is the analog of the area operator, $S(\chi_\alpha) = -Tr(\chi_\alpha \log \chi_\alpha)$ is the von Neumann entropy of χ_α, and $S(\rho_a : \mathcal{M})$ is the algebraic von Neumann entropy over the algebra $\mathcal{M}$. It is defined as

$$S(\rho_a : \mathcal{M}) \equiv \sum_\alpha p_\alpha S(\rho_{a_\alpha}) - \sum_\alpha p_\alpha \log(p_\alpha).$$

This entropy consists of an average of the von Neumann entropy of each block, plus a "classical" term that is the Shannon entropy of the probability distribution $\{p_\alpha\}$.

This error correcting code also satisfies the equivalence of "bulk" and "boundary" relative entropy. To see this, consider two states on the code subspace that are encoded in the usual way:

$$\tilde{\rho}_A = U_A \left[\oplus_\alpha (p_\alpha \rho_{a_\alpha} \otimes \chi_\alpha)\right] U_A^\dagger,\ \tilde{\sigma}_A = U_A \left[\oplus_\alpha (q_\alpha \sigma_{a_\alpha} \otimes \chi_\alpha)\right] U_A^\dagger.$$

We then compute the relative entropy, using the fact that it is invariant under unitary transformations

$$S(\tilde{\rho}_A || \tilde{\sigma}_A) = S(\oplus_\alpha (p_\alpha \rho_{a_\alpha} \otimes \chi_\alpha) || \oplus_\alpha (q_\alpha \sigma_{a_\alpha} \otimes \chi_\alpha))$$

In order to calculate this, we will need the logarithm of block diagonal matrices $\oplus_\alpha (p_\alpha \rho_{a_\alpha} \otimes \chi_\alpha)$. For a block diagonal matrix, $M = \oplus_\alpha M_\alpha$, we have that $M^n = \oplus M_\alpha^n$ and so (by the Taylor series for matrix exponentiation) $\exp(M) = \oplus_\alpha \exp(M_\alpha)$. Therefore, $\log M = \oplus_\alpha \log(M_\alpha)$. Therefore,

$$\log(\oplus_\alpha (p_\alpha \rho_{a_\alpha} \otimes \chi_\alpha)) = \oplus_\alpha \log p_\alpha I_{a_\alpha \bar{a}_\alpha} + \oplus_\alpha (\log \rho_{a_\alpha} \otimes I_{\bar{a}_\alpha}) + \oplus_\alpha (I_{a_\alpha} \otimes \log \chi_\alpha).$$

Hence,

$$Tr((\oplus_\alpha(p_\alpha\rho_{a_\alpha}\otimes\chi_\alpha))\log(\oplus_\alpha(p_\alpha\rho_{a_\alpha}\otimes\chi_\alpha))) = \sum_\alpha p_\alpha\log p_\alpha + \sum_\alpha p_\alpha Tr(\rho_\alpha\log\rho_{a_\alpha}) + \sum_\alpha p_\alpha Tr(\chi_\alpha\log\chi_\alpha), \tag{5.2}$$

and, similarly,

$$Tr((\oplus_\alpha(p_\alpha\rho_{a_\alpha}\otimes\chi_\alpha))\log(\oplus_\alpha(q_\alpha\sigma_{a_\alpha}\otimes\chi_\alpha))) = \sum_\alpha p_\alpha\log q_\alpha + \sum_\alpha p_\alpha Tr(\rho_\alpha\log\sigma_{a_\alpha}) + \sum_\alpha p_\alpha Tr(\chi_\alpha\log\chi_\alpha). \tag{5.3}$$

Hence,

$$\begin{aligned} S(\tilde{\rho}_A||\tilde{\sigma}_A) = {} & Tr((\oplus_\alpha(p_\alpha\rho_{a_\alpha}\otimes\chi_\alpha))\log(\oplus_\alpha(p_\alpha\rho_{a_\alpha}\otimes\chi_\alpha))) \\ & - Tr((\oplus_\alpha(p_\alpha\rho_{a_\alpha}\otimes\chi_\alpha))\log(\oplus_\alpha(q_\alpha\sigma_{a_\alpha}\otimes\chi_\alpha))) \\ = {} & \sum_\alpha p_\alpha\log\left(\frac{p_\alpha}{q_\alpha}\right) + \sum_\alpha p_\alpha S(\rho_{a_\alpha}||\sigma_{a_\alpha}) = S(\rho_a||\sigma_a:\mathcal{M}). \end{aligned} \tag{5.4}$$

As with the algebraic entropy considered above, this is the sum of two terms, an averaged quantum relative entropy, weighted by the probability distribution $\{p_\alpha\}$ and a "classical" term, which is the relative Shannon entropy of the probability distributions $\{p_\alpha\}$ and $\{q_\alpha\}$. Moreover, this algebraic relative entropy is the exact form one obtains from the theory of modular operators, as we discuss below.

A closely related concept in this construction is that of subregion duality. That is, for all operators on $\mathcal{O}\in M$, there are operators $\mathcal{O}_A$ which acts nontrivially only on $\mathcal{H}_A$ such that $\mathcal{O}|\psi\rangle = \mathcal{O}_A|\psi\rangle$ for all $|\psi\rangle\in\mathcal{H}_{code}$.

It was shown in [51] that the existence of an encoding map, the RT formula, subregion duality, and the equivalence of bulk and boundary relative entropy are all in fact equivalent for these kinds of finite-dimensional Hilbert spaces.

5.3 Sandwiched Renyi Relative Entropy in Holographic Quantum Error Correction

The so-called α-block decomposition described above has received considerable interest in recent years [39, 2, 42] and is now relatively well-understood. It is our aim in this section to discuss the sandwiched Renyi relative entropy in this quantum error-correction context and to provide a definition of sandwiched Renyi relative entropy that is suitable for this α-block setting. In the next section, we will show that this definition also follows from a modular-theoretic definition of sandwiched Renyi relative entropy.

In particular, we will show that the equality of sandwiched Renyi relative entropy is equivalent to the four statements above. Consider the same setup as in the previous section, and consider two states $\tilde{\rho}$ and $\tilde{\sigma}$ on the code subspace encoded in the usual way

$$\tilde{\rho}_A = U_A \left[\oplus_\alpha (p_\alpha \rho_{a_\alpha} \otimes \chi_\alpha)\right] U_A^\dagger,\ \tilde{\sigma}_A = U_A \left[\oplus_\alpha (q_\alpha \sigma_{a_\alpha} \otimes \chi_\alpha)\right] U_A^\dagger.$$

We calculate

$$\begin{aligned} S_n(\tilde{\rho}_A||\tilde{\sigma}_A) &= S_n(\oplus_\alpha (p_\alpha \rho_{a_\alpha} \otimes \chi_\alpha)|| \oplus_\alpha (q_\alpha \sigma_{a_\alpha} \otimes \chi_\alpha)) \\ &= \frac{1}{n-1} \log \left[\mathrm{Tr} \left[\left((\oplus_\alpha (q_\alpha \sigma_{a_\alpha} \otimes \chi_\alpha))^{\frac{1-n}{2n}} (\oplus_\alpha (p_\alpha \rho_{a_\alpha} \otimes \chi_\alpha)) (\oplus_\alpha (q_\alpha \sigma_{a_\alpha} \otimes \chi_\alpha))^{\frac{1-n}{2n}} \right)^n \right] \right] \\ &= \frac{1}{n-1} \log \left[\sum_\alpha p_\alpha^n q_\alpha^{1-n} \mathrm{Tr} \left[\left(\sigma_{a_\alpha}^{\frac{1-n}{2n}} \rho_{a_\alpha} \sigma_{a_\alpha}^{\frac{1-n}{2n}} \right)^n \otimes \chi_\alpha \right] \right] \\ &= \frac{1}{n-1} \log \left[\sum_\alpha p_\alpha^n q_\alpha^{1-n} \mathrm{Tr} \left[\left(\sigma_{a_\alpha}^{\frac{1-n}{2n}} \rho_{a_\alpha} \sigma_{a_\alpha}^{\frac{1-n}{2n}} \right)^n \right] \cdot \mathrm{Tr}(\chi_\alpha) \right] \\ &= \frac{1}{n-1} \log \left[\sum_\alpha p_\alpha^n q_\alpha^{1-n} \mathrm{Tr} \left[\left(\sigma_{a_\alpha}^{\frac{1-n}{2n}} \rho_{a_\alpha} \sigma_{a_\alpha}^{\frac{1-n}{2n}} \right)^n \right] \right], \end{aligned} \quad (5.5)$$

where in the first step, we have used the invariance of sandwiched relative Renyi entropy under unitary transformations, as discussed above. Note that we can write this as

$$S_n(\tilde{\rho}_A||\tilde{\sigma}_A) = \frac{1}{n-1} \log \left[\sum_\alpha p_\alpha^n q_\alpha^{1-n} \exp[(n-1) S_n(\rho_{a_\alpha}||\sigma_{a_\alpha})] \right].$$

As we discuss below, this is exactly the same as the Renyi relative entropy derived for such finite-dimensional von Neumann algebras using modular operators. (Similarly, the modular-theoretic definition of relative entropy reduces to the one defined above for finite-dimensional von Neumann algebras.) Note that this algebraic entropy is not of the form of a classical term plus a weighted average of the quantum entropies of each α-block. However, note that the classical relative Renyi entropy of two probability distributions $\{p_\alpha\}$ and $\{q_\alpha\}$ is given by

$$S_n(\{p_\alpha\}||\{q_\alpha\}) = \frac{1}{n-1} \log \left[\sum_\alpha p_\alpha^n q_\alpha^{1-n} \right].$$

This means that when the quantum states are purely classical probability distributions, our algebraic sandwiched relative Renyi entropy reduces to the classical relative Renyi entropy. Moreover, it is clear that when we only have one α-block, the algebraic sandwiched relative Renyi entropy reduces to the usual sandwiched relative Renyi entropy defined above. This is exactly as we would expect, in analogy with the corresponding special cases for the algebraic entropy and relative entropy described above.

The classical relative Renyi entropy described above is always greater than or equal to zero, and it is zero if and only if the probability distributions are identical, $p_\alpha = q_\alpha$. We claim that our algebraic relative Renyi entropy is greater than or equal to zero, and that it is zero if and only if the states are the same. To see this, consider the case where $n > 1$. $S_n(\rho_{a_\alpha}||\sigma_{a_\alpha}) \geq 0$, so

$$S_n(\tilde{\rho}_a||\tilde{\sigma}_a : \mathcal{M}) = \frac{1}{n-1} \log \left[\sum_\alpha p_\alpha^n q_\alpha^{1-n} \exp[(n-1) S_n(\rho_{a_\alpha}||\sigma_{a_\alpha})] \right]$$
$$\geq \frac{1}{n-1} \log \left[\sum_\alpha p_\alpha^n q_\alpha^{1-n} \right] = S_n(\{p_\alpha\}||\{q_\alpha\}). \quad (5.6)$$

since log is a monotone increasing function. Therefore, $S_n(\tilde{\rho}_a||\tilde{\sigma}_a : \mathcal{M}) \geq 0$. Moreover, the inequality in the above expression is saturated (i.e., $S_n(\tilde{\rho}_a||\tilde{\sigma}_a : \mathcal{M}) = S_n(\{p_\alpha\}||\{q_\alpha\})$) if and only if $\rho_{a_\alpha} = \sigma_{a_\alpha}$ for all α. Also, as discussed above, $S_n(\{p_\alpha\}||\{q_\alpha\}) = 0$ if and only if the probability distributions are identical, $p_\alpha = q_\alpha$. Therefore, $S_n(\tilde{\rho}_a||\tilde{\sigma}_a : \mathcal{M}) = 0$ if and only if $\rho_{a_\alpha} = \sigma_{a_\alpha}$ and $p_\alpha = q_\alpha$ for all α, i.e., the states are identical, as claimed. The case with $n < 1$ is similar.

In addition, we claim that our algebraic sandwiched Renyi relative entropy limits to the algebraic relative entropy defined above as $n \to 1$, just as the sandwiched Renyi relative entropy converges to the relative entropy when $n \to 1$. Note that

$$\lim_{n\to 1} S_n(\rho_{a_\alpha}||\sigma_{a_\alpha}) = S(\rho_{a_\alpha}||\sigma_{a_\alpha})$$

for all α. We have

$$\lim_{n\to 1} S_n(\tilde{\rho}_a||\tilde{\sigma}_a : \mathcal{M}) = \lim_{n\to 1} \frac{1}{n-1} \log \left[\sum_\alpha p_\alpha^n q_\alpha^{1-n} \exp[(n-1) S_n(\rho_{a_\alpha}||\sigma_{a_\alpha})] \right],$$

and

$$\lim_{n\to 1} \log \left[\sum_\alpha p_\alpha^n q_\alpha^{1-n} \exp[(n-1) S_n(\rho_{a_\alpha}||\sigma_{a_\alpha})] \right] = \log[\sum_\alpha p_\alpha] = 0.$$

Therefore, by L'Hospital's rule,

$$\begin{aligned}
&\lim_{n\to 1} S_n(\tilde{\rho}_a||\tilde{\sigma}_a : \mathcal{M}) \\
&\qquad = \lim_{n\to 1} \frac{1}{n-1} \log \left[\sum_\alpha \exp[n \log p_\alpha - (n-1)\log q_\alpha + (n-1) S_n(\rho_{a_\alpha}||\sigma_{a_\alpha})] \right] \\
&= \lim_{n\to 1} \frac{\sum_\alpha \exp[n \log p_\alpha - (n-1)\log q_\alpha + (n-1) S_n(\rho_{a_\alpha}||\sigma_{a_\alpha})](\log p_\alpha - \log q_\alpha + S_n(\rho_{a_\alpha}||\sigma_{a_\alpha}))}{\sum_\alpha \exp[n \log p_\alpha - (n-1)\log q_\alpha + (n-1) S_n(\rho_{a_\alpha}||\sigma_{a_\alpha})]} \\
&\quad + \lim_{n\to 1} \frac{\sum_\alpha \exp[n \log p_\alpha - (n-1)\log q_\alpha + (n-1) S_n(\rho_{a_\alpha}||\sigma_{a_\alpha})](n-1)\partial_n S_n(\rho_{a_\alpha}||\sigma_{a_\alpha})}{\sum_\alpha \exp[n \log p_\alpha - (n-1)\log q_\alpha + (n-1) S_n(\rho_{a_\alpha}||\sigma_{a_\alpha})]} \\
&= \frac{\sum_\alpha \exp[\log p_\alpha](\log p_\alpha - \log q_\alpha + S(\rho_{a_\alpha}||\sigma_{a_\alpha}))}{\sum_\alpha \exp[\log p_\alpha]} = \sum_\alpha p_\alpha \log\left(\frac{p_\alpha}{q_\alpha}\right) + \sum_\alpha p_\alpha S(\rho_{a_\alpha}||\sigma_{a_\alpha}),
\end{aligned} \tag{5.7}$$

which is the algebraic relative entropy, $S(\rho_a||\sigma_a : \mathcal{M})$, as claimed.

Now, as noted above, it was previously established that subregion duality, algebraic encoding, equality of bulk and boundary relative entropy, and the RT formula are all equivalent for this setting. We have shown that the algebraic encoding implies the equality of bulk and boundary sandwiched relative Renyi entropy (using the algebraic definition discussed above). Equality of bulk and boundary sandwiched relative Renyi entropy implies the equality of bulk and boundary relative entropy, by taking the limit $n \to 1$, since the algebraic sandwiched relative Renyi entropy converges to the algebraic relative entropy in this limit. Therefore, the equality of bulk and boundary sandwiched relative Renyi entropy is also equivalent to subregion duality, algebraic encoding, equality of bulk and boundary relative entropy, and the RT formula.

5.4 Sandwiched Renyi Relative Entropy using Modular Operators

We now discuss relative entropies and relative Renyi entropies using the theory of modular operators, closely following [97, 64]. We begin by reviewing modular operators.

Consider a Hilbert space $\mathcal{H}$ that has the following structure,

$$\mathcal{H} = \oplus_A (\mathcal{H}_A \otimes \mathcal{H}_{\bar{A}}),$$

and for simplicity we consider the case where $\dim \mathcal{H}_A = \dim \mathcal{H}_{\bar{A}}$. Consider two (normalized) states, $|\Psi\rangle, |\Phi\rangle \in \mathcal{H}$. We can write

$$|\Psi\rangle = \sum_A r_A |\psi_A\rangle,$$

where each $|\psi_A\rangle$ is normalized, and $\sum_A |r_A|^2 = 1$. We can write each $|\psi_A\rangle$ as

$$|\psi_A\rangle = \sum_i c(i,A)\,|i,i,A\rangle\,,$$

where $|i,i,A\rangle = |i,A\rangle \otimes |i,A\rangle'$, and $\{|i,A\rangle\}$ is an orthonormal basis for $\mathcal{H}_A$, and $\{|i,A\rangle'\}$ is an orthonormal basis for $\mathcal{H}_{\bar{A}}$. Each $|\psi_A\rangle$ is normalized, so $\sum_i |c(i,A)|^2 = 1$. In the exact same way, we can write

$$|\Phi\rangle = \sum_A s_A\,|\phi_A\rangle\,, |\phi_A\rangle = \sum_\alpha d(\alpha,A)\,|\alpha,\alpha,A\rangle\,,$$

where $|\alpha,\alpha,A\rangle = |\alpha,A\rangle \otimes |\alpha,A\rangle'$, and $\{|\alpha,A\rangle\}$ is an orthonormal basis for $\mathcal{H}_A$, and $\{|\alpha,A\rangle'\}$ is an orthonormal basis for $\mathcal{H}_{\bar{A}}$. Once again, we have the normalization conditions

$$\sum_A |s_A|^2 = 1, \sum_\alpha |d(\alpha,A)|^2 = 1.$$

Consider the algebra of operators $\mathcal{A}$ defined by operators on $\mathcal{H}$ that are block-diagonal and have the form $\oplus_A(\mathcal{O}_A \otimes I_{\bar{A}})$, where $I_{\bar{A}}$ is the identity operator on $\mathcal{H}_{\bar{A}}$. We first determine the relative Tomita operator, $S_{\Psi||\Phi}$, which is defined by

$$S_{\Psi||\Phi}\mathcal{O}\,|\Psi\rangle = \mathcal{O}^\dagger\,|\Phi\rangle \text{ for all } \mathcal{O} \in \mathcal{A}.$$

Consider an operator $\mathcal{O} \in \mathcal{A}$, which we can write as $\oplus_A(\mathcal{O}_A \otimes I_{\bar{A}})$, that acts as follows:

$$\mathcal{O}\,|i,A\rangle = |\alpha,A\rangle$$

and

$$\mathcal{O}_A\,|j,B\rangle = 0$$

for all $j \neq i$, and for all $B \neq A$. Then the adjoint acts as

$$\mathcal{O}^\dagger\,|\alpha,A\rangle = |i,A\rangle$$

and

$$\mathcal{O}^\dagger\,|\beta,B\rangle = 0$$

for all $\beta \neq \alpha$, and for all $B \neq A$. Therefore,

$$\mathcal{O}\,|\Psi\rangle = r_A c(i,A)\,|\alpha,i,A\rangle\,, \mathcal{O}^\dagger\,|\Phi\rangle = s_A d(\alpha,A)\,|i,\alpha,A\rangle\,.$$

Hence, the relative Tomita operator acts as

$$S_{\Psi||\Phi}\,|\alpha,i,A\rangle = \frac{s_A}{r_A}\frac{d(\alpha,A)}{c(i,A)}\,|i,\alpha,A\rangle\,.$$

The relative Tomita operator is an anti-linear operator, so the adjoint acts as

$$S^\dagger_{\Psi||\Phi}\left|i,\alpha,A\right\rangle = \frac{s_A^*}{r_A^*}\frac{d(\alpha,A)^*}{c(i,A)^*}\left|\alpha,i,A\right\rangle.$$

Using this, we can compute the relative modular operator, $\Delta_{\Psi||\Phi} = S^\dagger_{\Psi||\Phi}S_{\Psi||\Phi}$. We find

$$\Delta_{\Psi||\Phi}\left|\alpha,i,A\right\rangle = \frac{|s_A|^2}{|r_A|^2}\frac{|d(\alpha,A)|^2}{|c(i,A)|^2}\left|\alpha,i,A\right\rangle.$$

Define σ_A to be the reduced density matrix of $|\phi_A\rangle$ on $\mathcal{H}_A$, and $\bar{\rho}_A$ to be the reduced density matrix of $|\psi_A\rangle$ on $\mathcal{H}_{\bar{A}}$, and define $p_A \equiv |r_A|^2, q_A \equiv |s_A|^2$. With these definitions, and the expressions above for $|\psi_A\rangle$ and $|\phi_A\rangle$, we obtain

$$\Delta_{\Psi||\Phi} = \oplus_A\left(\frac{q_A}{p_A}\sigma_A\otimes\bar{\rho}_A^{-1}\right).$$

Having computed the relative modular operator, we now turn to the calculation of algebraic relative entropy. Recall that the Araki definition of relative entropy over our von Neumann algebra $\mathcal{A}$ is given by

$$S(\Psi||\Phi:\mathcal{A}) \equiv -\left\langle\Psi\right|\log\Delta_{\Psi||\Phi:\mathcal{A}}\left|\Psi\right\rangle.$$

Now, for a block diagonal matrix, $M = \oplus_A M_A$, $M^n = \oplus_A M_A^n$ so that (by the Taylor series definition of matrix exponentiation) $\exp M = \oplus_A \exp M_A$. which means that for a block-diagonal matrix $M = \oplus_A M_A$, $\log M = \oplus_A \log M_A$. Therefore,

$$\begin{aligned}S(\Psi||\Phi:\mathcal{A}) &= -\left\langle\Psi\right|\oplus_A\log\left(\frac{q_A}{p_A}\sigma_A\otimes\bar{\rho}_A^{-1}\right)\left|\Psi\right\rangle = -\left\langle\Psi\right|\oplus_A\log\left(\frac{q_A}{p_A}\sigma_A\otimes\bar{\rho}_A^{-1}\right)\left|\Psi\right\rangle \\ &= -\left\langle\Psi\right|\oplus_A\left[\log\left(\frac{q_A}{p_A}\right)I_A\otimes I_{\bar{A}}\right]\left|\Psi\right\rangle - \left\langle\Psi\right|\oplus_A\log\left(\sigma_A\otimes\bar{\rho}_A^{-1}\right)\left|\Psi\right\rangle. \quad (5.8)\end{aligned}$$

Now,

$$\log\left(\sigma_A\otimes\bar{\rho}_A^{-1}\right) = \log\sigma_A\otimes\bar{I}_{\bar{A}} - I_A\otimes\log\bar{\rho}_A,$$

and the first term in $S(\Psi||\Phi:\mathcal{A})$ becomes

$$\begin{aligned}-\left\langle\Psi\right|\oplus_A\left[\log\left(\frac{q_A}{p_A}\right)I_A\otimes I_{\bar{A}}\right]\left|\Psi\right\rangle &= -\sum_A\left\langle\psi_A\right|r_A^*r_A\log\left(\frac{q_A}{p_A}\right)\left|\psi_A\right\rangle \\ &= -\sum_A p_A\log\left(\frac{q_A}{p_A}\right) = \sum_A p_A\log\left(\frac{p_A}{q_A}\right). \quad (5.9)\end{aligned}$$

Therefore, the relative entropy becomes:

$$\begin{aligned} S(\Psi||\Phi:\mathcal{A}) &= \sum_A p_A \log\left(\frac{p_A}{q_A}\right) - \langle\Psi| \oplus_A \log\left(\sigma_A \otimes \bar{\rho}_A^{-1}\right)|\Psi\rangle \\ &= \sum_A p_A \log\left(\frac{p_A}{q_A}\right) + \langle\Psi| \oplus_A (I_A \otimes \log\bar{\rho}_A)|\Psi\rangle - \langle\Psi| \oplus_A (\log\sigma_A \otimes I_{\bar{A}})|\Psi\rangle \\ &= \sum_A p_A \log\left(\frac{p_A}{q_A}\right) + \sum_A p_A \langle\psi_A| I_A \otimes \log\bar{\rho}_A |\psi_A\rangle - \sum_A p_A \langle\psi_A| \log\sigma_A \otimes I_{\bar{A}} |\psi_A\rangle \\ &= \sum_A p_A \log\left(\frac{p_A}{q_A}\right) + \sum_A p_A \mathrm{Tr}(\bar{\rho}_A \log\bar{\rho}_A) - \sum_A p_A \mathrm{Tr}(\rho_A \log\sigma_A). \quad (5.10) \end{aligned}$$

Now, each $|\psi_A\rangle$ is a pure state for each A, so $\mathrm{Tr}(\bar{\rho}_A \log\bar{\rho}_A) = \mathrm{Tr}(\rho_A \log\rho_A)$ for each A, where ρ_A is of course the reduced density matrix of $|\psi_A\rangle$ on the Hilbert space $\mathcal{H}_A$. Thus,

$$\begin{aligned} S(\Psi||\Phi:\mathcal{A}) &= \sum_A p_A \log\left(\frac{p_A}{q_A}\right) + \sum_A p_A \mathrm{Tr}(\rho_A \log\rho_A) - \sum_A p_A \mathrm{Tr}(\rho_A \log\sigma_A) \\ &= \sum_A p_A \log\left(\frac{p_A}{q_A}\right) + \sum_A p_A \left[\mathrm{Tr}(\rho_A \log\rho_A) - \mathrm{Tr}(\rho_A \log\sigma_A)\right]. \quad (5.11) \end{aligned}$$

This is a sum of a purely classical "relative entropy" of the probability distributions $\{p_A\}$ and $\{q_A\}$, and a weighted sum of the quantum relative entropies of the density matrices ρ_A and σ_A, weighed by the probabilities p_A. This is the usual definition of algebraic relative entropy for this type of von Neumann algebra. Moreover, the above expression is the type of relative entropy that appears in the equality of bulk and boundary relative entropies in the context of holographic operator algebra quantum error correction.

The algebraic Renyi relative entropy is defined by Lashkari [64] using modular operators as

$$S_\alpha(\Phi||\Omega:\mathcal{A}) = \frac{1}{\alpha} \sup_{\Psi\in\mathcal{H}} \log\langle\Phi| \Delta^\alpha_{\Omega||\Psi} |\Phi\rangle,$$

for $\alpha > 0$, and similarly for $\alpha < 0$. Note that the index α is different than the index n above – they are related by $\alpha = \frac{n-1}{n}$. In order to analyze this, we first need to discuss various matrix norms. For a matrix X, its p-norm is defined to be

$$\|X\|_p \equiv Tr(|X|^p)^{1/p}.$$

This norm satisfies Holder's inequality

$$\|XY\|_1 \leq \|X\|_p \|Y\|_q,$$

where p and q satisfy $\frac{1}{p} + \frac{1}{q} = 1$, $p, q > 1$. Now, $Tr(XC) \leq \|XC\|_1$ so Holder's inequality tells us

$$\sup_{\|C\|_q=1} Tr(XC) \leq \|XC\|_1 \leq \|X\|_p \|C\|_q = \|X\|_p,$$

where $\frac{1}{p}+\frac{1}{q}=1$. The matrix X has polar decomposition $X=U|X|$. Consider an operator $C_0 = A|X|^{p/q}U^\dagger$, where A is a constant. We have that

$$\|C_0\|_q = A \cdot Tr(|X|^p)^{1/q}.$$

By requiring that $\|C_0\|_q = 1$, we find $A = \frac{1}{Tr(|X|^p)^{1/q}}$ so that

$$C_0 = \frac{|X|^{p/q}U^\dagger}{Tr(|X|^p)^{1/q}}.$$

We then find

$$Tr(XC_0) = \frac{Tr(U|X||X|^{p/q}U^\dagger)}{Tr(|X|^p)^{1/q}} = \frac{Tr(|X|^{1+p/q})}{Tr(|X|^p)^{1/q}}.$$

Now, $\frac{1}{p}+\frac{1}{q}=1$, so

$$Tr(XC_0) = \frac{Tr(|X|^p)}{Tr(|X|^p)^{1/q}} = Tr(|X|^p)^{1-1/q} = Tr(|X|^p)^{1/p} = \|X\|_p.$$

We know that $\sup_{\|C\|_q=1} Tr(XC) \leq \|X\|_p$, and that C_0 saturates this inequality with $\|C_0\|_q = 1$, so we conclude that

$$\sup_{\|C\|_q=1} Tr(XC) = \|X\|_p.$$

Now, recall that we wrote our state $|\Phi\rangle$ as $|\Phi\rangle = \sum_A s_A |\phi_A\rangle$. Each of the states $|\phi_A\rangle$ can in turn be written as $|\phi_A\rangle = \sum_\alpha d(\alpha, A) |\alpha, \alpha, A\rangle$. The reduced density matrix of $|\phi_A\rangle$ on $\mathcal{H}_A$ is then

$$\sigma_A = \sum_\alpha |d(\alpha, A)|^2 |\alpha, A\rangle \langle \alpha, A|.$$

Therefore, for full rank σ_A,

$$|\phi_A\rangle = (\sigma_A^{1/2} \otimes I_{\bar{A}}) \sum_\alpha |\alpha, \alpha, A\rangle.$$

Now, let X and Y be two Hermitian operators, so that

$$\begin{aligned}\langle\phi_A| X \otimes Y |\phi_A\rangle &= \sum_{\alpha,\beta} \langle \alpha, \alpha, A| \sigma_A^{1/2} X \sigma_A^{1/2} \otimes Y |\beta, \beta, A\rangle \\ &= \sum_{\alpha,\beta} \langle \alpha, A| \sigma_A^{1/2} X \sigma_A^{1/2} |\beta, A\rangle \langle \beta, A| Y |\alpha, A\rangle \\ &= \sum_{\alpha,\beta} \langle \alpha, A| \sigma_A^{1/2} X \sigma_A^{1/2} Y |\alpha, A\rangle = \mathrm{Tr}_{\mathcal{H}_A}(\sigma_A^{1/2} X \sigma_A^{1/2} Y). \quad (5.12)\end{aligned}$$

We can apply this result to the algebraic relative Renyi entropy. We use the same notation for the expansions of $|\Psi\rangle$ and $|\Phi\rangle$ as before. We can write the state $|\Omega\rangle$ as

$$|\Omega\rangle = \sum_A t_A |\omega_A\rangle ,$$

and write $|\omega_A\rangle$ as

$$|\omega_A\rangle = \sum_\mu g(\mu, A) |\mu, \mu, A\rangle ,$$

where $|\mu, \mu, A\rangle = |\mu, A\rangle \otimes |\mu, A\rangle'$, $\{|\mu, A\rangle\}$ is an orthonormal basis for $\mathcal{H}_A$, and $\{|\mu, A\rangle'\}$ is an orthonormal basis for $\mathcal{H}_{\bar{A}}$. We have our usual normalization conditions

$$\sum_A |t_A|^2 = 1, \sum_\mu |g(\mu, A)|^2 = 1.$$

We write τ_A for the reduced density matrix of $|\omega_A\rangle$ on $\mathcal{H}_A$, and $\bar{\tau}_A$ for the reduced density matrix of $|\omega_A\rangle$ on $\mathcal{H}_{\bar{A}}$.

Recall that our modular operator $\Delta_{\Omega||\Psi}$ is given by

$$\Delta_{\Omega||\Psi} = \oplus_A \left(\frac{p_A}{w_A} \rho_A \otimes \bar{\tau}_A^{-1} \right) ,$$

where $w_A \equiv |t_A|^2$. The algebraic relative Renyi entropy is then given by

$$\begin{aligned} S_\alpha(\Phi||\Omega : \mathcal{A}) &= \frac{1}{\alpha} \sup_{\Psi|\langle\Psi|\Psi\rangle=1} \log \langle\Phi| \Delta_{\Omega||\Psi} |\Phi\rangle \\ &= \frac{1}{\alpha} \sup_{\Psi|\langle\Psi|\Psi\rangle=1} \log \left(\sum_A q_A \frac{p_A^\alpha}{w_A^\alpha} \langle\phi_A| \rho_A^\alpha \otimes \bar{\tau}_A^{-\alpha} |\phi_A\rangle \right) . \end{aligned} \tag{5.13}$$

We can use our result above to write this as

$$\begin{aligned} S_\alpha(\Phi||\Omega : \mathcal{A}) &= \frac{1}{\alpha} \sup_{\Psi|\langle\Psi|\Psi\rangle=1} \log \left(\sum_A q_A \frac{p_A^\alpha}{w_A^\alpha} \mathrm{Tr}_{\mathcal{H}_A} (\sigma_A^{1/2} \rho_A^\alpha \sigma_A^{1/2} \tau_A^{-\alpha}) \right) \\ &= \frac{1}{\alpha} \sup_{\Psi|\langle\Psi|\Psi\rangle=1} \log \left(\sum_A q_A \frac{p_A^\alpha}{w_A^\alpha} \mathrm{Tr}_{\mathcal{H}_A} (\rho_A^\alpha \sigma_A^{1/2} \tau_A^{-\alpha} \sigma_A^{1/2}) \right) . \end{aligned} \tag{5.14}$$

We are taking the supremum over all $|\Psi\rangle \in \mathcal{H}$ that are normalized. This is equivalent to, in the notation used above, $\sum_A p_A = 1$ and $Tr(\rho_A) = 1$ for all A. So, we need to take the supremum over all probability distributions $\{p_A\}$ (which we write as $\sup_{\{p_A\}}$, where it is understood that we are taking the supremum over all p_A with all $p_A > 0$ and $\sum_A p_A = 1$), and

the supremum over all normalized density matrices ρ_A. Define $\eta_A = \rho_A^\alpha$, so that $Tr(\rho_A) = 1$ is equivalent to $\|\eta\|_{1/\alpha} = 1$. Putting this all together,

$$S_\alpha(\Phi||\Omega : \mathcal{A}) = \frac{1}{\alpha} \sup_{\{p_A\}} \log \left(\sum_A q_A \frac{p_A^\alpha}{w_A^\alpha} \sup_{\eta_A | \|\eta_A\|_{1/\alpha}=1} \mathrm{Tr}_{\mathcal{H}_A}(\eta_A \sigma_A^{1/2} \tau_A^{-\alpha} \sigma_A^{1/2}) \right).$$

Now define $X_A = \tau_A^{-\alpha/2} \sigma_A^{1/2}$ so that (using the equality of sup-norm and matrix norm derived above)

$$\begin{aligned} \sup_{\eta_A | \|\eta_A\|_{1/\alpha}=1} \mathrm{Tr}_{\mathcal{H}_A}(\eta_A \sigma_A^{1/2} \bar{\tau}_A^{-\alpha} \sigma_A^{1/2}) &= \sup_{\eta_A | \|\eta_A\|_{1/\alpha}=1} \mathrm{Tr}_{\mathcal{H}_A}(\eta_A X_A^\dagger X_A) = \left\| X_A^\dagger X_A \right\|_{\frac{1}{1-\alpha}} \\ &= \left\| X_A X_A^\dagger \right\|_{\frac{1}{1-\alpha}} = \left(Tr \left[(\tau_A^{-\alpha/2} \sigma_A \tau_A^{-\alpha/2})^{\frac{1}{1-\alpha}} \right] \right)^{1-\alpha} = \exp(\alpha S_\alpha(\sigma_A||\tau_A)), \quad (5.15) \end{aligned}$$

where

$$S_\alpha(\sigma_A||\tau_A) = \frac{1-\alpha}{\alpha} \log \left(Tr \left[(\tau_A^{-\alpha/2} \sigma_A \tau_A^{-\alpha/2})^{\frac{1}{1-\alpha}} \right] \right)$$

is the sandwiched relative Renyi entropy defined earlier, with a different index, α, related to n by $\alpha = \frac{n-1}{n}$. Therefore,

$$S_\alpha(\Phi||\Omega : \mathcal{A}) = \frac{1}{\alpha} \max_{\{p_A\}} \log \left(\sum_A q_A \frac{p_A^\alpha}{w_A^\alpha} \exp(\alpha S_\alpha(\sigma_A||\tau_A)) \right).$$

We need to maximize the quantity in the logarithm, subject to the constraint that $\sum_A p_A = 1$. To do this, we introduce a Lagrange multiplier λ to enforce the constraint. We then define

$$f(p_A, \lambda) \equiv \sum_A q_A \frac{p_A^\alpha}{w_A^\alpha} \exp(\alpha S_\alpha(\sigma_A||\tau_A)) - \lambda \left(\sum_A p_A - 1 \right).$$

The maximum will then be given by the solution to the system

$$\frac{\partial f}{\partial p_A} = 0, \sum_A p_A = 1.$$

This gives

$$q_A \frac{p_A^{\alpha-1}}{w_A^\alpha} \exp(\alpha S_\alpha(\sigma_A||\tau_A)) = \lambda, \sum_A p_A = 1,$$

which means

$$p_A^{\alpha-1} = \lambda \frac{w_A^\alpha}{q_A} \exp(-\alpha S_\alpha(\sigma_A||\tau_A)),$$

$$p_A^\alpha = \lambda^{\frac{\alpha}{\alpha-1}} \frac{w_A^{\frac{\alpha^2}{\alpha-1}}}{q_A^{\frac{\alpha}{\alpha-1}}} \exp\left(-\frac{\alpha^2}{\alpha-1} S_\alpha(\sigma_A||\tau_A) \right).$$

Therefore,

$$S_\alpha(\Phi||\Omega:\mathcal{A}) = \frac{1}{\alpha}\log\left(\sum_A q_A \lambda^{\frac{\alpha}{\alpha-1}} \frac{w_A^{\frac{\alpha^2}{\alpha-1}}}{q_A^{\frac{\alpha}{\alpha-1}}} \exp\left(-\frac{\alpha^2}{\alpha-1}S_\alpha(\sigma_A||\tau_A)\right)\frac{1}{w_A^\alpha}\exp(\alpha S_\alpha(\sigma_A||\tau_A))\right)$$
$$= \frac{1}{\alpha}\log\left(\sum_A q_A \frac{w_A^{\frac{\alpha^2}{\alpha-1}}}{q_A^{\frac{\alpha}{\alpha-1}}} \exp\left(-\frac{\alpha^2}{\alpha-1}S_\alpha(\sigma_A||\tau_A)\right)\frac{1}{w_A^\alpha}\exp(\alpha S_\alpha(\sigma_A||\tau_A))\right) + \frac{1}{\alpha}\log\left(\lambda^{\frac{\alpha}{\alpha-1}}\right). \tag{5.16}$$

Let us begin by considering the first term, which we call $\bar{S}_\alpha(\Phi||\Omega:\mathcal{A})$. We have

$$\bar{S}_\alpha(\Phi||\Omega:\mathcal{A}) = \frac{1}{\alpha}\log\left(\sum_A q_A \frac{w_A^{\frac{\alpha^2}{\alpha-1}}}{q_A^{\frac{\alpha}{\alpha-1}}} \exp\left(-\frac{\alpha^2}{\alpha-1}S_\alpha(\sigma_A||\tau_A)\right)\frac{1}{w_A^\alpha}\exp(\alpha S_\alpha(\sigma_A||\tau_A))\right)$$
$$= \frac{1}{\alpha}\log\left(\sum_A q_A^{\frac{\alpha-1}{\alpha-1}-\frac{\alpha}{\alpha-1}} w_A^{\frac{\alpha^2}{\alpha-1}-\frac{(\alpha^2-\alpha)}{\alpha-1}} \exp\left(\left[\frac{\alpha^2-\alpha}{\alpha-1}-\frac{\alpha^2}{\alpha-1}\right]S_\alpha(\sigma_A||\tau_A)\right)\right)$$
$$= \frac{1}{\alpha}\log\left(\sum_A q_A^{-\frac{1}{\alpha-1}} w_A^{\frac{\alpha}{\alpha-1}} \exp\left(\frac{-\alpha}{\alpha-1}S_\alpha(\sigma_A||\tau_A)\right)\right). \tag{5.17}$$

Next, we must solve for λ. We know that

$$p_A = \lambda^{\frac{1}{\alpha-1}} \frac{w_A^{\frac{\alpha}{\alpha-1}}}{q_A^{\frac{1}{\alpha-1}}} \exp\left(-\frac{\alpha}{\alpha-1}S_\alpha(\sigma_A||\tau_A)\right),$$

$$\sum_A p_A = 1.$$

Hence,

$$\lambda^{\frac{1}{\alpha-1}} \sum_A \left[\frac{w_A^{\frac{\alpha}{\alpha-1}}}{q_A^{\frac{1}{\alpha-1}}} \exp\left(-\frac{\alpha}{\alpha-1}S_\alpha(\sigma_A||\tau_A)\right)\right] = 1$$

so that

$$\lambda^{\frac{1}{\alpha-1}} = \frac{1}{\sum_A \left[\frac{w_A^{\frac{\alpha}{\alpha-1}}}{q_A^{\frac{1}{\alpha-1}}} \exp\left(-\frac{\alpha}{\alpha-1}S_\alpha(\sigma_A||\tau_A)\right)\right]}.$$

The second term in $S_\alpha(\Phi||\Omega:\mathcal{A})$ therefore becomes

$$\frac{1}{\alpha}\log\left(\lambda^{\frac{\alpha}{\alpha-1}}\right) = \log\left(\lambda^{\frac{1}{\alpha-1}}\right) = -\log\left(\sum_A q_A^{\frac{1}{\alpha-1}} w_A^{\frac{\alpha}{\alpha-1}} \exp\left(-\frac{\alpha}{\alpha-1}S_\alpha(\sigma_A||\tau_A)\right)\right).$$

Finally, putting everything together, we obtain an expression for the algebraic relative Renyi entropy,

$$\begin{aligned} S_\alpha(\Phi||\Omega:\mathcal{A}) &= \bar{S}_\alpha(\Phi||\Omega:\mathcal{A}) + \frac{1}{\alpha}\log\left(\lambda^{\frac{\alpha}{\alpha-1}}\right) \\ &= \frac{1}{\alpha}\log\left(\sum_A q_A^{-\frac{1}{\alpha-1}} w_A^{\frac{\alpha}{\alpha-1}} \exp\left(\frac{-\alpha}{\alpha-1}S_\alpha(\sigma_A||\tau_A)\right)\right) \\ &\quad - \log\left(\sum_A q_A^{\frac{1}{\alpha-1}} w_A^{\frac{\alpha}{\alpha-1}} \exp\left(-\frac{\alpha}{\alpha-1}S_\alpha(\sigma_A||\tau_A)\right)\right) \\ &= \frac{1-\alpha}{\alpha}\log\left(\sum_A q_A^{-\frac{1}{\alpha-1}} w_A^{\frac{\alpha}{\alpha-1}} \exp\left(\frac{-\alpha}{\alpha-1}S_\alpha(\sigma_A||\tau_A)\right)\right). \end{aligned} \tag{5.18}$$

We now rewrite this in terms of the index n, related to α by $\alpha = \frac{n-1}{n} = 1-\frac{1}{n}$ so that $n = \frac{1}{1-\alpha}$ and $\frac{\alpha}{1-\alpha} = n-1$. Thus, we find

$$S_n(\Phi||\Omega:\mathcal{A}) = \frac{1}{n-1}\log\left(\sum_A q_A^n w_A^{1-n}\exp((n-1)S_n(\sigma_A||\tau_A))\right),$$

which is exactly the form of relative Renyi entropy obtained in the holographic error-correction setting above.

5.5 Numerical Tensor Network Calculations

The discussion above established an equivalence between *exact* equality of bulk and boundary sandwiched Renyi relative entropy and other entries in the AdS/CFT dictionary, such as the exact equality of bulk and boundary relative entropy as well as exact quantum error correction. Previous work has shown that approximate equality of bulk and boundary relative entropy can lead to bounds on approximate error correction [35]. Thus, it is of interest to have an understanding of approximate equality of bulk and boundary Renyi relative entropy.

To this end, we consider random tensor networks as a model of AdS/CFT [56] (i.e., tensor networks where the tensors are drawn from probability distributions). Random tensor networks have been a very useful tool for understanding features of the entanglement structure of AdS/CFT, such as the RT formula, the equality of bulk and boundary relative entropy, reflected entropy and so on [63, 56, 3].

We study a simple random tensor network with 1 tensor, 1 bulk qudit, whose Hilbert space has dimension d_{bulk}, and two boundary qudits, whose Hilbert spaces have dimensions $d_{bdy,1}$ and $d_{bdy,2}$. We consider two states ρ_b, σ_b on the bulk qudit. We can calculate, for example, the bulk relative entropy between these states as usual. To find the corresponding boundary quantity, we proceed as follows. Let $|0_x\rangle$ be a fixed state on all the qudits. We

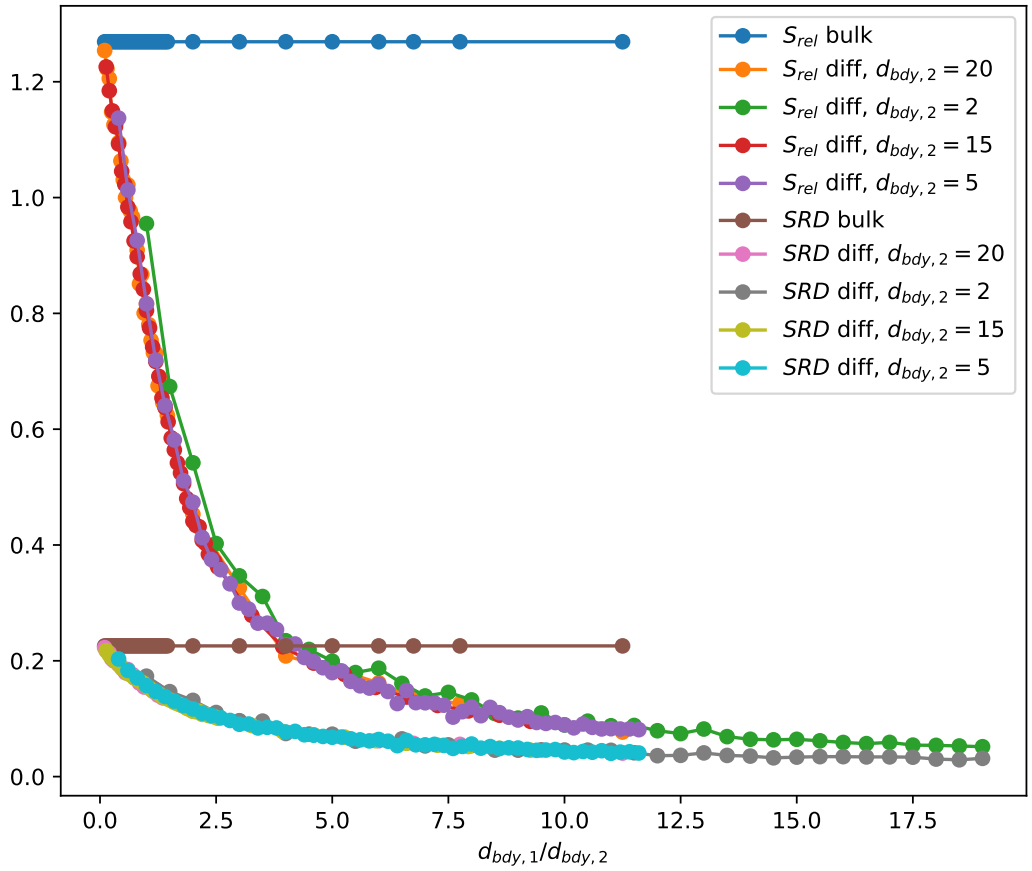

Figure 5.1: Difference between the bulk relative entropy and the (averaged) relative entropy of the states on boundary qudit 1 for various values of the boundary bond dimensions, and the difference between the bulk SRD and the (averaged) SRD on boundary qudit 1 for Renyi index $\alpha = 0.2$

then generate a Haar-random unitary U, and let $|V_x\rangle = U|0_x\rangle$. We then calculate the corresponding boundary state corresponding to our bulk state ρ_b:

$$\rho_{bdy} = Tr_{bulk}(\rho_{bulk} |V_x\rangle \langle V_x|),$$

where Tr_{bulk} is a trace over the bulk leg. The state on, e.g., boundary qudit 1 can obtained by taking a further partial trace $\rho_1 = Tr_2\rho_{bdy}$. To obtain the sandwiched Renyi divergence on boundary qudit 1, we compute the SRD of ρ_1 and σ_1, and average over Haar-random unitary matrices U.

We now consider specific cases, setting $d_{bulk} = 2$ throughout. First, we calculate the difference between the bulk relative entropy and the (averaged) relative entropy of the states on boundary qudit 1 for various values of the boundary bond dimensions, and the difference between the bulk SRD and the (averaged) SRD on boundary qudit 1 for Renyi index $\alpha = 0.2$. The results are shown for a specific example in Figure 5.1. From this figure, we see that these differences only depend on the ratio of our boundary bond dimensions $x \equiv \frac{d_{bdy,1}}{d_{bdy,2}}$. As we increase x, the difference converges to 0, so that equality of bulk and boundary relative entropy (as well as bulk and boundary SRD) holds.

In Figure 5.2, we plot the SRD difference as a function of $d_{bdy,1}$ (with $d_{bdy,2} = 20$) for two different values of $\alpha = 0.8, 7.4$. The $\alpha = 7.4$ difference seems to fall off somewhat faster.

In Figure 5.3, we plot the bulk and boundary qudit 1 SRD (and their difference) as a function of Renyi index α, with $d_{bdy,1} = 6, d_{bdy,2} = 2$. In addition, we plot the data from Figure 5.1 on a log-log plot, shown in Figure 5.4. It seems that the SRD difference is has a peak close to (but not equal to) $\alpha = 1$. At $\alpha = 1$, of course, the SRD is the usual relative entropy. Thus, there are values of the index α where the difference in SRD is smaller than the difference in relative entropy. It would be very interesting to see if these leads to new bounds on, for example, approximate reconstruction of bulk operators. We leave such investigations for future work.

5.6 Conclusions

In this chapter, we have explored the role of the sandwiched Renyi relative entropy in AdS/CFT. In particular, we have shown that the equivalence of bulk and boundary sandwiched Renyi relative entropy is equivalent to the RT formula, algebraic encoding, subregion duality, and the equivalence of bulk and boundary relative entropy, expanding the equivalence theorem (established in [51]) of the latter four statements. We then discussed the Renyi relative entropies from the perspective of modular operators. In the context of finite-dimensional von Neumann algebras, this algebraic definition of the sandwiched Renyi relative entropy was shown to reduce to the form found in the context of the holographic error-correction setting. Finally, we explored numerical calculations of the sandwiched Renyi relative entropy in a simple random holographic tensor network.

There are several possible avenues for further investigation. Previous work has shown that the corrections to the equality of bulk and boundary relative entropy can bound errors

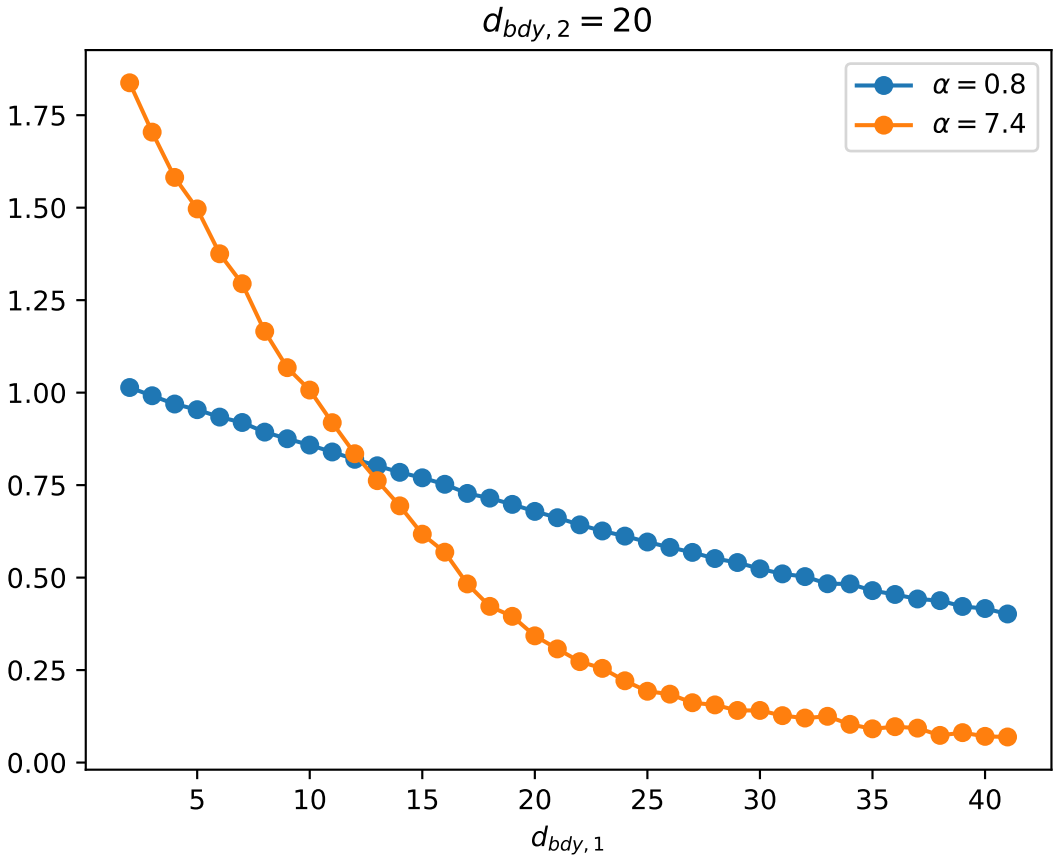

Figure 5.2: The SRD difference as a function of $d_{bdy,1}$ (with $d_{bdy,2} = 20$) for two different values of $\alpha = 0.8, 7.4$.

on the reconstruction of low-energy bulk operators [35] using the twirled Petz map. It would interesting to see if the corrections to the sandwiched Renyi relative entropies can place a similar bound on the accuracy of the reconstruction of low-energy bulk operators, perhaps using some channel other than the twirled Petz map. In particular, it would be of great interest if there were situations in AdS/CFT where the bounds on the differences between bulk and boundary SRD's lead to a more accurate reconstruction of bulk operators than the bound on the difference between bulk and boundary relative entropies. It would also be interesting to continue to do numerical simulations on larger tensor networks, in addition to investigating possible analytic results on sandwiched Renyi relative entropies in various tensor network models of holography.

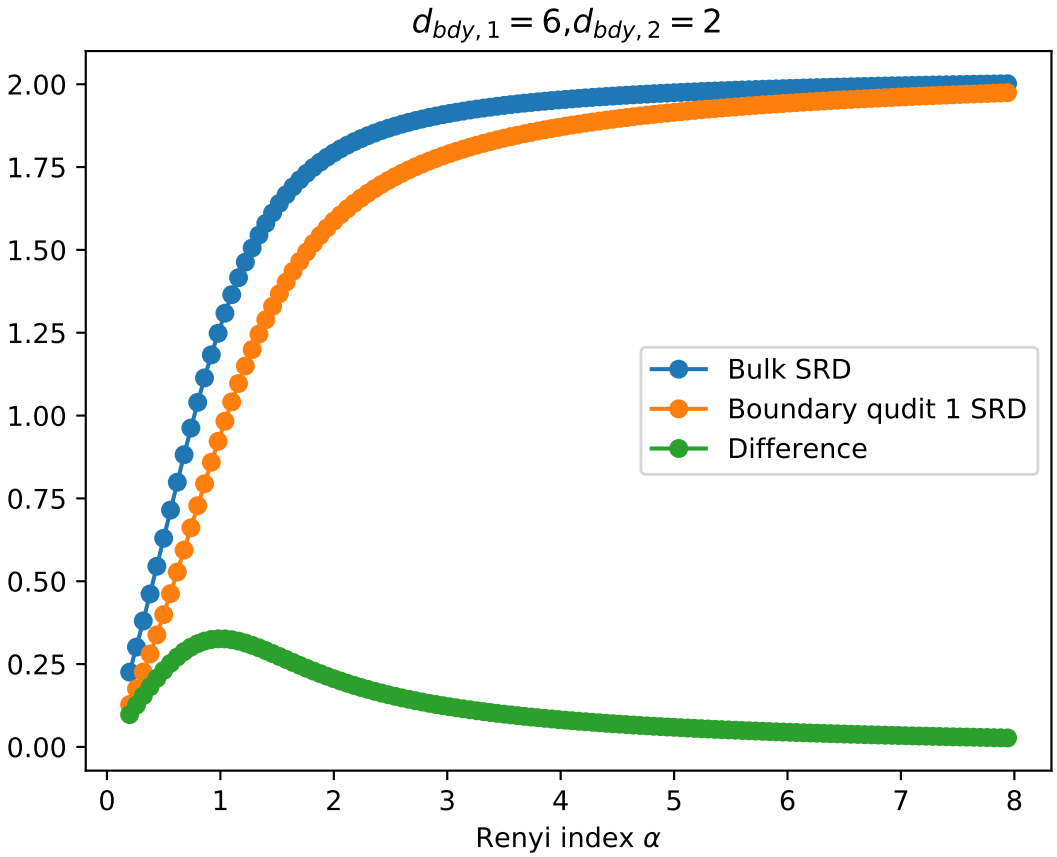

Figure 5.3: Bulk and boundary qudit 1 SRD (and their difference) as a function of Renyi index α, with $d_{bdy,1} = 6, d_{bdy,2} = 2$

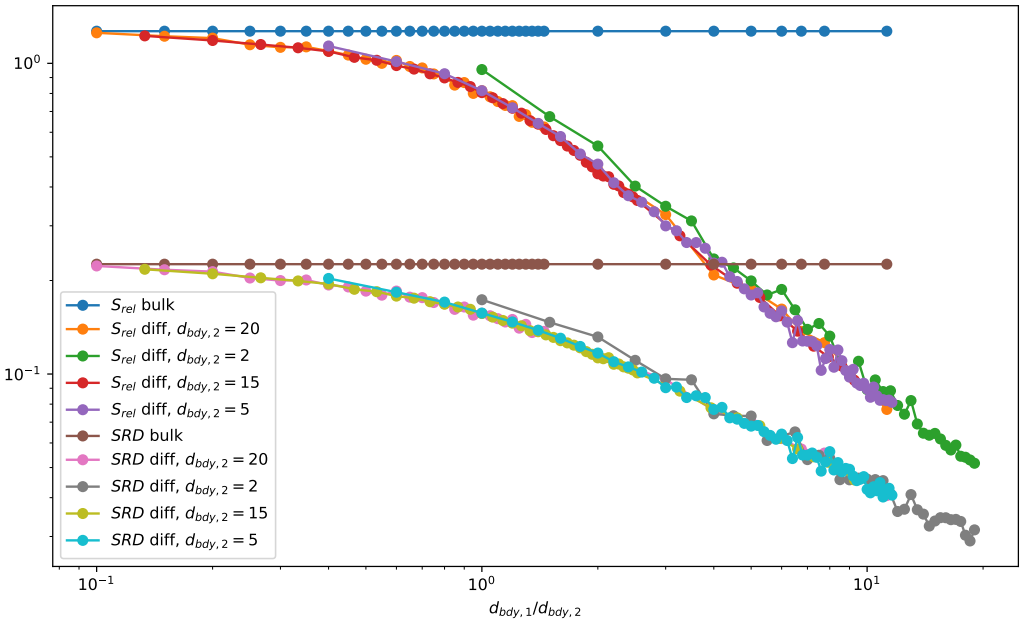

Figure 5.4: The data from Figure 5.1 on a log-log plot

Bibliography

[1] Gerard 't Hooft. "Dimensional reduction in quantum gravity". In: *Conf. Proc. C* 930308 (1993), pp. 284–296. arXiv: gr-qc/9310026.

[2] Chris Akers and Pratik Rath. "Holographic Renyi Entropy from Quantum Error Correction". In: *JHEP* 05 (2019), p. 052. DOI: 10.1007/JHEP05(2019)052. arXiv: 1811.05171 [hep-th].

[3] Chris Akers et al. "Reflected entropy in random tensor networks". In: *JHEP* 05 (2022), p. 162. DOI: 10.1007/JHEP05(2022)162. arXiv: 2112.09122 [hep-th].

[4] Andrea Allais and Erik Tonni. "Holographic evolution of the mutual information". In: *JHEP* 01 (2012), p. 102. DOI: 10.1007/JHEP01(2012)102. arXiv: 1110.1607 [hep-th].

[5] Ahmed Almheiri, Xi Dong, and Daniel Harlow. "Bulk Locality and Quantum Error Correction in AdS/CFT". In: *JHEP* 04 (2015), p. 163. DOI: 10.1007/JHEP04(2015)163. arXiv: 1411.7041 [hep-th].

[6] Ahmed Almheiri et al. "Replica Wormholes and the Entropy of Hawking Radiation". In: *JHEP* 05 (2020), p. 013. DOI: 10.1007/JHEP05(2020)013. arXiv: 1911.12333 [hep-th].

[7] Ahmed Almheiri et al. "The entropy of bulk quantum fields and the entanglement wedge of an evaporating black hole". In: *JHEP* 12 (2019), p. 063. DOI: 10.1007/JHEP12(2019)063. arXiv: 1905.08762 [hep-th].

[8] Vijay Balasubramanian et al. "Binding Complexity and Multiparty Entanglement". In: *JHEP* 02 (2019), p. 069. DOI: 10.1007/JHEP02(2019)069. arXiv: 1811.04085 [hep-th].

[9] Vijay Balasubramanian et al. "Quantum Complexity of Time Evolution with Chaotic Hamiltonians". In: *JHEP* 01 (2020), p. 134. DOI: 10.1007/JHEP01(2020)134. arXiv: 1905.05765 [hep-th].

[10] Ning Bao and Márk Mezei. "On the Entropy Cone for Large Regions at Late Times". In: (Oct. 2018). arXiv: 1811.00019 [hep-th].

[11] Ning Bao, Mudassir Moosa, and Ibrahim Shehzad. "The holographic dual of Rényi relative entropy". In: *JHEP* 08 (2019), p. 099. DOI: 10.1007/JHEP08(2019)099. arXiv: 1904.08433 [hep-th].

[12] Ning Bao et al. "The Holographic Entropy Cone". In: *JHEP* 09 (2015), p. 130. DOI: 10.1007/JHEP09(2015)130. arXiv: 1505.07839 [hep-th].

[13] James M. Bardeen, B. Carter, and S. W. Hawking. "The Four laws of black hole mechanics". In: *Commun. Math. Phys.* 31 (1973), pp. 161–170. DOI: 10.1007/BF01645742.

[14] Jacob D. Bekenstein. "A Universal Upper Bound on the Entropy to Energy Ratio for Bounded Systems". In: *Phys. Rev. D* 23 (1981), p. 287. DOI: 10.1103/PhysRevD.23.287.

[15] Jacob D. Bekenstein. "Black holes and entropy". In: *Phys. Rev. D* 7 (1973), pp. 2333–2346. DOI: 10.1103/PhysRevD.7.2333.

[16] Raphael Bousso. "A Covariant entropy conjecture". In: *JHEP* 07 (1999), p. 004. DOI: 10.1088/1126-6708/1999/07/004. arXiv: hep-th/9905177.

[17] Raphael Bousso. "The Holographic principle". In: *Rev. Mod. Phys.* 74 (2002), pp. 825–874. DOI: 10.1103/RevModPhys.74.825. arXiv: hep-th/0203101.

[18] Raphael Bousso and Netta Engelhardt. "Generalized Second Law for Cosmology". In: *Phys. Rev. D* 93.2 (2016), p. 024025. DOI: 10.1103/PhysRevD.93.024025. arXiv: 1510.02099 [hep-th].

[19] Raphael Bousso and Netta Engelhardt. "New Area Law in General Relativity". In: *Phys. Rev. Lett.* 115.8 (2015), p. 081301. DOI: 10.1103/PhysRevLett.115.081301. arXiv: 1504.07627 [hep-th].

[20] Raphael Bousso and Netta Engelhardt. "Proof of a New Area Law in General Relativity". In: *Phys. Rev. D* 92.4 (2015), p. 044031. DOI: 10.1103/PhysRevD.92.044031. arXiv: 1504.07660 [gr-qc].

[21] Raphael Bousso et al. "Quantum focusing conjecture". In: *Phys. Rev. D* 93.6 (2016), p. 064044. DOI: 10.1103/PhysRevD.93.064044. arXiv: 1506.02669 [hep-th].

[22] Adam R. Brown and Leonard Susskind. "Complexity geometry of a single qubit". In: *Phys. Rev. D* 100.4 (2019), p. 046020. DOI: 10.1103/PhysRevD.100.046020. arXiv: 1903.12621 [hep-th].

[23] Adam R. Brown and Leonard Susskind. "Second law of quantum complexity". In: *Phys. Rev. D* 97.8 (2018), p. 086015. DOI: 10.1103/PhysRevD.97.086015. arXiv: 1701.01107 [hep-th].

[24] Adam R. Brown, Leonard Susskind, and Ying Zhao. "Quantum Complexity and Negative Curvature". In: *Phys. Rev. D* 95.4 (2017), p. 045010. DOI: 10.1103/PhysRevD.95.045010. arXiv: 1608.02612 [hep-th].

[25] Adam R. Brown et al. "Complexity, action, and black holes". In: *Phys. Rev. D* 93.8 (2016), p. 086006. DOI: 10.1103/PhysRevD.93.086006. arXiv: 1512.04993 [hep-th].

[26] Adam R. Brown et al. "Holographic Complexity Equals Bulk Action?" In: *Phys. Rev. Lett.* 116.19 (2016), p. 191301. DOI: 10.1103/PhysRevLett.116.191301. arXiv: 1509.07876 [hep-th].

[27] Reginald J. Caginalp. "Holographic Complexity in FRW Spacetimes". In: *Phys. Rev. D* 101.6 (2020), p. 066027. DOI: 10.1103/PhysRevD.101.066027. arXiv: 1906.02227 [hep-th].

[28] Reginald J. Caginalp. "Holographic entropy cone in AdS-Vaidya spacetimes". In: *Phys. Rev. D* 101.2 (2020), p. 026010. DOI: 10.1103/PhysRevD.101.026010. arXiv: 1905.00544 [hep-th].

[29] Reginald J. Caginalp. "Sandwiched Renyi Relative Entropy in AdS/CFT". In: (Apr. 2022). arXiv: 2204.07694 [hep-th].

[30] Reginald J. Caginalp and Samuel Leutheusser. "Complexity in One- and Two-Qubit Systems". In: (Oct. 2020). arXiv: 2010.15099 [hep-th].

[31] Robert Callan, Jian-Yang He, and Matthew Headrick. "Strong subadditivity and the covariant holographic entanglement entropy formula". In: *JHEP* 06 (2012), p. 081. DOI: 10.1007/JHEP06(2012)081. arXiv: 1204.2309 [hep-th].

[32] Dean Carmi et al. "On the Time Dependence of Holographic Complexity". In: *JHEP* 11 (2017), p. 188. DOI: 10.1007/JHEP11(2017)188. arXiv: 1709.10184 [hep-th].

[33] Shira Chapman, Hugo Marrochio, and Robert C. Myers. "Holographic complexity in Vaidya spacetimes. Part II". In: *JHEP* 06 (2018), p. 114. DOI: 10.1007/JHEP06(2018)114. arXiv: 1805.07262 [hep-th].

[34] Shira Chapman et al. "Toward a Definition of Complexity for Quantum Field Theory States". In: *Phys. Rev. Lett.* 120.12 (2018), p. 121602. DOI: 10.1103/PhysRevLett.120.121602. arXiv: 1707.08582 [hep-th].

[35] Jordan Cotler et al. "Entanglement Wedge Reconstruction via Universal Recovery Channels". In: *Phys. Rev. X* 9.3 (2019), p. 031011. DOI: 10.1103/PhysRevX.9.031011. arXiv: 1704.05839 [hep-th].

[36] Josiah Couch et al. "Holographic complexity and noncommutative gauge theory". In: *JHEP* 03 (2018), p. 108. DOI: 10.1007/JHEP03(2018)108. arXiv: 1710.07833 [hep-th].

[37] Bartlomiej Czech and Xi Dong. "Holographic Entropy Cone with Time Dependence in Two Dimensions". In: *JHEP* 10 (2019), p. 177. DOI: 10.1007/JHEP10(2019)177. arXiv: 1905.03787 [hep-th].

[38] Xi Dong. "The Gravity Dual of Renyi Entropy". In: *Nature Commun.* 7 (2016), p. 12472. DOI: 10.1038/ncomms12472. arXiv: 1601.06788 [hep-th].

[39] Xi Dong, Daniel Harlow, and Donald Marolf. "Flat entanglement spectra in fixed-area states of quantum gravity". In: *JHEP* 10 (2019), p. 240. DOI: 10.1007/JHEP10(2019)240. arXiv: 1811.05382 [hep-th].

[40] Xi Dong, Daniel Harlow, and Aron C. Wall. "Reconstruction of Bulk Operators within the Entanglement Wedge in Gauge-Gravity Duality". In: *Phys. Rev. Lett.* 117.2 (2016), p. 021601. DOI: 10.1103/PhysRevLett.117.021601. arXiv: 1601.05416 [hep-th].

[41] Xi Dong, Aitor Lewkowycz, and Mukund Rangamani. "Deriving covariant holographic entanglement". In: *JHEP* 11 (2016), p. 028. DOI: 10.1007/JHEP11(2016)028. arXiv: 1607.07506 [hep-th].

[42] William Donnelly et al. "Living on the Edge: A Toy Model for Holographic Reconstruction of Algebras with Centers". In: *JHEP* 04 (2017), p. 093. DOI: 10.1007/JHEP04(2017)093. arXiv: 1611.05841 [hep-th].

[43] Mark R. Dowling and Michael A. Nielsen. *The geometry of quantum computation*. 2006. arXiv: quant-ph/0701004 [quant-ph].

[44] Christian Ecker et al. "Quantum Null Energy Condition and its (non)saturation in 2d CFTs". In: *SciPost Phys.* 6.3 (2019), p. 036. DOI: 10.21468/SciPostPhys.6.3.036. arXiv: 1901.04499 [hep-th].

[45] Netta Engelhardt and Aron C. Wall. "Quantum Extremal Surfaces: Holographic Entanglement Entropy beyond the Classical Regime". In: *JHEP* 01 (2015), p. 073. DOI: 10.1007/JHEP01(2015)073. arXiv: 1408.3203 [hep-th].

[46] Johanna Erdmenger et al. "Time evolution of entanglement for holographic steady state formation". In: *JHEP* 10 (2017), p. 034. DOI: 10.1007/JHEP10(2017)034. arXiv: 1705.04696 [hep-th].

[47] Mario Flory et al. "Time dependence of entanglement for steady state formation in AdS_3/CFT_2". In: *J. Phys. Conf. Ser.* 942.1 (2017). Ed. by Piero Nicolini et al., p. 012010. DOI: 10.1088/1742-6596/942/1/012010. arXiv: 1709.08614 [hep-th].

[48] Mile Gu, Andrew Doherty, and Michael A. Nielsen. "Quantum control via geometry: An explicit example". In: *Physical Review A* 78.3 (Sept. 2008). ISSN: 1094-1622. DOI: 10.1103/physreva.78.032327. URL: http://dx.doi.org/10.1103/PhysRevA.78.032327.

[49] S. S. Gubser, Igor R. Klebanov, and Alexander M. Polyakov. "Gauge theory correlators from noncritical string theory". In: *Phys. Lett. B* 428 (1998), pp. 105–114. DOI: 10.1016/S0370-2693(98)00377-3. arXiv: hep-th/9802109.

[50] Daniel Harlow. "TASI Lectures on the Emergence of Bulk Physics in AdS/CFT". In: *PoS* TASI2017 (2018), p. 002. DOI: 10.22323/1.305.0002. arXiv: 1802.01040 [hep-th].

[51] Daniel Harlow. "The Ryu–Takayanagi Formula from Quantum Error Correction". In: *Commun. Math. Phys.* 354.3 (2017), pp. 865–912. DOI: 10.1007/s00220-017-2904-z. arXiv: 1607.03901 [hep-th].

[52] Thomas Hartman and Juan Maldacena. "Time Evolution of Entanglement Entropy from Black Hole Interiors". In: *JHEP* 05 (2013), p. 014. DOI: 10.1007/JHEP05(2013)014. arXiv: 1303.1080 [hep-th].

[53] S. W. Hawking. "Black hole explosions". In: *Nature* 248 (1974), pp. 30–31. DOI: 10.1038/248030a0.

[54] S. W. Hawking. "Particle Creation by Black Holes". In: *Commun. Math. Phys.* 43 (1975). Ed. by G. W. Gibbons and S. W. Hawking. [Erratum: Commun.Math.Phys. 46, 206 (1976)], pp. 199–220. DOI: 10.1007/BF02345020.

[55] Patrick Hayden, Matthew Headrick, and Alexander Maloney. "Holographic Mutual Information is Monogamous". In: *Phys. Rev. D* 87.4 (2013), p. 046003. DOI: 10.1103/PhysRevD.87.046003. arXiv: 1107.2940 [hep-th].

[56] Patrick Hayden et al. "Holographic duality from random tensor networks". In: *JHEP* 11 (2016), p. 009. DOI: 10.1007/JHEP11(2016)009. arXiv: 1601.01694 [hep-th].

[57] Matthew Headrick. "General properties of holographic entanglement entropy". In: *JHEP* 03 (2014), p. 085. DOI: 10.1007/JHEP03(2014)085. arXiv: 1312.6717 [hep-th].

[58] Matthew Headrick and Tadashi Takayanagi. "A Holographic proof of the strong subadditivity of entanglement entropy". In: *Phys. Rev. D* 76 (2007), p. 106013. DOI: 10.1103/PhysRevD.76.106013. arXiv: 0704.3719 [hep-th].

[59] Sergio Hernández Cuenca. "Holographic entropy cone for five regions". In: *Phys. Rev. D* 100.2 (2019), p. 026004. DOI: 10.1103/PhysRevD.100.026004. arXiv: 1903.09148 [hep-th].

[60] Veronika E. Hubeny, Mukund Rangamani, and Tadashi Takayanagi. "A Covariant holographic entanglement entropy proposal". In: *JHEP* 07 (2007), p. 062. DOI: 10.1088/1126-6708/2007/07/062. arXiv: 0705.0016 [hep-th].

[61] Daniel L. Jafferis et al. "Relative entropy equals bulk relative entropy". In: *JHEP* 06 (2016), p. 004. DOI: 10.1007/JHEP06(2016)004. arXiv: 1512.06431 [hep-th].

[62] Ro Jefferson and Robert C. Myers. "Circuit complexity in quantum field theory". In: *JHEP* 10 (2017), p. 107. DOI: 10.1007/JHEP10(2017)107. arXiv: 1707.08570 [hep-th].

[63] Jonah Kudler-Flam and Pratik Rath. "Large and small corrections to the JLMS Formula from replica wormholes". In: *JHEP* 08 (2022), p. 189. DOI: 10.1007/JHEP08(2022)189. arXiv: 2203.11954 [hep-th].

[64] Nima Lashkari. "Constraining Quantum Fields using Modular Theory". In: *JHEP* 01 (2019), p. 059. DOI: 10.1007/JHEP01(2019)059. arXiv: 1810.09306 [hep-th].

[65] Felix Leditzky. *Relative entropies and their use in quantum information theory*. 2016. arXiv: 1611.08802 [quant-ph].

[66] Luis Lehner et al. "Gravitational action with null boundaries". In: *Phys. Rev. D* 94.8 (2016), p. 084046. DOI: 10.1103/PhysRevD.94.084046. arXiv: 1609.00207 [hep-th].

[67] Aitor Lewkowycz and Juan Maldacena. "Generalized gravitational entropy". In: *JHEP* 08 (2013), p. 090. DOI: 10.1007/JHEP08(2013)090. arXiv: 1304.4926 [hep-th].

[68] E. H. Lieb and M. B. Ruskai. "Proof of the strong subadditivity of quantum-mechanical entropy". In: *J. Math. Phys.* 14 (1973), pp. 1938–1941. DOI: 10.1063/1.1666274.

[69] Elliott H. Lieb and Mary Beth Ruskai. "A Fundamental Property of Quantum-Mechanical Entropy". In: *Phys. Rev. Lett.* 30 (1973), pp. 434–436. DOI: 10.1103/PhysRevLett.30.434.

[70] Seth Lloyd. "Ultimate physical limits to computation". In: *Nature* 406 (2000), pp. 1047–1054. DOI: 10.1038/35023282.

[71] Juan Martin Maldacena. "The Large N limit of superconformal field theories and supergravity". In: *Adv. Theor. Math. Phys.* 2 (1998), pp. 231–252. DOI: 10.4310/ATMP.1998.v2.n2.a1. arXiv: hep-th/9711200.

[72] Mudassir Moosa, Pratik Rath, and Vincent Paul Su. "A Rényi quantum null energy condition: proof for free field theories". In: *JHEP* 01 (2021), p. 064. DOI: 10.1007/JHEP01(2021)064. arXiv: 2007.15025 [hep-th].

[73] Martin Müller-Lennert et al. "On quantum Rényi entropies: A new generalization and some properties". In: *J. Math. Phys.* 54.12 (2013), p. 122203. DOI: 10.1063/1.4838856. arXiv: 1306.3142 [quant-ph].

[74] Michael A. Nielsen. *A geometric approach to quantum circuit lower bounds*. 2005. arXiv: quant-ph/0502070 [quant-ph].

[75] Michael A. Nielsen et al. "Optimal control, geometry, and quantum computing". In: *Physical Review A* 73.6 (June 2006). ISSN: 1094-1622. DOI: 10.1103/physreva.73.062323. URL: http://dx.doi.org/10.1103/PhysRevA.73.062323.

[76] Michael A. Nielsen et al. "Quantum Computation as Geometry". In: *Science* 311.5764 (Feb. 2006), pp. 1133–1135. ISSN: 1095-9203. DOI: 10.1126/science.1121541. URL: http://dx.doi.org/10.1126/science.1121541.

[77] Yasunori Nomura, Pratik Rath, and Nico Salzetta. "Spacetime from Unentanglement". In: *Phys. Rev. D* 97.10 (2018), p. 106010. DOI: 10.1103/PhysRevD.97.106010. arXiv: 1711.05263 [hep-th].

[78] Yasunori Nomura and Nico Salzetta. "Butterfly Velocities for Holographic Theories of General Spacetimes". In: *JHEP* 10 (2017), p. 187. DOI: 10.1007/JHEP10(2017)187. arXiv: 1708.04237 [hep-th].

[79] Yasunori Nomura et al. "Toward a Holographic Theory for General Spacetimes". In: *Phys. Rev. D* 95.8 (2017), p. 086002. DOI: 10.1103/PhysRevD.95.086002. arXiv: 1611.02702 [hep-th].

[80] Fernando Pastawski et al. "Holographic quantum error-correcting codes: Toy models for the bulk/boundary correspondence". In: *JHEP* 06 (2015), p. 149. DOI: 10.1007/JHEP06(2015)149. arXiv: 1503.06237 [hep-th].

[81] Geoff Penington et al. "Replica wormholes and the black hole interior". In: *JHEP* 03 (2022), p. 205. DOI: 10.1007/JHEP03(2022)205. arXiv: 1911.11977 [hep-th].

[82] Geoffrey Penington. "Entanglement Wedge Reconstruction and the Information Paradox". In: *JHEP* 09 (2020), p. 002. DOI: 10.1007/JHEP09(2020)002. arXiv: 1905.08255 [hep-th].

[83] Andrea Prudenziati. "Strong subadditivity and holography". In: *Phys. Rev. D* 93.10 (2016), p. 106003. DOI: 10.1103/PhysRevD.93.106003. arXiv: 1509.07885 [hep-th].

[84] Massimiliano Rota and Sean J. Weinberg. "New constraints for holographic entropy from maximin: A no-go theorem". In: *Phys. Rev. D* 97.8 (2018), p. 086013. DOI: 10.1103/PhysRevD.97.086013. arXiv: 1712.10004 [hep-th].

[85] Shinsei Ryu and Tadashi Takayanagi. "Holographic derivation of entanglement entropy from AdS/CFT". In: *Phys. Rev. Lett.* 96 (2006), p. 181602. DOI: 10.1103/PhysRevLett.96.181602. arXiv: hep-th/0603001.

[86] Fabio Sanches and Sean J. Weinberg. "Holographic entanglement entropy conjecture for general spacetimes". In: *Phys. Rev. D* 94.8 (2016), p. 084034. DOI: 10.1103/PhysRevD.94.084034. arXiv: 1603.05250 [hep-th].

[87] Stephen H. Shenker and Douglas Stanford. "Black holes and the butterfly effect". In: *JHEP* 03 (2014), p. 067. DOI: 10.1007/JHEP03(2014)067. arXiv: 1306.0622 [hep-th].

[88] Douglas Stanford and Leonard Susskind. "Complexity and Shock Wave Geometries". In: *Phys. Rev. D* 90.12 (2014), p. 126007. DOI: 10.1103/PhysRevD.90.126007. arXiv: 1406.2678 [hep-th].

[89] Leonard Susskind. "Computational Complexity and Black Hole Horizons". In: *Fortsch. Phys.* 64 (2016). [Addendum: Fortsch.Phys. 64, 44–48 (2016)], pp. 24–43. DOI: 10.1002/prop.201500092. arXiv: 1403.5695 [hep-th].

[90] Leonard Susskind. "The World as a hologram". In: *J. Math. Phys.* 36 (1995), pp. 6377–6396. DOI: 10.1063/1.531249. arXiv: hep-th/9409089.

[91] Leonard Susskind. "Three Lectures on Complexity and Black Holes". In: SpringerBriefs in Physics. Springer, Oct. 2018. DOI: 10.1007/978-3-030-45109-7. arXiv: 1810.11563 [hep-th].

[92] Leonard Susskind and Ying Zhao. "Switchbacks and the Bridge to Nowhere". In: (Aug. 2014). arXiv: 1408.2823 [hep-th].

[93] Brian Swingle and Yixu Wang. "Holographic Complexity of Einstein-Maxwell-Dilaton Gravity". In: *JHEP* 09 (2018), p. 106. DOI: 10.1007/JHEP09(2018)106. arXiv: 1712.09826 [hep-th].

[94] Aron C. Wall. "Maximin Surfaces, and the Strong Subadditivity of the Covariant Holographic Entanglement Entropy". In: *Class. Quant. Grav.* 31.22 (2014), p. 225007. DOI: 10.1088/0264-9381/31/22/225007. arXiv: 1211.3494 [hep-th].

[95] Mark M. Wilde, Andreas Winter, and Dong Yang. "Strong Converse for the Classical Capacity of Entanglement-Breaking and Hadamard Channels via a Sandwiched Renyi Relative Entropy". In: *Commun. Math. Phys.* 331.2 (2014), pp. 593–622. DOI: 10.1007/s00220-014-2122-x. arXiv: 1306.1586 [quant-ph].

[96] Edward Witten. "Anti-de Sitter space and holography". In: *Adv. Theor. Math. Phys.* 2 (1998), pp. 253–291. DOI: 10.4310/ATMP.1998.v2.n2.a2. arXiv: hep-th/9802150.

[97] Edward Witten. "APS Medal for Exceptional Achievement in Research: Invited article on entanglement properties of quantum field theory". In: *Rev. Mod. Phys.* 90.4 (2018), p. 045003. DOI: 10.1103/RevModPhys.90.045003. arXiv: 1803.04993 [hep-th].

Appendix A

Appendix

A.1 Geodesic Kinematics for the Vaidya spacetime

In this Appendix, we describe some of the details of the geodesic kinematics for the Vaidya spacetime. The geodesic equation for v is given by

$$\ddot{v} + \frac{1}{2}\partial_r f \dot{v}^2 - r\dot{x}^2 = 0,$$

where an overdot denotes a derivative with respect to the affine parameter τ. In addition, the tangent vector $dx^\mu/d\tau$ has unit norm, so that

$$-f(r,v)\dot{v}^2 + 2\dot{v}\dot{r} + r^2\dot{x}^2 = 1.$$

Because the metric has no explicit x-dependence, the quantity $p_x \equiv g_{xx}\dot{x} = r^2\dot{x}$ is conserved along the geodesic. When we express the metric in terms of t and r (instead of v and r), we found that the metric takes the form

$$ds^2 = -h(r)dt^2 + \frac{1}{h(r)}dr^2 + r^2dx^2,$$

where $h(r) = r^2$ in AdS, and $h(r) = r^2 - m$ in BTZ. For simplicity, we will set $m = 1$ throughout. Other than at the shell, there is no explicit dependence in the metric on t, so there is a quantity that is conserved except at the shell. It is given by

$$E \equiv g_{tt}\dot{t} = h(r)\dot{t}.$$

In these coordinates, the normalization condition for the vector $dx^\mu/d\tau$ becomes

$$-h(r)\dot{t}^2 + \frac{\dot{r}^2}{h(r)} + r^2\dot{x}^2 = 1$$

$$\dot{r}^2 = h + E^2 - \frac{hp_x^2}{r^2}$$

Alternatively, we can write this in terms of r', where the prime denotes a derivative with respect to x. Then we obtain

$$r'^2 = \frac{r^4 h}{p_x^2} + \frac{r^4 E^2}{p_x^2} - hr^2.$$

We will first solve these equations for constant time intervals, and then solve them for general covariant regions.

Constant Time Intervals for Positive-Energy Metric

We begin by considering a region A on the boundary that is constant in time, and is a single interval in x. That is,

$$A = \{(x,t) \in \text{CFT} | x \in [0, \ell_x], t = const = t_b\}.$$

To calculate the entanglement entropy $S(A)$ of this region in the CFT, the HRT prescription tells us that we need to find the extremal boundary-anchored curve (i.e., spacelike geodesic) χ_A such that $\partial\chi_A = \partial A$ and χ_A is homologous to A.

There are three cases (i) the geodesic is entirely in the AdS bulk, (ii) the geodesic is entirely in the BTZ bulk, or (iii) the geodesic is in both the BTZ bulk and the AdS bulk. See Figure A.1. We consider each of these cases in turn.

Geodesics Entirely in the AdS Bulk

We are considering a constant time geodesic in the AdS bulk, so $E = 0$. Therefore, we have

$$\frac{dr}{d\tau} = \sqrt{r^2 - p_x^2},$$

which has solution

$$r(\tau) = \frac{1}{2}(p_x^2 e^{-\tau} + e^{\tau}).$$

Now, x obeys the equation

$$\dot{x} = \frac{p_x}{r^2},$$

which has solution

$$x(\tau) = Const - \frac{2p_x}{p_x^2 + e^{2\tau}}.$$

This means that

$$\ell_x = x(\tau = \infty) - x(\tau = -\infty) = \frac{2}{p_x}.$$

We have normalized our affine parameter so that τ measures the length of the curve. For τ approaching $\pm\infty$, r approaches ∞. For large R, there are two roots of τ., one large and positive, the other large and negative. They are

$$\tau_{b-} = -\log(2R) + 2\log(p_x)$$

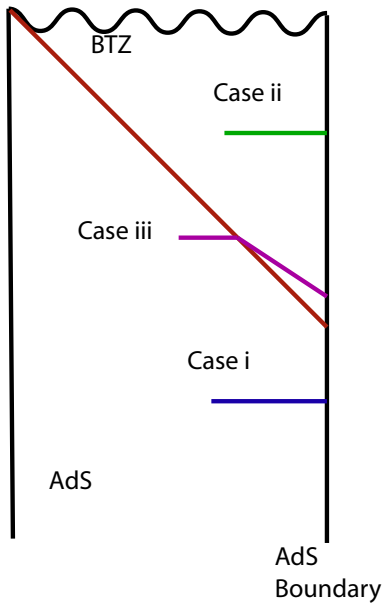

Figure A.1: A Penrose diagram of the Vaidya spacetime (the red line represents the shell of null matter), showing the three cases for the spacelike geodesics. (i) Entirely in the AdS bulk, (ii) entirely in the BTZ bulk, and (iii) partially in the BTZ bulk, and partially in the AdS bulk.

$$\tau_{b+} = \log(2R),$$

so the total length of the curve is

$$L = \tau_{b+} - \tau_{b-} = 2\log(2R) - 2\log(p_x).$$

To get to the boundary, of course, we need to send $R \to \infty$, and the length diverges. Thus, to obtain a regularized, finite length, we need to subtract the UV-divergent term. Thus, we obtain:

$$L_{reg} = 2\log\frac{\ell_x}{2}.$$

This is a concave function, so it satisfies strong subadditivity.

Geodesics Entirely in the BTZ bulk

In this case we have

$$\dot{r} = \sqrt{r^2 - 1 + E^2 - p_x^2 + \frac{p_x^2}{r^2}}.$$

There are two solutions to this equation:

$$r_1(\tau) = \frac{1}{2}\sqrt{-2E^2 + 2p_x^2 + 2 + e^{2\tau} - E^4 e^{-2\tau} + 2E^2(p_x^2+1)e^{-2\tau} - (p^2-1)^2 e^{-2\tau}}, \quad \text{(A.1)}$$

$$r_2(\tau) = \frac{1}{2}\sqrt{(-E^2 + 2E^2 p_x^2 + 2E^2 - p_x^4 + 2p_x^2 - 1)e^{2\tau} - e^{-2\tau} - 2E^2 + 2p_x^2 + 2}. \quad \text{(A.2)}$$

With a few lines of algebra, we can cast these in the following form:

$$r_1(\tau)^2 = \frac{1}{4}(e^\tau + B_+ e^{-\tau})(e^\tau + B_- e^{-\tau}),$$

$$r_2(\tau)^2 = -\frac{1}{4}(B_+ e^\tau - e^{-\tau})(B_- e^\tau - e^{-\tau}),$$

where we have defined the quantities

$$B_\pm = (p_x \pm 1)^2 - E^2.$$

We are, of course, looking for geodesics that are boundary anchored. As τ goes to minus infinity, r_2^2 goes to $-1/4$. Thus, the solution r_2 can never describe the geodesics we are interested in. Therefore, we restrict our attention to the solution r_1. We first obtain expressions for x and t. We find

$$t(\tau) = const + \frac{1}{2}\log\left(\frac{A_- + e^{2\tau}}{A_+ + e^{2\tau}}\right),$$

$$x(\tau) = const - \frac{1}{2}\log\left(\frac{B_- + e^{2\tau}}{B_+ + e^{2\tau}}\right),$$

where we have defined

$$A_\pm = p_x^2 - (1 \pm E)^2.$$

An analysis exactly the same as above gives us that the regularized length is (subtracting off the UV-divergent term $2\log(2R)$)

$$L_{reg} = -\frac{1}{2}\log(B_+ B_-).$$

Meanwhile,

$$\Delta t = \frac{1}{2}\log(A_-/A_+),\ \ell_x = -\frac{1}{2}\log(B_-/B_+).$$

In particular, if we have a constant-time interval, then $E = 0$ and

$$L_{reg} = -\frac{1}{2}\log\left(p_x^2 - 1\right)^2, \ell_x = \frac{1}{2}\log\left(\frac{p_x+1}{p_x-1}\right).$$

Finally, we turn to geodesics that are partially in AdS and partially in BTZ.

Geodesics in both AdS and BTZ

Because the shell is located at $v = 0$, if the interval is at boundary time $t_b < 0$, it will be in pure AdS. If $t_b > 0$, then we calculate $v(\tau) = t(\tau) - \tanh^{-1}(1/r(\tau))$ for the pure BTZ geodesic, and see if it dips below 0. If it does, then it will have a component that is in the AdS bulk. If not, it will be contained entirely in the BTZ bulk.

We begin by considering what happens at the junction of AdS and BTZ. Because we do not want a delta function in v'', then v' needs to be continuous. This means:

$$v' = 2(r'_A - r'_B).$$

In AdS space, we have that

$$v' = t' + \frac{r'_A}{r_c^2} = \frac{E_A}{p_x} + \frac{r'_A}{r_c^2},$$

where r_c is the value of r when the geodesic crosses the shell, and E_A is the value of E in the AdS region. We combine these two to get

$$r'_B = -\frac{E_A}{2p_x} + \left(1 - \frac{1}{2r_c^2}\right) r'_A$$

From the BTZ side we know that

$$v' = t' + \frac{r'_B}{r_c^2 - 1} = \frac{r_c^2}{r_c^2 - 1}\frac{E_B}{p_x} + \frac{r'_B}{r_c^2} = \frac{r_c^2}{r_c^2 - 1}\frac{E_B}{p_x} + \frac{r'_B}{r_c^2 - 1}.$$

This gives us:

$$(r_c^2 - 1)\frac{E_A}{p_x} + r'_A - \frac{r'_A}{r_c^2} = r_c^2\frac{E_B}{p_x} + r'_B$$

$$(r_c^2 - \frac{1}{2})\frac{E_A}{p_x} - \frac{r'_A}{2r_c^2} = r_c^2\frac{E_B}{p_x}$$

$$E_B = (1 - \frac{1}{2r_c^2})E_A - \frac{p_x r'_A}{2r_c^4}.$$

In addition, we know that

$$r'_A = \sqrt{\frac{r_c^6}{p_x^2} + \frac{r_c^4 E_A^2}{p_x^2} - r_c^4}.$$

The value of the affine parameter in the BTZ geodesic when $r = r_c$ is given by

$$\begin{aligned}\alpha_c \equiv \exp(2\tau_c) = \frac{1}{2}[-(B_+ + B_-) + 4r_c^2 \\ + \sqrt{-4B_+B_- + (B_+ + B_- - 4r_c^2)^2}].\end{aligned} \tag{A.3}$$

There are two BTZ components. For second component, from τ_c to $\tau = \infty$, we have

$$\Delta x_B = x(\tau = \infty) - x(\tau_c) = -\frac{1}{2}\log\left(\frac{B_- + \alpha_c}{B_+ + \alpha_c}\right),$$

$$\Delta t_B = \frac{1}{2}\log\left(\frac{A_- + \alpha_c}{A_+ + \alpha_c}\right).$$

At the shell, we have that $t_c = \tanh^{-1}(1/r_c)$, so the boundary time is

$$t_b = \tanh^{-1}(1/r_c) + \Delta t_B.$$

Meanwhile, the length of the curve is

$$L_B = \log 2R - \frac{1}{2}\log\alpha_c.$$

By symmetry, the portion of the curve in AdS has $E = 0$, and the two BTZ components have the same Δx and the same length. The curve in AdS obeys

$$r(\tau) = \frac{1}{2}(p_x^2 e^{-\tau} + e^{\tau})$$

This satisfies $r = r_c$ at two values of the affine parameter

$$\tau_\pm = \log\Big(r_c \pm \sqrt{r_c^2 - p_x^2}\Big).$$

Using our expression for $x(\tau)$, we find that

$$\Delta x_A = x(\tau_+) - x(\tau_-) = \frac{2}{r_c p_x}\sqrt{r_c^2 - p_x^2}$$

and that

$$L_A = \tau_+ - \tau_- = \log\left(\frac{r_c + \sqrt{r_c^2 - p_x^2}}{r_c - \sqrt{r_c^2 - p_x^2}}\right).$$

We know that $L = L_A + 2L_B$ and $\ell_x = 2\Delta x_B + \Delta x_A$. We then find

$$\ell_x = \frac{2}{r_c p_x}\sqrt{r_c^2 - p_x^2} + \frac{1}{2}\log\left(\frac{B_+ + \alpha_c}{B_- + \alpha_c}\right),$$

$$L_{reg} = \log\left(\frac{r_c + \sqrt{r_c^2 - p_x^2}}{r_c - \sqrt{r_c^2 - p_x^2}}\right) - \log\alpha_c.$$

For given values of t_b and ℓ_x, we can solve numerically to find the corresponding values of r_c and p_x. We do this numerically for $t_b = 0.8$, and show the result in Figure A.2.

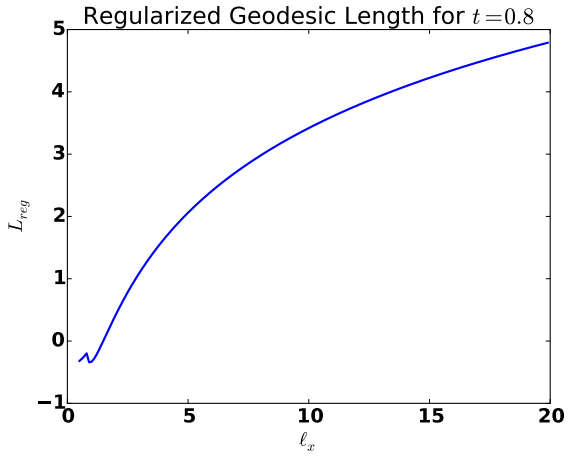

Figure A.2: The regularized geodesic length L_{reg} as a function of the boundary interval length, ℓ_x at boundary time $t_b = 0.8$.

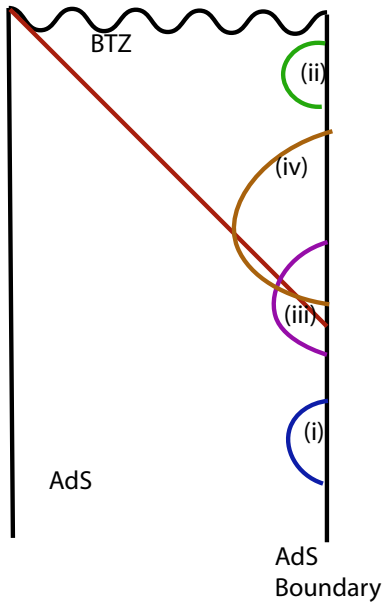

Figure A.3: A Penrose diagram of the Vaidya spacetime (the red line represents the shell of null matter), showing the four cases for the general spacelike geodesics. (i) Entirely in the AdS bulk, (ii) entirely in the BTZ bulk, (iii) starts in AdS, crosses into BTZ, and (iv) starts in BTZ, crosses into AdS, and crosses back into BTZ.

Spacelike Intervals with Nonzero Δt for Positive-Energy Metric

In this situation, there are four cases: (i) entirely in AdS, (ii) entirely in BTZ, (iii) starts in AdS, crosses into BTZ, (iv) starts in BTZ, crosses into AdS, crosses back into BTZ. See Figure A.3. Without loss of generality, suppose $\Delta t \geq 0$. Then the interval is characterized by three parameters, $\Delta x, \Delta t$, and the starting boundary time of the interval t_b. Again, because the shell is located at $v = 0$, if $t_b < 0$, the curve is either (i) or (iii). If $t_b \geq 0$, the curve is either (ii) or (iv).

Geodesics entirely in AdS or BTZ

We begin with the AdS case. The solution is:

$$r(\tau) = \frac{1}{2}((p_x^2 - E^2)e^{-\tau} + e^{\tau}),$$

$$t(\tau) = Const - \frac{2E}{p_x^2 - E^2 + e^{2\tau}},$$

$$x(\tau) = Const - \frac{2p_x}{p_x^2 - E^2 + e^{2\tau}}.$$

This is very similar to the case considered above with $E = 0$. We calculate

$$\Delta x = \frac{2p_x}{p_x^2 - E^2}, \Delta t = \frac{2E}{p_x^2 - E^2}, L_{reg} = -\log\left(p_x^2 - E^2\right).$$

We calculated the solution to the BTZ case with $E \neq 0$ above. The solution is

$$r(\tau)^2 = \frac{1}{4}(e^{\tau} + B_+ e^{-\tau})(e^{\tau} + B_- e^{-\tau}),$$

$$t(\tau) = Const + \frac{1}{2}\log\left(\frac{A_- + e^{2\tau}}{A_+ + e^{2\tau}}\right),$$

$$x(\tau) = Const - \frac{1}{2}\log\left(\frac{B_- + e^{2\tau}}{B_+ + e^{2\tau}}\right),$$

where we have defined the quantities

$$B_\pm = (p_x \pm 1)^2 - E^2, A_\pm = p_x^2 - (1 \pm E)^2.$$

This tells us that

$$\Delta x = \frac{1}{2}\log\left(\frac{A_-}{A_+}\right), \Delta t = -\frac{1}{2}\log\left(\frac{B_-}{B_+}\right), L_{reg} = -\frac{1}{2}\log(B_+ B_-).$$

We now turn our attention to the geodesics that cross the shell.

Geodesics that start in AdS, end in BTZ

In this case, the geodesic intersects the shell once, say at coordinate r_c. The affine parameter (in the AdS portion) at which the crossing occurs is

$$\tau_c = \log\left(r_c + \sqrt{r_c^2 + E_A^2 - p_x^2}\right)$$

Because this occurs at the shell, we need $t_c = t(\tau_c) = 1/r_c$, which fixes the constant in the equation for $t(\tau)$. The length of the geodesic in AdS is given by

$$L_A = \log 2R + \log\left(r_c + \sqrt{r_c^2 + E_A^2 - p_x^2}\right) - \log\left(p_x^2 - E_A^2\right).$$

Meanwhile,

$$\begin{aligned} \Delta x_A &= \frac{2p_x}{p_x^2 - E_A^2} - \frac{p_x}{r_c(r_c + \sqrt{r_c^2 + E_A^2 - p_x^2})}, \\ \Delta t_A &= \frac{E_A}{p_x}\Delta x_A. \end{aligned} \tag{A.4}$$

As we calculated above, the value of E in the BTZ portion is given by

$$E_B = (1 - \frac{1}{2r_c^2})E_A - \frac{p_x r'_A}{2r_c^4},\ r'_A = \sqrt{\frac{r_c^6}{p_x^2} + \frac{r_c^4 E_A^2}{p_x^2} - r_c^4}.$$

The value of the affine parameter in the BTZ portion of the crossing is

$$\begin{aligned} \alpha_B \equiv \exp(2\tau_B) = \frac{1}{2}[-(B_+ + B_-) + 4r_c^2 \\ + \sqrt{-4B_+B_- + (B_+ + B_- - 4r_c^2)^2}], \end{aligned} \tag{A.5}$$

where $B_\pm$ is as defined above, using the energy E_B. Furthermore, we have

$$\Delta x_B = x(\tau = \infty) - x(\tau_B) = -\frac{1}{2}\log\left(\frac{B_- + \alpha_B}{B_+ + \alpha_B}\right),$$

$$\Delta t_B = \frac{1}{2}\log\left(\frac{A_- + \alpha_B}{A_+ + \alpha_B}\right),$$

$$L_B = \log 2R - \frac{1}{2}\log\alpha_B.$$

In the AdS region, the time of the boundary crossing is given by $t_c = 1/r_c$. Therefore, the starting time of the interval is

$$t_b = \frac{1}{r_c} - \Delta t_A.$$

The total (regularized) length of the curve is

$$\begin{aligned} L_{reg} &= -\frac{1}{2}\log\alpha_c = \log 2R + \\ &\log\left(r_c + \sqrt{r_c^2 + E_A^2 - p_x^2}\right) - \log\left(p_x^2 - E_A^2\right), \end{aligned} \tag{A.6}$$

while

$$\Delta x = \Delta x_A + \Delta x_B, \Delta t = \Delta t_A + \Delta t_B.$$

Geodesics that start in BTZ, cross into AdS, end in BTZ

Finally we consider the geodesics that start in the BTZ bulk (so that $t_b = 0$), cross over into the AdS bulk, and then cross back to the BTZ bulk. These geodesics cross the shell twice, say at r_1 and r_2, with $r_1 > r_2$. If the part of the geodesic in AdS has E_A, then the length of the AdS portion is given by

$$\begin{aligned} L_A = \tau_1 - \tau_2 &= \log\left(r_1 + \sqrt{r_1^2 + E_A^2 - p_x^2}\right) \\ &- \log\left(r_2 + \sqrt{r_2^2 + E_A^2 - p_x^2}\right). \end{aligned} \tag{A.7}$$

Also,

$$\Delta t_A = \frac{1}{r_2} - \frac{1}{r_1}, \Delta x_A = \frac{p_x}{E_A}\Delta t_A.$$

We now consider the BTZ portions of the geodesics. Consider the upper BTZ arc of the geodesic. The shell is at $v = 0$, so since $r_1 > r_2$, $r_1' < 0$. Thus, we obtain

$$r_A^{1\prime} = -\sqrt{\frac{r_1^6}{p_x^2} + \frac{r_1^4 E_A^2}{p_x^2} - r_1^4},$$

and

$$E_{B1} = (1 - \frac{1}{2r_1^2})E_A - \frac{p_x r_A^{1\prime}}{2r_1^4}.$$

We know r x and t as functions of τ for the BTZ curve for these values of the conserved momenta. We can numerically solve for τ_B^1 when r_{B1} is equal to r_1. Because $t_{B1}(\tau_B^1)$ has to be equal to $\tanh^{-1}(1/r_1)$, this fixes the constant. We then compute

$$\begin{aligned} &\Delta x_{B1} = x_{B1}(\tau_\infty) - x_{B1}(\tau_B^1), \Delta x_{B1} = x_{B1}(\infty) - x_{B1}(\tau_B^1), \\ &L_{B1} = \tau_\infty - \tau_B^1. \end{aligned} \tag{A.8}$$

We repeat this procedure for the bottom BTZ arc. For r_2, however, $r_A^{2\prime} > 0$, so that

$$r_A^{1\prime} = \sqrt{\frac{r_2^6}{p_x^2} + \frac{r_2^4 E_A^2}{p_x^2} - r_2^4},$$

which means

$$E_{B2} = (1 - \frac{1}{2r_2^2})E_A - \frac{p_x r_A^{1\prime}}{2r_2^4}.$$

We then follow the same procedure to compute $\Delta x_{B2}, \Delta t_{B2}$ and L_{B2}. The totals are, of course,

$$\Delta x = \Delta x_A + \Delta x_{B1} + \Delta x_{B2}, \Delta t = \Delta t_A + \Delta t_{B1} + \Delta t_{B2}.$$

To obtain the regularized geodesic length, we have to subtract off the usual UV-divergent term:

$$L_{reg} = L_A + L_{B1} + L_{B2} - 2\log(2R).$$

The boundary time of the start point of the interval is given by

$$t_b = \frac{1}{r_1} - \Delta t_{B1}.$$

If we are given r_1 and E_A, we can calculate r_2 as follows. In the AdS region, we can solve for the value of τ at which r is equal t or_1. We know that t evaluated at this value is $1/r_1$, which fixes the value of the integration constant in the $t(\tau)$ function. We then find the other value of τ for which the function $v(\tau) = r(\tau) - \frac{1}{t(\tau)}$ vanishes. Evaluating the function $r(\tau)$ at this value then gives us r_2. Therefore, the geodesic is specified by three parameters: E_A, p_x, and r_1. From these we can calculate the starting time t_b and the values of Δx and Δt. For values of t_b, Δx and Δt, we can numerically find the corresponding values of E_A, p_x, and r_1, and then use these to calculate the geodesic lengths.

Geodesic Kinematics for Constant-Time Intervals for Negative-Energy Metric

We consider constant-time intervals. For boundary time $t_b < 0$ the geodesics will be entirely in the BTZ bulk, while for large enough t_b it will be entirely in the AdS bulk. These cases were treated above; we will now consider the case where the geodesic is partially in the AdS region, and partially in the BTZ region. We first consider the BTZ part. By the symmetry of the problem, $E = 0$ in the BTZ arc. Suppose that the geodesic crosses the shell at r_c. The value of the affine parameter at this value of r is

$$\tau_c = \log\Big(\sqrt{|r_c^2 - 1|} + \sqrt{|r_c^2 - p_x^2|}\Big).$$

From the equation for $\dot{r}$, it is clear that $r = p_x$ is the turning point. Therefore, by symmetry, the length of the BTZ part of the geodesic is

$$L_B = 2(\tau_c - \tau_{p_x}) = 2\log\left(\frac{\sqrt{|r_c^2 - 1|} + \sqrt{|r_c^2 - p_x^2|}}{\sqrt{|p_x^2 - 1|}}\right).$$

Similarly, the change in x is given by

$$\begin{aligned}\Delta x_B = &-\log\left(\frac{(p_x-1)^2+(\sqrt{|r_c^2-1|}+\sqrt{|r_c^2-p_x^2|})^2}{(p_x+1)^2+(\sqrt{|r_c^2-1|}+\sqrt{|r_c^2-p_x^2|})^2}\right)\\ &+\log\left(\frac{(p_x-1)^2+(\sqrt{|p_x^2-1|})^2}{(p_x+1)^2+(\sqrt{|p_x^2-1|})^2}\right).\end{aligned} \tag{A.9}$$

We now turn to the AdS components. Similar to the positive-energy case, we require that at the shell $v=0$ we must have

$$v' = 2(r'_A - r'_B).$$

$E_B = 0$ so

$$v' = \frac{r'_B}{r_c^2-1},$$

which means that

$$r'_A = r'_B + \frac{v'}{2} = r'_B + \frac{r'_B}{2(r_c^2-1)} = \frac{(2r_c^2-1)r'_B}{2(r_c^2-1)}.$$

Note that this means that r'_A becomes negative when $r_c < \frac{1}{2}$. In AdS, we know that

$$r'^2_A = \frac{r_c^6}{p_x^2} + \frac{r_c^4 E_A^2}{p_x^2} - r_c^4,$$

$$r'^2_A p_x^2 = r_c^6 + r_c^4 E_A^2 - r_c^4 p_x^2,$$

$$\frac{r'^2_A p_x^2}{r_c^4} + p_x^2 - r_c^2 = E_A^2,$$

$$E_A^2 = \frac{(2r_c^2-1)^2 r'^2_B p_x^2}{4r_c^4(r_c^2-1)^2} + p_x^2 - r_c^2.$$

Also, we know that

$$r'^2_B = (r_c^2-1)r_c^2\left(\frac{r_c^2}{p_x^2}-1\right),$$

which means

$$\begin{aligned}E_A^2 &= \frac{(2r_c^2-1)^2(r_c^2-p_x^2)}{4r_c^2(r_c^2-1)} + p_x^2 - r_c^2\\ &= \frac{((2r_c^2-1)^2 - 4r_c^4 + 4r_c^2)(r_c^2-p_x^2)}{4r_c^2(r_c^2-1)}\\ &= \frac{(r_c^2-p_x^2)}{4r_c^2(r_c^2-1)}.\end{aligned} \tag{A.10}$$

If $r_c > \frac{1}{2}$ then $r' > 0$ and $\dot{r} > 0$, and the solution is

$$r(\tau) = \frac{1}{2}(e^{\tau} + (p_x^2 - E^2)e^{-\tau}).$$

We have that

$$\tau_c = \log\left(r_c + \sqrt{r_c^2 + E_A^2 - p_x^2}\right).$$

For large R, the corresponding (large, positive) value of τ is $\log 2R$ so the length of the AdS arc is

$$L_A = \log 2R - \log\left(r_c + \sqrt{r_c^2 + E_A^2 - p_x^2}\right).$$

The change in x is given by

$$\Delta x_A = \frac{p_x}{r_c(r_c + \sqrt{r_c^2 + E_A^2 - p_x^2})}.$$

We find the starting point of the interval in the usual way:

$$t_b = t_c - \Delta t_A = \frac{1}{r_c} - \frac{E_A}{r_c(r_c + \sqrt{r_c^2 + E_A^2 - p_x^2})},$$

since $\Delta t_A = \Delta x_A \frac{E_A}{p_x}$. The total arc length and displacement are

$$L = L_B + 2L_A, \Delta x = 2\Delta x_A + \Delta x_B.$$

On the other hand, if $r_c < \frac{1}{2}$, $\dot{r} < 0$ and the solution is given by

$$r(\tau) = \frac{1}{2}(e^{-\tau} + (p_x^2 - E^2)e^{\tau}),$$

and we have that

$$\tau_c = -\log\left(r_c + \sqrt{r_c^2 + E_A^2 - p_x^2}\right).$$

The positive affine parameter for large R is given by

$$\tau_\infty = \log(2R) - \log\big(p_x^2 - E_A^2\big),$$

which means that the total length of the AdS arc is given by

$$\begin{aligned} L_A = \tau_\infty - \tau_c = \log(2R) - \log\big(p_x^2 - E_A^2\big) \\ + \log\left(r_c + \sqrt{r_c^2 + E_A^2 - p_x^2}\right). \end{aligned} \tag{A.11}$$

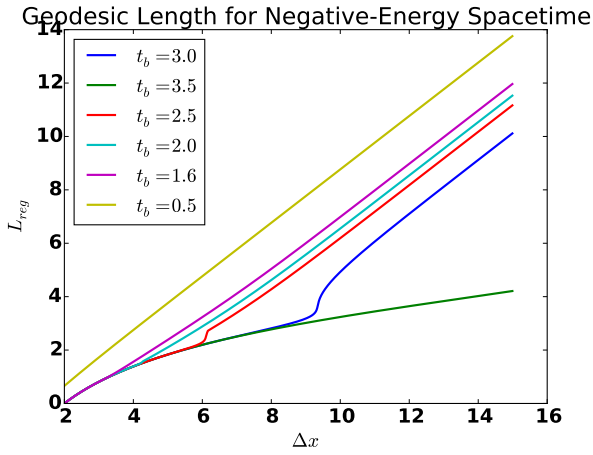

Figure A.4: The regularized geodesic length L_{reg} as a function of the boundary interval length, Δx for various values of the boundary time t_b in the negative-energy Vaidya spacetime. We see that the curves are not convex, meaning there will be violations of strong subadditivity

Meanwhile,

$$\Delta x_A = x(\tau_\infty) - x(\tau_c) = \frac{p_x}{r_c(r_c + \sqrt{r_c^2 + E_A^2 - p_x^2})} - \frac{2p_x}{-E_A^2 + p_x^2 + (p_x^2 - E_A^2)^2} \tag{A.12}$$

and

$$t_b = \frac{1}{r_c} - \frac{E_A}{p_x}\Delta x_A.$$

Once again, the total geodesic length and displacement are

$$L = L_B + 2L_A, \Delta x = 2\Delta x_A + \Delta x_B.$$

To find the geodesic for the negative-energy metric for a given interval, we proceed as follows. First, if $t_b \leq 0$, the geodesic is of course entirely in BTZ. If $t_b > 0$, we find the trajectory of the geodesic in AdS, and calculate $v(\tau)$. If at any point it dips below 0, then there will be a portion of the geodesic that is in the BTZ bulk. We then use a numerical algorithm to find the values of r_c and p_x that correspond to the desired t_b and Δx. We show a plot of the (regularized) geodesic length as a function of the displacement for various values of the boundary time t_b in Figure A.4. We see the non-convex behavior of some of these curves, which means that strong subadditivity will be violated.

A.2 Null Boundary and Corner Terms in the Action of a Spacetime Patch

Consider a spacetime region W. Its gravitational action will consist of the bulk Einstein-Hilbert and boundary Gibbons-Hawking-York term, as well as null boundary terms and corner terms. This prescription was first worked out in [66]. Suppose the boundary ∂W consists of several smooth pieces that are connected at "corners." Consider one such smooth, null component N, with corners B_1 and B_2. The boundary and corner terms are:

$$\begin{aligned}\mathcal{I}_N &= \frac{sgn(N)}{8\pi G_N}\int_N d\lambda d\theta\sqrt{\gamma}\kappa \\ &+ \frac{sgn(N)}{8\pi G_N}\int_N d\lambda d\theta\sqrt{\gamma}\Theta\log(l_c|\Theta|) + \frac{1}{8\pi G_N}\int_{B_1} d\theta\sqrt{\gamma}a_1 \\ &+ \frac{1}{8\pi G_N}\int_{B_2} d\theta\sqrt{\gamma}a_2,\end{aligned} \tag{A.13}$$

where $sgn(N)$ is +1 if N is to the future of W, and -1 if it is to the past of W. The quantities a_1, a_2 depend on the precise nature of the joint. In the case where we have a joint between two null surfaces, with normal vectors k and m, the joint will have

$$a = \pm\log\left|\frac{k\cdot m}{2}\right|.$$

The sign is determined is follows. If $W \subset J^+(N)$, and the corner is at the past end of N, or if $W \subset J^-(N)$, and the corner is at the future end of N, then the sign is positive. In all other cases, it is negative.

As was first demonstrated in [66], the above action is independent of the parameterization of the null generators of N. We demonstrate that here. Suppose, for definiteness, that W lies to the past of N. Let B_2 be at the future end of N, and let B_1 be at its past end. The boundary and corner terms associated to N are given by

$$\begin{aligned}\mathcal{A}_N &= \frac{-1}{8\pi G_N}\int_N d\lambda d\theta\sqrt{\gamma}\kappa - \frac{1}{8\pi G_N}\int_N d\lambda d\theta\sqrt{\gamma}\Theta\log(l_c|\Theta|) \\ &- \frac{1}{8\pi G_N}\int_{B_1} d\theta\sqrt{\gamma}A_1 + \frac{1}{8\pi G_N}\int_{B_2} d\theta\sqrt{\gamma}A_2,\end{aligned} \tag{A.14}$$

where A_i denotes the positive sign of a_i.

We now show that $\mathcal{I}_N$ is independent of the geodesic parameterization. Suppose that we parameterize the null geodesics by a new parameter, $\bar{\lambda}(\lambda,\theta)$, and define $e^{-\beta} \equiv d\bar{\lambda}/d\lambda$. Clearly, we have

$$\bar{k} = \frac{\partial\lambda}{\partial\bar{\lambda}}k = e^{\beta}k,$$

and that

$$\bar{\Theta} = \frac{1}{\sqrt{\gamma}} \frac{\partial \sqrt{\gamma}}{\partial \bar{\lambda}} = e^{\beta} \Theta.$$

We define the vector N^{α} to be the null vector such that $k^{\alpha} N_{\alpha} = -1$ so that

$$\kappa = -N_{\nu} k^{\mu} \nabla_{\mu} k^{\nu}.$$

Of course, $\bar{N} = e^{-\beta} N$ (since $\bar{k} \cdot \bar{N} = -1$), which means that

$$\bar{\kappa} = -N_{\nu} k^{\mu} \nabla_{\mu} (e^{\beta} k^{\nu}) = e^{\beta} \kappa - N_{\nu} k^{\nu} k^{\mu} \nabla_{\mu} e^{\beta} = e^{\beta} (\kappa + \partial_{\lambda} \beta).$$

Thus, since $\bar{A} = A + \beta$, we obtain

$$\begin{aligned}
\bar{\mathcal{I}}_N &= -\frac{1}{8\pi G_N} \int_N d\lambda d\theta \sqrt{\gamma} (\kappa + \partial_{\lambda} \beta) - \frac{1}{8\pi G_N} \int_N d\lambda d\theta \sqrt{\gamma} \Theta \log(l_c |\Theta|) \\
&- \frac{1}{8\pi G_N} \int_N d\lambda d\theta \sqrt{\gamma} \Theta \beta - \frac{1}{8\pi G_N} \int_{B_1} d\theta \sqrt{\gamma} A_1 + \frac{1}{8\pi G_N} \int_{B_2} d\theta \sqrt{\gamma} A_2 \\
&- \frac{1}{8\pi G_N} \int_{B_1} d\theta \sqrt{\gamma} \beta + \frac{1}{8\pi G_N} \int_{B_2} d\theta \sqrt{\gamma} \beta \\
&= -\frac{1}{8\pi G_N} \int_N d\lambda d\theta \sqrt{\gamma} \kappa + \frac{1}{8\pi G_N} \int_N d\lambda d\theta \beta \partial_{\lambda} \sqrt{\gamma} \\
&- \frac{1}{8\pi G_N} \int_N d\lambda d\theta \sqrt{\gamma} \Theta \log(l_c |\Theta|) - \frac{1}{8\pi G_N} \int_N d\lambda d\theta \sqrt{\gamma} \Theta \beta \\
&- \frac{1}{8\pi G_N} \int_{B_1} d\theta \sqrt{\gamma} A_1 + \frac{1}{8\pi G_N} \int_{B_2} d\theta \sqrt{\gamma} A_2 \\
&= -\frac{1}{8\pi G_N} \int_N d\lambda d\theta \sqrt{\gamma} \kappa - \frac{1}{8\pi G_N} \int_N d\lambda d\theta \sqrt{\gamma} \Theta \log(l_c |\Theta|) \\
&- \frac{1}{8\pi G_N} \int_{B_1} d\theta \sqrt{\gamma} A_1 + \frac{1}{8\pi G_N} \int_{B_2} d\theta \sqrt{\gamma} A_2 = \mathcal{I}_N.
\end{aligned}$$

Hence, we see that $\mathcal{I}_N$ is invariant under reparameterization.

A.3 Parameterization of One-Qubit Operators and Recurrence Times

In this Appendix, we give an analytic discussion of the parameterization of one-qubit operators and of recurrence times for time-evolution operators. Much of our discussion here overlaps with that in [9]. A general single-qubit "easy" Hamiltonian in our setup may be

described by a real three-dimensional vector J_i with[1]

$$H = \sum_{i=1}^{2} J_i \ \sigma^i.$$

Accordingly, we may introduce the magnitude $J = \sqrt{\sum_{i=1}^{2} J_i^2}$. The time-evolution unitary is then

$$U(t) = \cos(Jt) - i \sin(Jt) \ \hat{J}_i \sigma^i$$

with $\hat{J}_i \equiv J_i/J$. This makes it clear that the recurrence time-scale of the system is $t_{rec} = 2\pi/J$. It is clear that the coordinates describing the time-evolution unitary are $x^I(t) = -J_I t$ for the easy directions, and $x^3 = 0$ for the hard direction, since we have $U(t) = \exp(-iJ_i\sigma^i t)$. This is certainly true for small times $t << t_{rec}$; however, at large times, we can see that our parameterization of $SU(2)$ 'breaks down'.[2] Thus we see that the unitary described by $x^I(t)$ is equivalent to that described by $\tilde{x}_n^I(t) = -J_I t_n$ with $t_n \equiv t + 2\pi n/J$, for $n \in \mathbb{Z}$, and $I \in \{1, 2\}$, $\tilde{x}_n^3 = 0$. This is an example of a 'topological obstruction' discussed earlier.

It was shown in [9] that in the submanifold generated by easy directions, there are linear geodesics γ_n between the identity and any point in the "easy" submanifold. These geodesics are described by coordinate functions of the parameter $s \in [0, 1]$:

$$x_n^I(s; t) = -J_I \cdot t_n \cdot s,$$

for $I \in \{1, 2\}$, and $x_n^3(s; t) = 0$. It is clear from the metric in the space of unitaries, Eq 4.1, that the metric at the identity will be proportional to the cost factor, since our generators T_I are orthogonal. The above solution solves the geodesic equation, so s is an affine parameter, and therefore, the metric projected along the geodesic (expressed in terms of s) is a constant along the geodesic, since $x^I \propto s$. The geodesic passes through the identity, so the metric on the one-dimensional space (the geodesic) is the metric projected onto the tangent vector of our geodesic, which we call $h(s)$. This is

$$h(s) = g_{IJ} \frac{dx_n^I}{ds} \frac{dx_n^J}{ds} = 4 \sum_{I=1}^{2} J_I^2 \mathcal{I}_{II} \cdot (t_n)^2.$$

The length of these geodesics in the Nielsen metric are therefore given by

$$l(\gamma_n) = 2 \sqrt{\sum_{I=1}^{2} J_I^2 \mathcal{I}_{II}} \cdot |t_n|,$$

[1] In principle one should add a multiple of identity to H to ensure it is positive definite; however, this will not be important for our discussion.

[2] That this should happen is clear since, topologically, $SU(2) \sim S^3$ so it should be described by three angles, not an arbitrary three-dimensional vector. In geometric language, the coordinate chart, x^I, we have been using is really only valid for a subset of the x^I, not for $x^I \in \mathbb{R}^3$.

and minimizing over this family of geodesics gives the complexity

$$\mathcal{C}[U(t)] = 2\sqrt{\sum_{I=1}^{2} J_I^2 \mathcal{I}_{II}} \cdot \min_{n\in\mathbb{Z}} |t + 2\pi n/J|.$$

It is clear from this formula that the complexity of the time-evolution unitary will have initial linear growth until $t = \pi/J$ at which point it will decay linearly to zero and then the same curve will repeat with period $2\pi/J$. The geodesics with non-minimal n describe paths that 'wind' around the group many times before finally ending at the desired unitary.

The formula above for $\mathcal{C}[U(t)]$ shows us that the unitary complexity always grows linearly with time, and the only feature that is sensitive to the precise details of the complexity geometry is its slope. On the other hand, the qualitative behavior of the precursor complexity is sensitive to the precise details of the complexity metric.

We now briefly discuss precursor operators. We wish to discuss Pauli operators, however, these have determinant -1 and thus are not in $SU(2)$ so we choose to "re-phase by i" so that the operator $\tilde{\sigma}^i = i\sigma^i$ is described by coordinates $x^j = \frac{\pi}{2}\delta^{ji}$. Conjugation of $\tilde{\sigma}^i$ by the time evolution unitary yields an operator that is rotated by angle $2Jt$ around the $\hat{J}$ axis. Clearly this operator $\tilde{\sigma}^i(t)$ is still described by coordinate vector $x^j(t)$ of magnitude $\pi/2$. The complexity of the precursor is given by the length of the geodesic from the identity to the vector $x^j(t)$ in the Nielsen metric.

One finds that, for an initial operator $W_0 = F_i\tilde{\sigma}^i$ (with $|F|^2 = 1$ for unitary) we find the coordinates of the precursor $W(t)$ to be

$$\beta^k(t) = \frac{\pi}{2}\left(\cos(2Jt)F_k + (1-\cos(2Jt))(F_l\hat{J}_l)\hat{J}_k + \sin(2Jt)(\epsilon_{ijk}\hat{J}_iF_j)\right).$$

As we mentioned in the main text, the complexity of precursors will be equivalent for large classes of J_i (corresponding to the Hamiltonian) and F_i (corresponding to the choice of W_0). From the above equation, we see that the coordinates, β^k, are a sum of three terms. The first two terms are only in the X and Y directions. The time dependence is always of the form Jt, so any overall rescaling in J can be absorbed into a redefinition of the time parameter t. The second term involves the dot product of $\hat{J}_i$ and F_i so it only depends on the angle between F_i and J_i. The third term is proportional to the cross product between $\hat{J}_i$ and F_i, so it is in the Z direction and again only depends on the angle between $\hat{J}_i$ and F_i. Therefore, since the sub-manifold generated by the X and Y directions is isotropic, up to a rescaling of time, the complexity of the precursor only depends on the angle between F_i and J_i.